REGIONAL HETEROGENEITY OF ADVENTITIAL ELASTIN IN THE ARTERIOLAR WALL REFLECTS DIFFERENCES IN THE MECHANICAL ENVIRONMENT

A Thesis
presented to
the Faculty at the Graduate School
of the University of Missouri

In Partial Fulfillment
of the Requirements for the Degree

Master of Science

By
AARON J. STUPICA

Dr. Michael A. Hill, Thesis Supervisor

DECEMBER 2011

The undersigned, appointed by the dean of the Graduate School, have examined the thesis entitled

REGIONAL HETEROGENEITY OF ADVENTITIAL ELASTIN
IN THE ARTERIOLAR WALL REFLECT DIFFERENCES
IN THE MECHANICAL ENVIRONMENT

presented by Aaron Stupica,

a candidate for the degree of Master of Science,

and hereby certify that, in their opinion, it is worthy of acceptance.

_____

Dr. Michael Hill, Biological Engineering,
Medical Pharmacology and Physiology

_____

Dr. Gerald Meininger, Medical Pharmacology and Physiology,
Biological Engineering

_____

Dr. Luis Martinez-Lemus, Medical Pharmacology and Physiology,

_____

Dr. Philip Clifford, Medical College of Wisconsin, Visiting Professor

ACKNOWLEDGEMENTS

I'd like to take this time to thank everyone who has made my graduate school experience a success. My mentor and advisor, Dr. Michael A. Hill, has given me constant guidance and support throughout my entire learning curve. I cannot fully express how much it means to me to be given the opportunity he has provided for me. Even after numerous and costly mistakes, the support was unwavering. After two months of unsuccessful results, the guidance never faltered. I greatly appreciate the constant contact whether it be from across the hall or across the ocean. My thesis would never have been appropriate for submission without his continuous comments and suggestions.

I would also like to thank each member of my committee: Dr. Luis Martinez-Lemus, who taught me the intricacies of confocal microscopy and how to produce the results that have made this thesis possible, Dr. Gerald Meininger, who helped me keep everything in perspective and never forget the big picture, and last but not least Dr. Philip Clifford, who has worked closely with the Hill lab and myself. Dr. Clifford helped me realize what exactly I know and what I don't know. Such simple things can really advance the process of such a comprehensive study.

I would like to thank Dr. Srikanth Ella, member of Hill lab, with whom I have worked so closely with over the past two years. His close instruction assisted me with everything from fluorescent microscopy to writing my thesis. I cannot fully express how much his guidance has helped me in the laboratory and in graduate school life.

All members of the Hill lab: Dr. Yan Yang, Dr. Zahra Nourian, Dr. Min Li, Srijita Dhar (MS) have provided me with support above and beyond what is asked of lab members. They have gone out of their way to look for ways to help me. Being the only American student in the lab, they provided me with culture and food to make me feel welcome. I would also like specially thank Dr. Zahra Nourian for reviewing my thesis and helping me develop a paper that I am happy to submit.

I would like to thank all lab collaborators and Dalton staff. Lab collaborators: Dr. Michael Davis, Dr. Steven Segal, Dr. Robert Mecham, and Dr. Jessica Wagenseil have helped add different dimensions to my studies. The Dalton Cardiovascular Research Center staff and support team have also gone beyond their duties to help me personally and their work has been greatly appreciated. Dr. Mark Ellersieck, of the MU Department of Statistics, also provided support in the form of statistical analysis.

Finally, I would like to thank all my family and friends have supported me throughout the past two years and especially during the late hours of thesis writing. The support shown by my parents, John and Carol Stupica, has been unwavering and greatly appreciated.

TABLE OF CONTENTS

LIST OF FIGURES

Figure Page

LIST OF TABLES

ABBREVIATIONS

1A- First order arteriole
ACh- Acetylcholine
ANOVA- Analysis of variance
Ca^{2+}- Calcium
DAPI- 4'6-diamino-2-Phenylindol
EBP- Elastin binding protein
ECM- Extracellular matrix
EEL- External elastic lamina
IEL- Internal elastic lamina
K^{+}- Potassium
MMP- Matrix metalloproteinase
NA- Numerical aperture
PE- Phenylephrine
PMT- Photomultiplier tube
PSS- Physiological salt solution
ROS- Reactive oxygen species
SMC- Smooth muscle cell

REGIONAL HETEROGENEITY OF ADVENTITIAL ELASTIN IN THE ARTERIOLAR WALL REFLECTS DIFFERENCES IN THE MECHANICAL ENVIRONMENT

Aaron Stupica

Dr. Michael Hill, Thesis Supervisor

ABSTRACT

The mechanical properties of arteries are determined, in large part, by the extracellular matrix (ECM) composition and organization. Vessel stiffness and elasticity, vascular smooth muscle cell (SMCs) location, and stability are all influenced by the ECM proteins. The proteins that make up the ECM include elastin, collagen, and a number of glycoproteins: fibronectin, tenascin, vitronectin, and laminin. All of these proteins provide the vessel with mechanical support and functional strength. Elastic layers have been observed in throughout the vessel wall, specifically in the adventitia, external elastic lamina (EEL), and internal elastic lamina (IEL). The two elastic laminas act to constrain and presumably protect vascular SMCs from excessive mechanical forces. Each section of elastin has a distinct arrangement which hypothetically provide the vessel with a specific type of support.

The ECM protein elastin is the most hydrophobic of all known ECM proteins, which stems from its composition. This composition also provides a high degree of cross-linking, which leads to the most important property elastin confers on the vessel, elasticity. In the ECM, elastic fibers are assembled on microfibrils and these longitudinal fibers are especially common in tissues that undergo repetitive distention or passive lengthening movements. For example, skeletal muscle and mesenteric arteries are known

to contain elastin fibers in the adventitia. Elastin also exists in the IEL which separates the SMCs and endothelial cells but still allows for communication between the two. Holes (fenestrae) are common throughout the IEL in small arteries and arterioles of cerebral, mesenteric, and skeletal muscle vessels. This IEL assists vessel mechanics by contributing elasticity in response to shear stresses. However, with all that is understood about elastin content and ECM influence in vascular signaling in microvessels, the 3D structure of elastin distribution is currently not known.

Preliminary experiments in which adventitial elastin protein was degraded with the enzyme elastase, revealed a significant and irreversible lengthening of cannulated and pressurized cremasteric arterioles. These treated vessels still hold pressure, are myogenically active, and respond to vasoactive agents, suggesting that SMC and endothelial function were not impaired. Therefore we hypothesized that adventitial elastin is responsible for bearing longitudinal stress in blood vessels that would be exposed to longitudinal stretch.

This hypothesis was examined through the use of 3D confocal microscopy in isolated arterioles from cremaster skeletal muscle and small arteries from cerebral and mesenteric tissues. The isolated blood vessels (diameters= 180-220 μm) from Sprague Dawley rats were cannulated, pressurized, and fixed. Three different non-selective Alexa Hydrazides (350, 488, and 633) were initially studied for their ability to stain ECM, EEL, and IEL proteins/structure. Cell nuclei were stained with fluorescent nuclear indicators to allow cellular orientation and position within the wall to be observed. The staining pattern of the Alexa dyes were compared and Alexa 633 Hydrazide consistently and reproducibly labeled an extensive network of longitudinal adventitial fibers, shorter,

more branched fibers in the EEL, and the IEL. The fibers stained with Alexa 633 were also found to co-label with a fluorescent elastin antibody confirming that these fibers were elastin. Treatment with elastase in cremaster arterioles cleaved these longitudinal fibers and a significant and irreversible lengthening of the isolated arteriolar segment was observed. These longitudinal fibers were seen in the adventitia of cremaster and mesenteric vessels while a complete absence of fluorescently labeled adventitial fibers was noted in the cerebral artery. Fluorescence images confirmed the presence of the IEL in each of the three vessel types, although a structural heterogeneity within the IEL was observed.

Through focus image stacks of the arteriolar wall were acquired using 3D confocal microscopy. To our knowledge, these are the first data to provide a detailed 3D structure of elastin in arterioles from small arterioles. The arterioles collected from two mechanically active tissue environments, that are known to undergo frequent stretching, cremaster and mesentery, exhibited an ECM containing a population of longitudinal fibers, as well as an EEL containing shorter, circumferential fibers, and a fenestrated, but otherwise continuous IEL. The small cerebral arteries were selected as an example of a tissue with a stable and protected environment (i.e. within the skull). Consistent with our hypothesis, the cerebral vessel did not exhibit any adventitial elastin content associated with an EEL and in contrast to cremaster vessels, cerebral vessels showed no lengthening when treated with elastase.

Collectively, these results suggest that the elastin fibers in the adventitia of cremaster and mesenteric arterioles are responsible for bearing forces exerted along the longitudinal axis of the vessel, giving the vessel increased longitudinal support in the

presence of stretch. Furthermore, the absence of adventitial elastin in cerebral vessels suggests that the differences in adventitial elastin content may be related to the mechanical environment in which the vessels functionally exist.

In related studies, the developed ECM imaging approaches were also applied to aged vessels using an aging model, the Fischer 344 strain of rat. The results collected from aged rats exhibited noticeable differences in the elastin structure in mesenteric and cremaster vessels between young and old animals. The images produced in this preliminary study from microvessels could provide evidence showing the changes in elastin which could result in increased stiffness in aged blood vessels.

In conclusion, the fluorescence labeling techniques developed in the course of the research project should provide a valuable tool for investigation of the vessel wall ECM in a number of pathological states, such as diabetes mellitus and hypertension. The protocol has been shown to reveal microstructural details of the ECM structure in small blood vessels. Comparing the physiological state of the vascular wall with those of the pathological state could provide a basis for deeper understanding the changes that occur during vascular disease.

CHAPTER 1

INTRODUCTION

The principal function of the human circulatory system is to provide nutrients to cells and remove waste products produced throughout the body. The circulation is a closed system consisting of a heart acting as a pump and the blood vessels as the loop of the system that transports the oxygenated blood to organs and various tissue beds throughout the body. Post capillary blood vessels assist with returning the de-oxygenated blood containing metabolic byproducts to the heart to start the process over again. The vessels transporting blood are arteries, veins, and capillaries.

Across the arterial tree there are subtypes of blood vessels; each specialized to perform its specific function. Arteries are designed to transport blood from the heart to organs and different tissue beds and are therefore structured differently than the other vessel types. As the arteries continually branch into smaller vessels to help with blood distribution, a subtype of arteries are designated arterioles. For the current study, arterioles are defined as the feed artery, which enters muscle tissue or organs, and all arterial vessels that branch off the feed artery. Arterioles are typically under 220 μm in passive lumen diameter. Arterioles are also structured differently from the larger arteries (van den Akker et al., 2010).

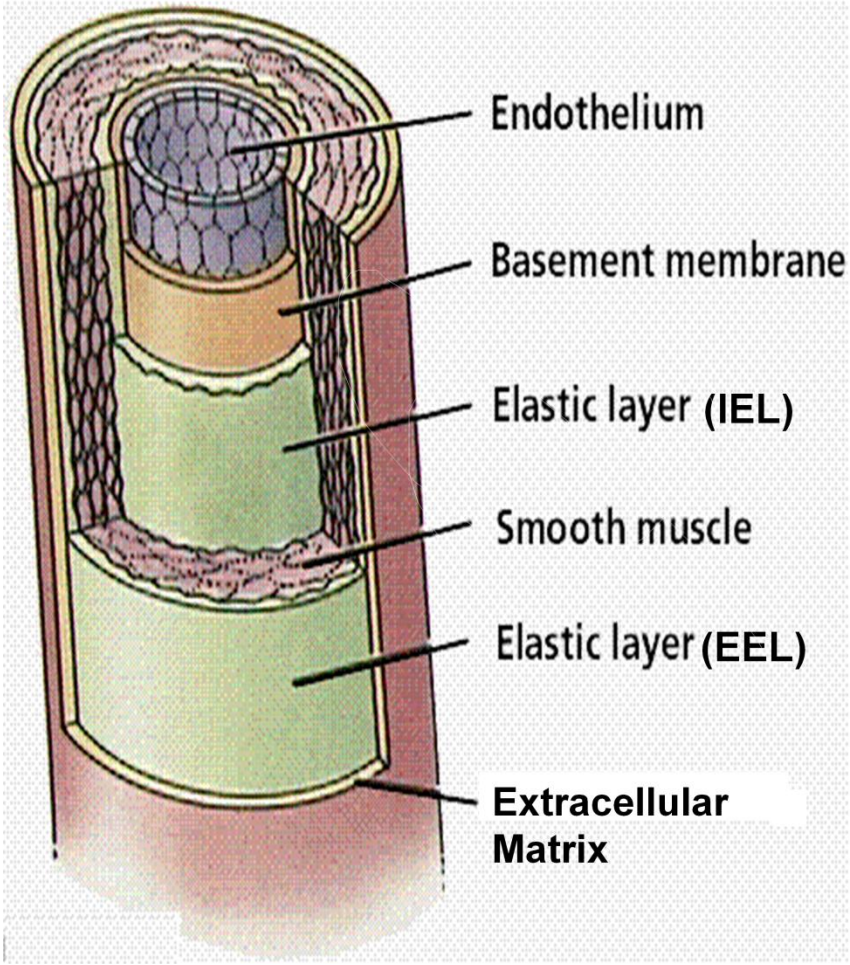

Figure 1.1: Cross section of a small artery. Endothelial cells line the lumen. Smooth muscle cells wrap around the vessel and are responsible for vessel constriction or dilation.

Source: (Purves et al., 1995)

As shown in Figure 1.1, arterioles are a conduit system for delivery of blood and well suited to perform their purpose. The major difference in the vascular wall composition of an artery and an arteriole is that an arteriole has only one or two layers of vascular smooth muscle cells. By convention, arterioles have been broken down into three layers: intima, media, and adventitia. In the intima, endothelial cells, typically oriented parallel to the direction of blood flow are in contact with the blood and line the

inside of the basement membrane. The basement membrane is composed principally of collagen type-IV and laminins (Ng and Ikeda, 2011). The internal elastic lamina (IEL) separates the intima and medial layers (Sims et al., 1993). In small arterioles, the medial layer consists of a single layer of vascular smooth muscle cells (SMCs), which are oriented perpendicular to blood flow and wrap circumferentially around the vessel. Larger arterioles may contain multiple layers of smooth muscle cells (Shiraishi et al., 1990). The smooth muscle cells in the media are responsible for the ability of the blood vessel to constrict and dilate in response to chemical or mechanical signals. On the outside of the smooth muscle cell layer is the adventitial layer, mainly composed of extracellular matrix (ECM) proteins. The medial and adventitial layers are separated by another elastic layer named the external elastic lamina (EEL) (Briones et al., 2003). The ECM is made up primarily of a number of proteins, proteoglycans, and glycoproteins. The structure and function of the adventitial proteins, such as elastin, can significantly influence the mechanical properties of the vascular wall and influence functional characteristics of the cardiovascular system.

While experiments pertaining to the functional significance of the ECM of arterioles are increasing in number, historically the main focus has been on the structural support that the ECM provides. Proteins of the ECM, such as collagen and elastin, are two of the most important fibrillar components that offer strength and flexibility for the vessel wall (Wagenseil and Mecham, 2009). Elastin in particular is believed to be a major determinate of the mechanical properties of arterioles, specifically vascular elasticity and stiffness (Borisov et al., 2000). Since arterioles are constantly undergoing changes in pressure, the importance of the protein scaffold composition in the ECM

cannot be overstated. However, the contribution of the ECM to vessel function is more than just structural support.

A number of proteins in the ECM are in contact with SMCs through membrane spanning receptors called integrins (Alenghat and Ingber, 2002; van den Akker et al., 2010). These possible connections would allow for the mechanical forces to be transmitted both directions, indicating the importance of ECM proteins to vessel function. Non-fibrillar elastin in the IEL also influences the vascular processes of remodeling and angiogenesis (Bakker et al., 2008).

1.1 Anatomy of the Cardiovascular System

There are three major types of blood vessels: arteries, veins, and capillaries. Arteries are responsible for controlling resistance throughout the blood system. Veins are capacitance vessels which can hold or transport large amounts of oxygen depleted blood back to the heart. Capillaries, which are very small in diameter, allow for passage of single blood cells between the arterial and venous networks during which nutrients and waste are exchanged in the tissue. The small arteries and arterioles are capable of controlling pressure and therefore, blood flow, independent of any central control (Davis and Hill, 1999). Veins are mostly responsible for transporting the deoxygenated blood back to the heart, but are also capable of holding significant quantities of blood. While variations in the structure of blood vessels from different networks exist, each vessel type is well designed to perform its purpose.

The arterial network begins at the aorta leaving the heart and continuously branching throughout the vasculature into smaller blood vessels. When these small, branched arteries finally enter an organ or tissue bed, they are termed feed arteries or arterioles (Segal et al., 1999). Control of blood flow to organs and tissue beds is vital to overall survival since not all organs and tissue beds require maximal blood flow at all times. As illustrated in Figure 1.2, the arterial network, in particular, specializes in pressure control. Although this recording is from a hamster cheek pouch, the pressure profile is similar to that observed in the circulation of rat skeletal muscle (Bohlen et al., 1977). The largest change in overall blood pressure is observed in the small arteries and arterioles of the arterial network even though at any given time the venous network contains 70% of the blood in circulation (Davis et al., 1986; Gelman, 2008). For this reason, small arteries and arterioles are considered to be large contributors to the resistance of the network.

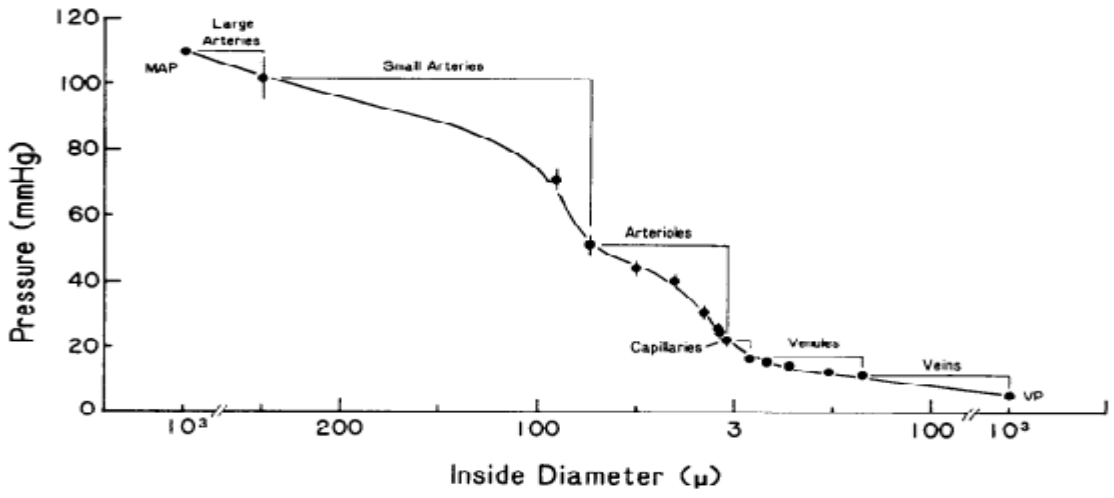

Figure 1.2: Pressure drops through skeletal muscle in the hamster cheek pouch circulation. The largest change in pressure is seen in the arterial network and specifically in small arteries and arterioles. MAP, mean arterial pressure, from femoral artery; VP, venous pressure, from external maxillary vein.

Source: (Davis et al., 1986)

The hemodynamic properties of blood vessels explain the importance of the resistance network. Any given pressure drop (ΔP) is directly related to flow rate (Q) and the resistance (R) to blood flow: $\Delta P = Q \times R$ (Dodds et al., 1996). Resistance is also shown to be inversely proportional to radius of the vessel to the fourth power (r^4) using a variation of Poiseuille's equation characterizing pressure drop through a long cylindrical pipe:$R \propto \frac{\eta \times L}{r^4}$, where η is viscosity of blood and L is length of the vessel (Fedosov et al., 2010). As the vessels branch and become smaller, their slight decreases in radius lead to significant increases in resistance, thus giving the small arteries and arterioles the name of the resistance network (Christensen and Mulvany, 2001). These small arteries and arterioles allow for control of blood flow to any specific tissue at a given time.

This pressure control in the arteries and arterioles largely stems from the contractile nature of vascular SMCs. Where large arteries are more passive in nature, their changes in diameter are largely controlled by neural inputs (Pickering et al., 2008). The control of pressure in small arteries and arterioles is more dependent on SMC function and an intrinsic property of these vessels described in the next section (Coats, 2003). The activity of the SMC is largely responsible for this dramatic change in vascular pressure recorded in the small vessels. The upstream pressure from larger arteries to the following, smaller arteries move the blood through the arterial network. The movement of blood is also assisted though neurotransmitters, such as phenylephrine and acetylcholine, circulating in the blood stream.

1.2 Myogenic Response

Arterioles, as part of the resistance network, contain either one or two layers of smooth muscle cells that have the capability to constrict and completely close the blood vessel to blood flow or dilate and allow for maximal blood flow (Berne, 2004). This regulation of blood flow is controlled by a number of factors including an intrinsic property of these vessels named the myogenic response. Briefly, when intraluminal pressure is increased in arterioles, a slight distention occurs, which is immediately followed by constriction and a new level of myogenic tone (Davis and Hill, 1999). Similarly, decreases in intraluminal pressure produce a similar but opposite effect with an overall dilation of the vessel (Johnson, 1981). This phenomenon is also observed, to a lesser degree, in arteries, veins, venules, and lymphatics (Davis and Hill, 1999).

1.2.1 History of the Myogenic Response

The first description of the myogenic response was provided by Sir William Bayliss in 1902, while measuring changes in volume of the dog hind limb in response to brief aortic occlusions. He recorded significant increases in volume when the occlusion was released. Bayliss decided that this was not due to an accumulation of metabolites because of the short time lapse but in fact due to an intrinsic mechanism. He supported this contention with studies in isolated arteries, which constricted after sudden distention (Bayliss, 1902). Due to contemporaries of Bayliss' favoring a metabolic mechanism for his findings including the publications of Anrep (von Anrep, 1912), research on the

myogenic response stayed relatively unchanged until the late 1940's. Folkow (1949) then confirmed and extended Bayliss' findings providing firm evidence to support a pressure-based mechanism for local vasoregulation.

1.2.2 Definition of the Myogenic Response

Descriptions of the myogenic response often vary between research groups because levels of myogenic tone differ in blood vessels depending on the size and tissue from which the vessel is isolated. For this report, the myogenic behavior of arterioles will be considered as a transient distension that is followed by active myogenic constriction to a new level of tone when intraluminal pressure is increased (Figure 1.3). Often the level of steady state constriction achieves a diameter significantly less than the initial baseline. When intraluminal pressure is reduced, the myogenic response acts in the opposite manner of pressure increase. An initial passive collapse is followed by vessel dilation to a larger diameter than before the downward pressure step (Davis and Hill, 1999). The vessel would be considered to be under myogenic tone if these conditions are met. A tracing of diameter in a functional coronary arteriole exhibiting myogenic tone as intraluminal pressure is acutely increased is shown in Figure 1.4A. The following recording of Figure 1.4B, in similar arterioles from the coronary circulation shows that myogenic constriction is independent of endothelium activity (Kuo et al., 1990).

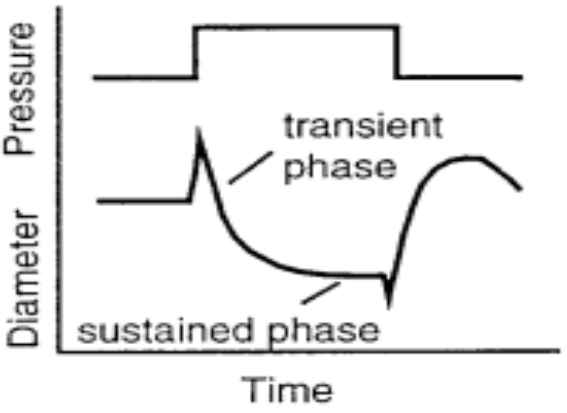

Figure 1.3: Myogenic behavior in arterioles. Shown is an example tracing of diameter change in response to a 2 min pressure step.

Source: (Davis and Hill, 1999)

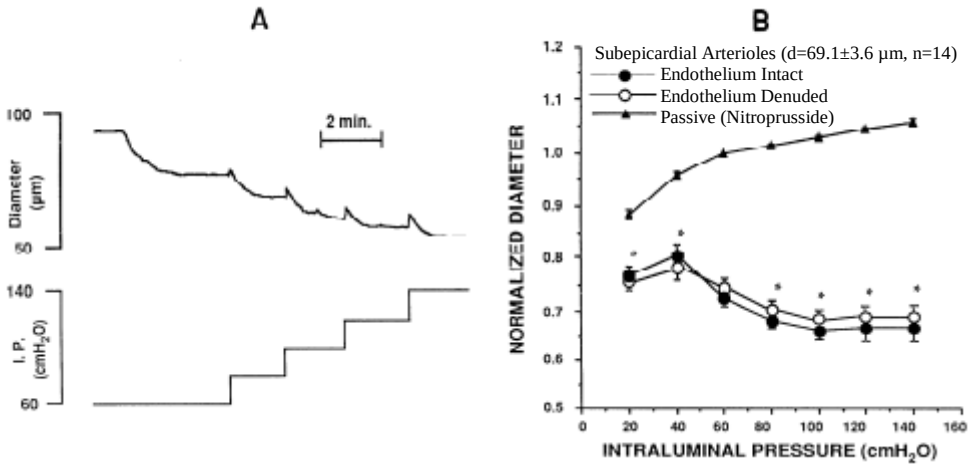

Figure 1.4: Coronary arterioles constrict in response to pressure increases when under myogenic tone (A). This response is independent of endothelial cell functionality (B); d, Average luminal diameter.

Source: (Kuo et al., 1990)

The myogenic response acts to protect vessels downstream from sudden increases in arterial pressure. This holds especially true in vessels feeding tissue beds and encapsulated organs, such as the brain, heart, and kidneys. Sudden changes in pressure in

the blood vessels carrying blood to these organs could lead to development of edema having significant, negative consequences. The myogenic response is an important autoregulation mechanism contributing to the regulation of blood pressure, capillary pressure, and peripheral resistance. Although all blood vessels maintain some level of myogenic tone *in-vivo*, the myogenic response is strongest in the microcirculation, where the changes in resistance are the greatest (Shepherd and Riedel, 1982; Chilian et al., 1993). Resting levels of myogenic tone in three vessels from the cremaster muscle arterial networks are shown in Figure 1.5. The larger artery, pudic-epigastric (internal diameter = 217 μm) does in fact maintain levels of tone, however the levels of resting myogenic tone are significantly stronger in the smaller vessels, external spermatic artery and cremasteric arteriole (both had internal diameter = 126 μm).

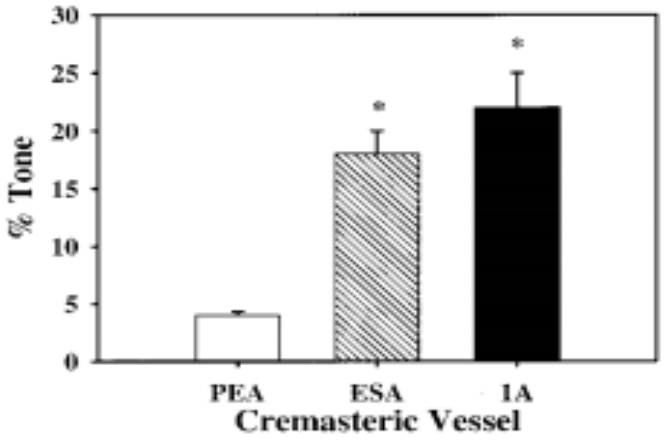

Figure 1.5: Resting tone of rat cremaster vessels. PEA, Pudic-epigastric artery; ESA, External spermatic artery; 1A, First order cremasteric arteriole.

Source: (Sylvester et al., 2000)

1.2.3 Mechanisms Underlying the Myogenic Response

The myogenic response is a complex vasoregulatory mechanism designed to react to changes in intraluminal pressure (Davis and Hill, 1999). Experiments into the intracellular mechanisms first started impacting the current theories in the late 1960's. Uchida and Bohr (1969) first stated that the myogenic response stemmed from SMC membrane depolarization and increased Ca^{2+} permeability. Increases in $[Ca^{2+}]_i$ levels have been shown to be fundamental to the development and maintenance of myogenic tone. The current prevailing theory still implicates membrane depolarization of vascular SMCs. SMC membrane depolarization could occur through modulation of ion channels, molecular signaling cascades, and modulation of levels of reactive oxygen species (ROS). However, the pathways that mechanical forces could take to influence myogenic activity have been suggested (Figure 1.6). In order to initiate a contractile response to an increase in intraluminal pressure, SMCs activate non-selective cation channels, which are thought to lead to SMC membrane depolarization. This in turn opens voltage gated calcium ion channels, which increases intracellular calcium levels and ultimately activates vessel constriction (Jackson, 2000).

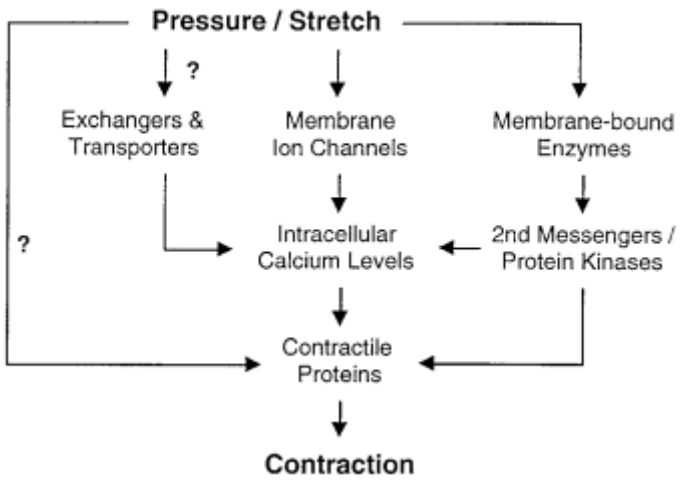

Figure 1.6: Pathways for the influence of mechanical forces, pressure or stretch, to affect the myogenic response.

Source: (Davis and Hill, 1999)

Activation of mechanosensitive ion channels is one of the many pathways implicated in causing membrane depolarization. Mechanosensitive ion channels, also known as stretch activated calcium channels, have been identified in virtually all cell types in numerous animals (Davis et al., 1992; Ahmed et al., 2004). One particular aspect of interest with these channels is how the mechanical forces impact the behavior of the vascular cells. One possible pathway for transmission of these forces throughout the vessel wall is through membrane spanning proteins called integrins. In a study by Mogford (1997), isolated skeletal muscle arterioles from rats, displaying spontaneous myogenic tone, were shown to result in vasoconstriction when exposed to an integrin binding peptide. Vasoconstriction was inhibited by blocking both α_5 and β_3 integrins separately. Furthermore, in a 2008 study, Sun et al. used atomic force microscopy to examine focal adhesions between various ECM proteins and isolated, vascular SMCs. Fibronectin caused strong focal adhesions through the $\alpha_5\beta_3$ integrin and when the

fibronectin coated bead was pulled away from the cell, the SMC reacted with a "myogenic-like, force generating response" (Sun et al., 2008).

1.3 Extracellular Matrix

The extracellular matrix (ECM) is known to provide structural support and protect the functional properties of arterioles (Badylak et al., 2009). Proteins found in the ECM, such as collagen, elastin, and glycoproteins are also seen throughout the vessel wall. In reference to Figure 1.1, non-fibrillar proteins compose the basement membrane and internal elastic lamina (IEL) respectively, while individual protein fibers make up the external elastic lamina (EEL) and ECM. The IEL appears as a continuous sheet-like structure that wraps circumferentially around the vessel. There are however holes, or fenestrae, in the IEL whose purpose is thought to allow for pathways of myoendothelial gap junctions between SMCs and endothelial cells (Garland et al., 2010). The EEL is another elastic layer separating the SMCs from the ECM. This elastic layer is mainly composed of protein fibers, rather than having a sheet-like structure like the IEL. Finally, the composition and organization of individual proteins in the ECM in large part determines the mechanical properties of the vascular wall and assist with vessel recoil after contraction or dilation (Wagenseil and Mecham, 2009). ECM proteins give the arterioles a highly flexible vascular wall which loses little energy during the constriction and dilation cycle (Mithieux and Weiss, 2005). While cellular mechanisms, such as the myogenic response, have been focused on during increases in pressure, the ECM also

assists with vessel stability. In arterioles, the elastic protein elastin is responsible for bearing stress at low pressures, up to 40 mmHg (Briones et al., 2003). The ECM provides a limit of distention at higher levels of pressure by transferring the load to collagen bundles, which prevents rupture of the vessel (Burton, 1954; Fomovsky et al., 2010). This protection of the vessel wall following an increase in pressure is shown in Figure 1.7. The passive response is characterized by a rapid distension following an increase in pressure but reaches a plateau, where the vessel is prevented from further distending and possible vessel rupture. This plateau is dependent on the vascular wall and ECM proteins more heavily than actual cellular responses.

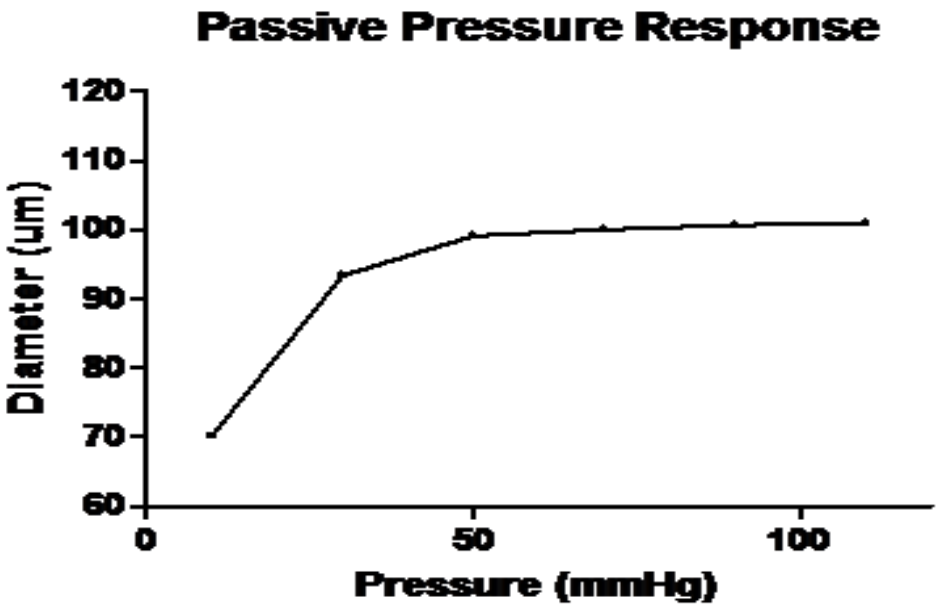

Figure 1.7: Example tracing of the passive distention qualities of the arteriolar wall. Increases in pressure cause an increase in diameter until a maximum distention is reached.

The ECM is coupled with the vascular cells through mechanosensing connections called integrins (Martinez-Lemus et al., 2005). The ability of vascular SMCs and endothelial cells to sense mechanical forces and turn them into signals for specific

cellular responses is known as mechanotransduction (Huang et al., 2004). Integrins are membrane spanning α- and β-, heterodimeric proteins that act as the mechanosensing mechanism through which the ECM communicates with SMCs, endothelial cells, and the cytoskeleton. These integrins have extracellular segments that bind with the ECM and short cytoplasmic tails that bind to focal adhesion proteins (Vuori, 1998). As pressure in the vessel increases, the vessel distends and places strain on both SMCs and proteins in the ECM. As shown in Figure 1.8, this strain is relayed via cell-matrix and cell-cell integrin connections, which ultimately elicits a response from SMCs (Martinez-Lemus et al., 2005). For example, fibronectin has been shown to potentiate SMC contraction through activation of voltage gated Ca^{2+} channels via integrin binding in a process called "outside-in signaling" (Wu et al., 2008). Two integrins that have been specifically implicated in the influence of cellular function are $\alpha_5\beta_1$ and $\alpha_v\beta_3$. Bonding between fibronectin and the $\alpha_5\beta_1$ integrin has been confirmed by atomic force microscopy (Martinez-Lemus et al., 2005; Sun et al., 2008). Contractile proteins attach to the extracellular domain of integrins through adhesion to dense plaques of integrins on the plasma membrane. Dense plaques refer to the in situ clusters of anchoring points on the plasma membrane for the cytoskeleton (Small and Gimona, 1998). These signal pathways to the vascular cells also send signals from the cells to the ECM proteins. These communications to the adventitial proteins have been shown to result in ECM remodeling or assembly. Application of mechanical stress across SMC- integrin adhesion sites results in a proportional stiffening of the cytoskeleton through a process called "inside-out signaling." Wang showed in 1993 that cytoskeleton reorganization

resulted from twisting of cells by magnetic beads that were applied to cell surface receptors (Wang et al., 1993).

ECM-integrin mechanosensing is not limited to vascular SMC function. In endothelial cells, when the extracellular domain of the integrin would bind to vitronectin, fibronectin, laminin, or collagen, mechanosensing of shear stress resulted in cytoskeletal remodeling (Shyy and Chien, 2002). Despite results provided for these interactions comparatively little research has focused on the impact the ECM has on cellular functions in the functional/active vessel. At present, however, integrins offer a possible and direct pathway for mechanosensing between the ECM and cytoskeleton.

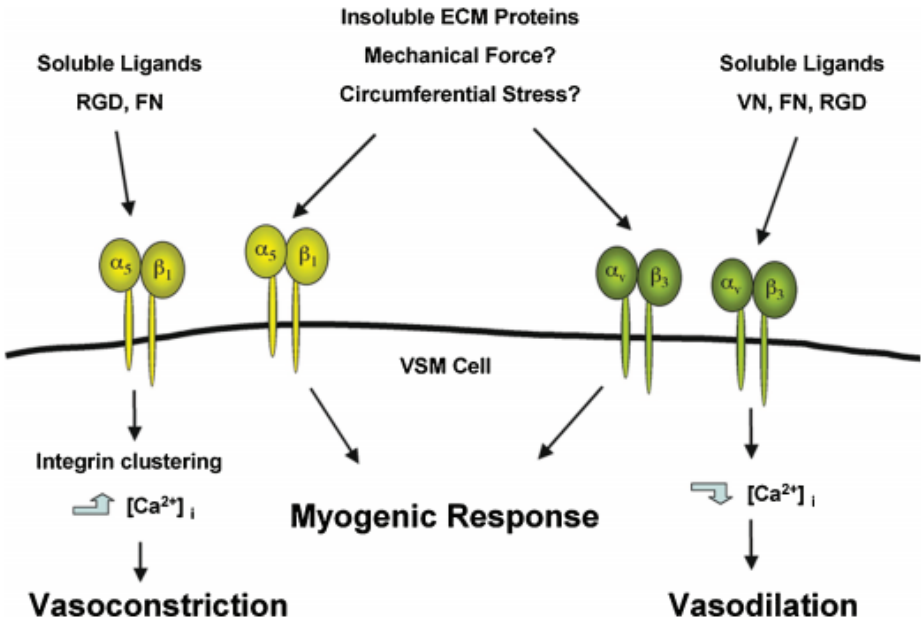

Figure 1.8: Integrin influence on the vessel functions. Soluble ligands can induce vasoconstriction or vasodilation through separate integrins. However, both integrins have been implicated in mechanotransduction in arterioles. FN, fibronectin; VN, vitronectin; RGD, Asp-Gly-Asp recognition site.

Source: (Martinez-Lemus et al., 2005)

1.3.1 Elastin

Elastin as a member of the ECM protein family is the major source of elasticity in the vasculature. Elastin has been found in many tissues, such as the aorta and carotid arteries, lungs, tendons, skin, and microvessels. The quantities of elastin vary greatly between tissues such as more than 50% in large arteries or as little as 2-4% of the dry weight of skin (Greenlee et al., 1966). Adventitial elastin is observed in large, conduit arteries and remains a significant component of the wall, even in very small arterioles. Elastin contributes to the overall vessel composition and arteriolar distensibility. After longitudinal vessel lengthening, elastin is primarily responsible for bringing the vessel back to its resting state (Kielty et al., 2002). Being a highly cross-linked structure, the protein is insoluble, extremely hydrophobic, long lived, and resilient to stretch. A good example of the degree of elasticity of elastin is given by Young's Modulus. Young's Modulus is tensile stress divided by tensile strain, with lower values being more elastic and higher values being stiffer. Elastic fibers have an average value 450 kPa, whereas collagen has an approximate value of 1,000,000 kPa (Fung, 1993). While elastin and elastic fibers are not one and the same, elastin composes 90% of the elastic fiber with the remaining constituents being fibrillins and microfibrillar-associated glycoproteins (Wagenseil and Mecham, 2009). An important property of stretch, the elasticity allows for significant deformation followed by recoil without requiring energy input for recoil.

1.3.2 Synthesis of Elastin

As previously mentioned, the cross-linking structure of elastin is very important to providing blood vessels with their resilient nature. This cross-linking is a result of the

mechanism by which elastin is synthesized. A single gene encodes for 60-70 kDa protein named tropoelastin. This gene is found in SMC, fibroblasts, endothelial cells, chondroblasts, and mesothelial cells (Uitto et al., 1991). The tropoelastin protein consists of hydrophobic sequences alternating with lysine containing cross-linking motifs. In SMCs, tropoelastin is transported out of the plasma membrane by the $\alpha_v\beta_3$ integrin, which binds to the C- terminal motif (Bax et al., 2009). Tropoelastin is guided by an elastin binding protein (EBP) to the site of elastogenesis on microfibrils (Figure 1.9). However, the exact relationship between tropoelastin and EBP is not currently known (Patel et al., 2011). Microfibrils are 10-12 nm filaments that act as a scaffold for tropoelastin deposition, orientation, and assembly. Microfibrils are mainly composed of glycoproteins: fibrillin-1, fibrillin-2, and microfibril-associated glycoprotein-1 (Mithieux and Weiss, 2005). This chaperone prevents intracellular self-aggregation or premature degradation. Microfibrils facilitate elastin assembly and provide an overall structure for the growing elastin fiber. Tropoelastin is organized on the microfibril through a process known as "coacervation", in which tropoelastin molecules aggregate with increasing temperatures (Mithieux and Weiss, 2005). This has been shown *in-vitro* by Bellingham (2001) with a similar process is believed to occur *in*-vivo. Defects in the process of coacervation have been linked to incomplete elastin formation as well as supravalvular aortic stenosis (Wu and Weiss, 1999). Following coacervation, cross-linking of the tropoelastin occurs through the enzyme, lysyl oxidase. This enzyme begins the oxidative deamination of the ε-amino group of the lysine chains (Kagan and Li, 2003). Following this, a reactive precursor, aldehyde, for inter- and intramolecular cross-links for elastin remains. This aldehyde is then able to condense with another aldehyde residue or with an

unoxidized lysyl amino group. Four separate cross-link types, with subtypes, can then be created, but the two most important cross links are the tetrafunctional desmosine and isodesmosine as shown in Figure 1.10 (Mithieux and Weiss, 2005). The cross-linking step is essential for structural integrity and to provide the function for elastin for vessel stability.

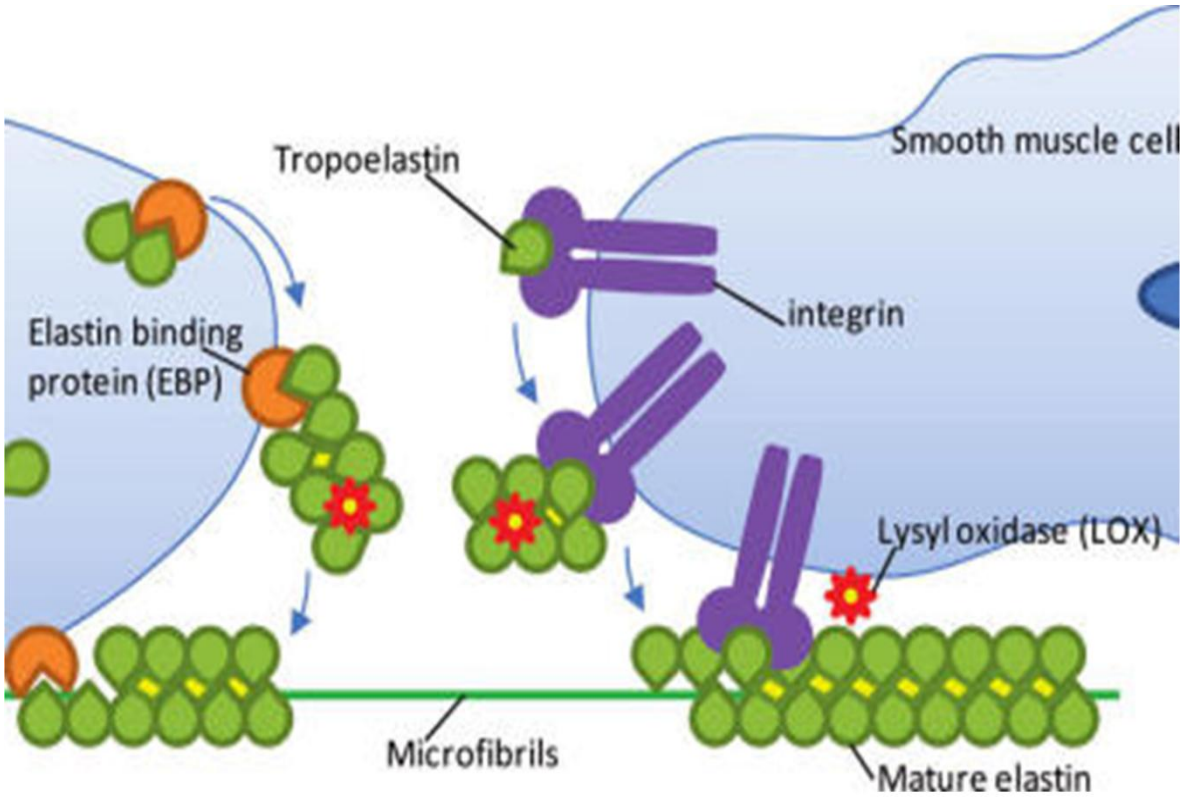

Figure 1.9: Schematic for elastin synthesis. Tropoelastin is made in smooth muscle cells and guided to the microfibril by EBP. Not shown is coacervation, where tropoelastin is organized on the microfibril, and cross-linking, which provides the integrity and function of elastin.

Source: (Patel et al., 2011)

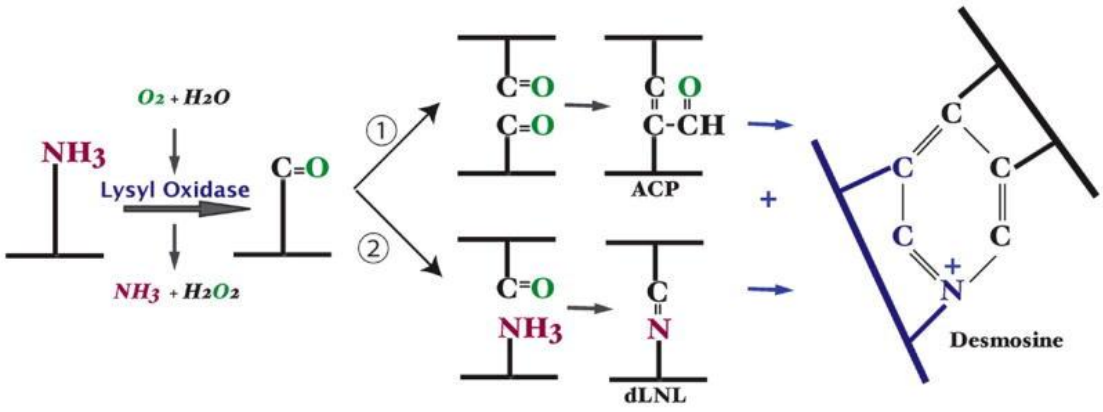

Figure 1.10: Alteration of lysine side chains of tropoelastin into the tetrafunctional cross-link desmosine. Post coacervation, cross-linking begins with lysyl oxidase in the process of deamination of the lysine side chains. The resultant aldehyde can then pair with another aldehyde or with an unoxidized lysyl amino group. The result is desmosine or its isomer isodesmosine.

Source: (Mecham, 2008)

This cross-linking of elastin is its signature feature and provides the protein with the elasticity and long life required for vessel function. Medium to small arteries are described as muscular arteries because of the existence and strength of the elastic fiber. The result of coacervation is the addition of hydrophobic segments to elastin. Cross-linking produces bifunctional, trifunctional, and tetrafunctional cross-links. Bifunctional and tetrafunctional cross links each have at least two subtypes. Other proteins in the ECM also contain cross-links, but the tetrafunctional cross-links, desmosine and isodesmosine, are found exclusively in elastin (Mithieux and Weiss, 2005). While lysyl oxidase also produces cross-links in collagen, the major difference between collagen and elastin is the magnitude of the cross-links. Collagen has 1-4 cross links per collagen unit, while elastin contains 15-20 cross-links per unit (Wagenseil and Mecham, 2009). This cross-linking also provides the protein with a very long working life. Indeed, the half-life of elastin is estimated to be approximately 70 years (Petersen et al., 2002). The vast

majority of elastin expression is completed early in the life cycle, as demonstrated in the mouse aorta in Figure 1.11. The units and degree of cross-linking gives elastin, and therefore the blood vessel, its long life and ability to regain its resting structure without requiring energy input.

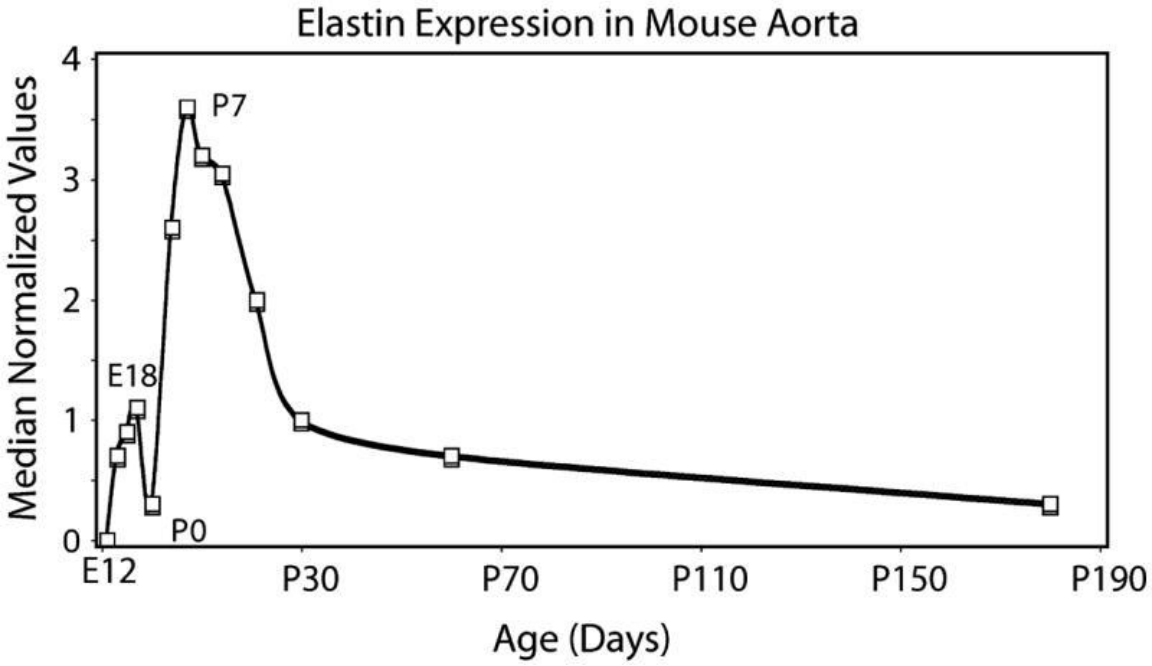

Figure 1.11: Time profile of elastin expression in mouse aorta. Elastin expression is highest from embryonic day 14 through postnatal day 7-10**.** Expression falls rapidly after this point.

Source: (Mecham, 2008)

1.3.3 Pathological States Involving Elastin

In healthy individuals, elastin is a stable, insoluble, and resilient protein. However, there are many pathological states that cause ECM remodeling and degradation of elastin, such as aging, hypertension, and aneurysms (Urban and Boyd, 2000). The most common case of elastin degradation is seen in aged blood vessels. The many cross

links existing in elastin slows this process, which also helps the longevity of the protein. The overall deterioration of elastin is accomplished through a group of proteolytic enzymes, known as elastases, the non-enzymatic process of glycation, and simply fatigue (O'Rourke, 2007). These can cause the elastic fibers to degenerate, thin, branch, fracture and decrease in volume. Elastase is an enzyme of the serine protease class which degrades elastin (Faury, 2001). Matrix metalloproteinase (MMP)7, produced in the vessel wall, and MMP12, secreted during differentiation of monocytes into macrophages, both also assist with degradation of elastin. The regulation of MMP production is tightly controlled, but over time and during pathological processes, this regulation can become unbalanced. Konova *et al.* (2004) showed that even in normoglycemia, age related changes in healthy human aorta caused increased non-enzymatic glycation. This is not surprising considering that greater glycation occurs in diabetic states (Nozynski et al., 2011). Finally, it is believed that elastic fibers are able to undergo billions of cycles of extension and recoil without failure, but elastin fatigue over the span of a lifetime and other environmental factors such as nutrition, physical activity, and smoking also influence the longevity of elastin (Keeley et al., 2002). Whatever the cause, a decrease in the elastin specific cross links, desmosine and isodesmosine, is observed in the human aorta, which directly decreases elasticity (Figure 1.12). These effects of aging result in an increase in arterial stiffness and therefore decreased distensibility and systemic compliance (Watanabe et al., 1996).

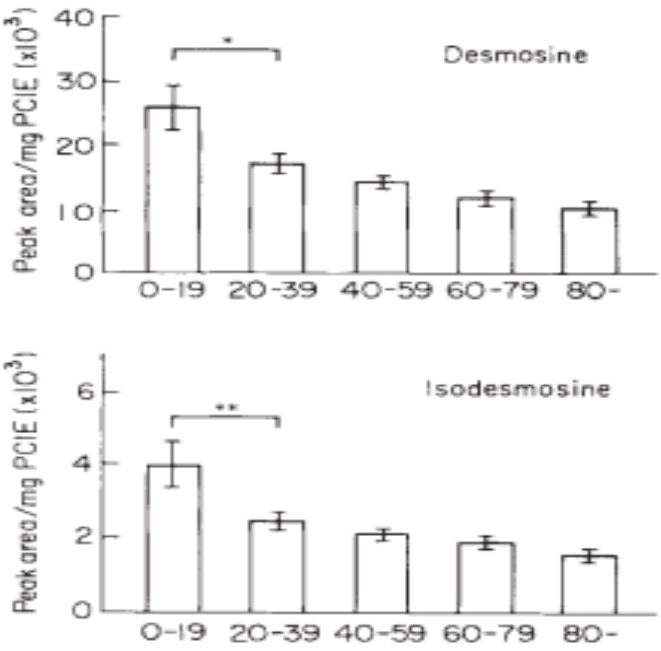

Figure 1.12: A significant decrease in the overall amount of the elastin specific cross links desmosine and isodesmosine is seen over time. x-axis is age in years of human aorta studied.

Source: (Watanabe et al., 1996)

Dramatic differences have been seen in ECM composition in hypertension and aneurysms. ECM remodeling has been proposed as both a causal and secondary factor in hypertension. Hypertensive remodeling involves both eutrophic and hypertrophic remodeling. Eutrophic remodeling results in a decrease in the outer diameter and in the lumen (Baumbach and Heistad, 1989). Hypertrophic remodeling results in a thickening of the medial section which reduces the lumen diameter (Deng and Schiffrin, 1992). Both states give a higher media-lumen ratio, which ultimately increases arterial blood pressure as shown in Figure 1.13. Vascular remodeling is also seen in aneurysms with an end result that can lead to rupture of the vessel wall. In this situation, remodeling has been seen as disorganization and destruction of the EEL as a result of adventitial fibrosis

and degradation of adventitial elastin through increases in elastase and MMP-9 and MMP-12 activity as described above (Tamarina et al., 1997). While other factors exist as a possible cause or result of these pathological states, the ECM changes in elastin alone can be seen as a significant contributor to the pathological problems.

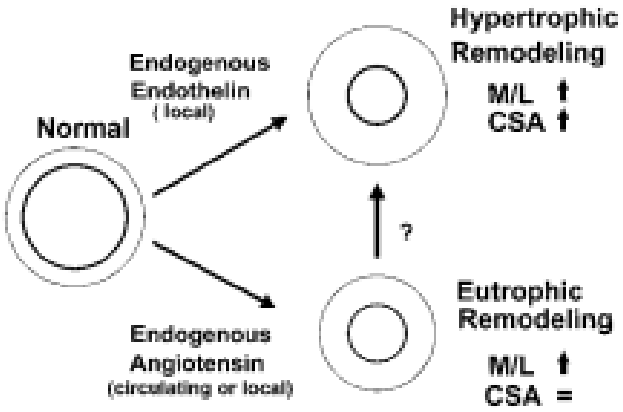

Figure 1.13: ECM remodeling in hypertension. Eutrophic remodeling decreases lumen size and total diameter so the cross sectional area stays the same while the media to lumen ratio increases. Hypertrophic remodeling results in a thickening of the media so the cross sectional area and media to lumen ratio are both increased.

Source: (Intengan and Schiffrin, 2000)

The necessity for elastin is firmly illustrated in genetic mouse models in which the elastin gene has been knocked out. As shown in Figure 1.11, the majority of elastin expression is accomplished within the first two postnatal weeks (Mecham, 2008). Elastin knockout mice do not survive more than a day or two postnatally. Close to birth, intravascular pressure is greatly increased from the embryonic stage. Without the appropriate elastin content, the normal development of blood vessels is impaired. The elastin heterozygote mouse had lengthened blood vessels and smaller diameters. The absence of elastin during the first days postnatal produced blood vessels with that were very stiff, narrow, and tortuous (Wagenseil et al., 2009). This is highlighted in Figure

1.14, where in the Eln -/- panel it can be seen that the right and left carotid artery, in particular, are extremely tortuous.

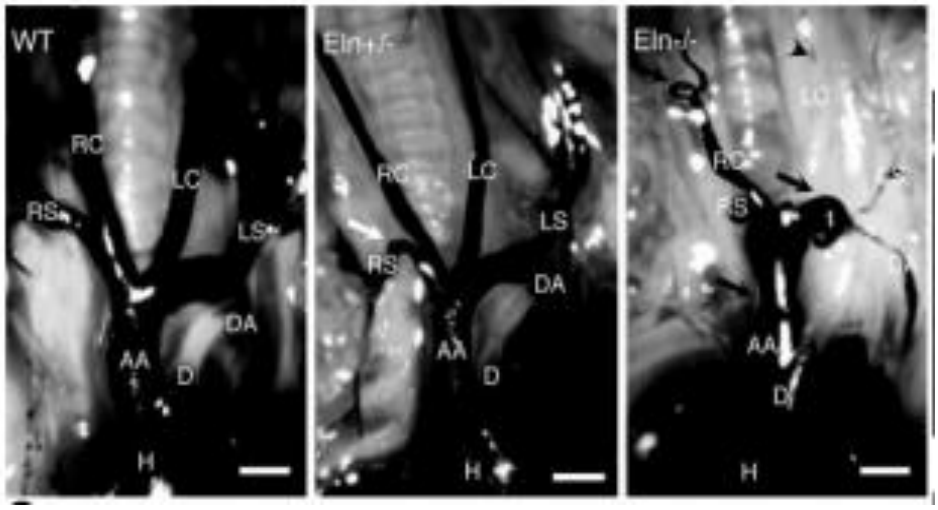

Figure 1.14: Elastin content influences vessel stability. Left panel is wildtype. Middle panel is elastin heterozygote missing half of the elastin gene. The white arrow shows a bend in the vessel. Right panel is elastin knockout. Black arrowhead shows where the LC is. Black arrow highlights tortuosity. H, heart; AA, ascending aorta; RS, right subclavian; LS, left subclavian; RC, right carotid; LC, left carotid; DA, descending aorta. Arrows highlight vessel tortuosity. Scale bar is 0.5mm.

Source: (Wagenseil et al., 2009)

1.3.4 Elastase Degradation

In the physiological and the pathological states highlighted above, elastin proteins are degraded by elastase. When isolated, cremaster arterioles were exposed to elastase (0.05 U/ml) for 5 minutes, lengthening of the vessel was observed as shown in Figure 1.15 (Clifford et al., 2009). The degradation of adventitial elastin resulted in significant and irreversible vessel lengthening by 35% in cremaster arterioles with little response in cerebral arteries (Figure 1.16A). Although myogenic reactivity was attenuated, the lengthening following elastase treatment did not cause gross damage to the vessel as

assessed by the absence of pressure leaks (Figure 1.16B). Further, no difference in responsiveness to vasoactive agents was observed after the elastase treatment (Figure 1.16C). A significant shift in the pressure-diameter relationship at low pressures was however evident after elastase treatment (Figure 1.16D). This data suggested that elastin may constrain the vessels along the axis of blood flow at resting state (Clifford et al., Unpublished data). The leftward shift in the pressure-diameter relationship recorded at low pressures is attributable to degradation of elastin, which is responsible for bearing stress at low pressures in the vascular wall of small arteries. Therefore, one significant difference that is directly attributable to elastin degradation is vessel lengthening.

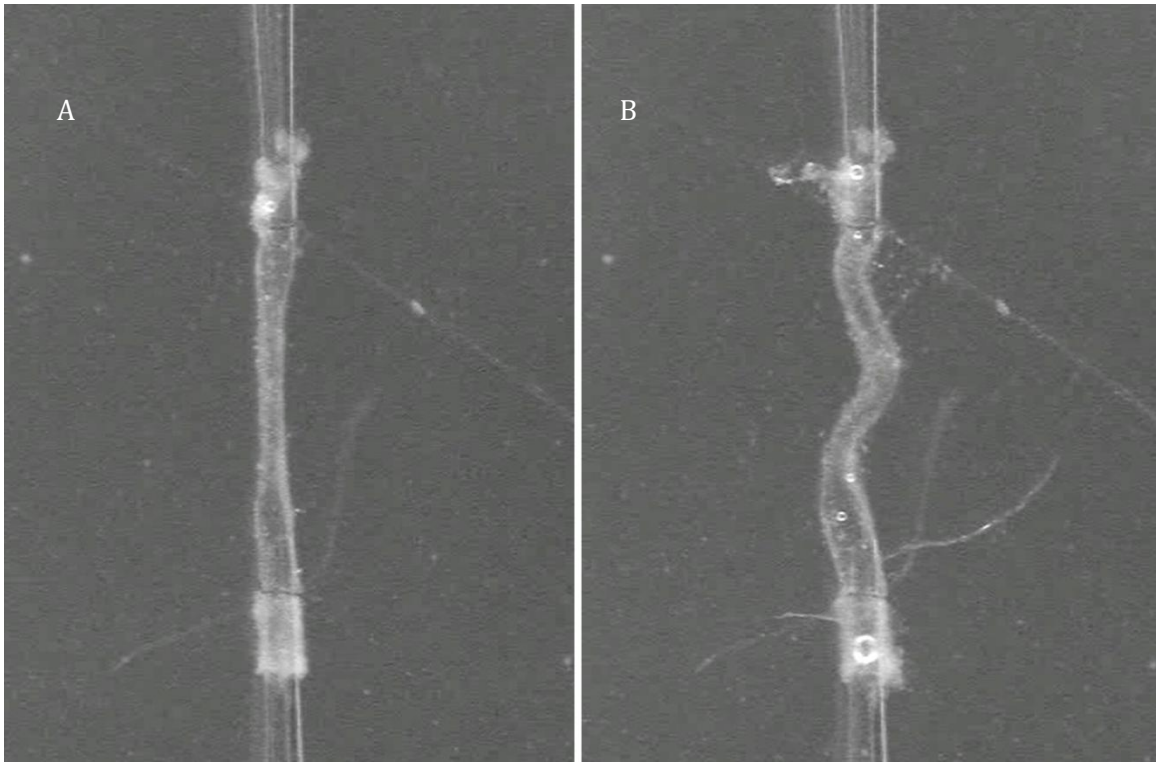

Figure 1.15: Isolated cremaster arteriole exposed to elastase resulted in significant vessel lengthening. A) Control B) Elastase treated.

Source: (Clifford et al., 2009)

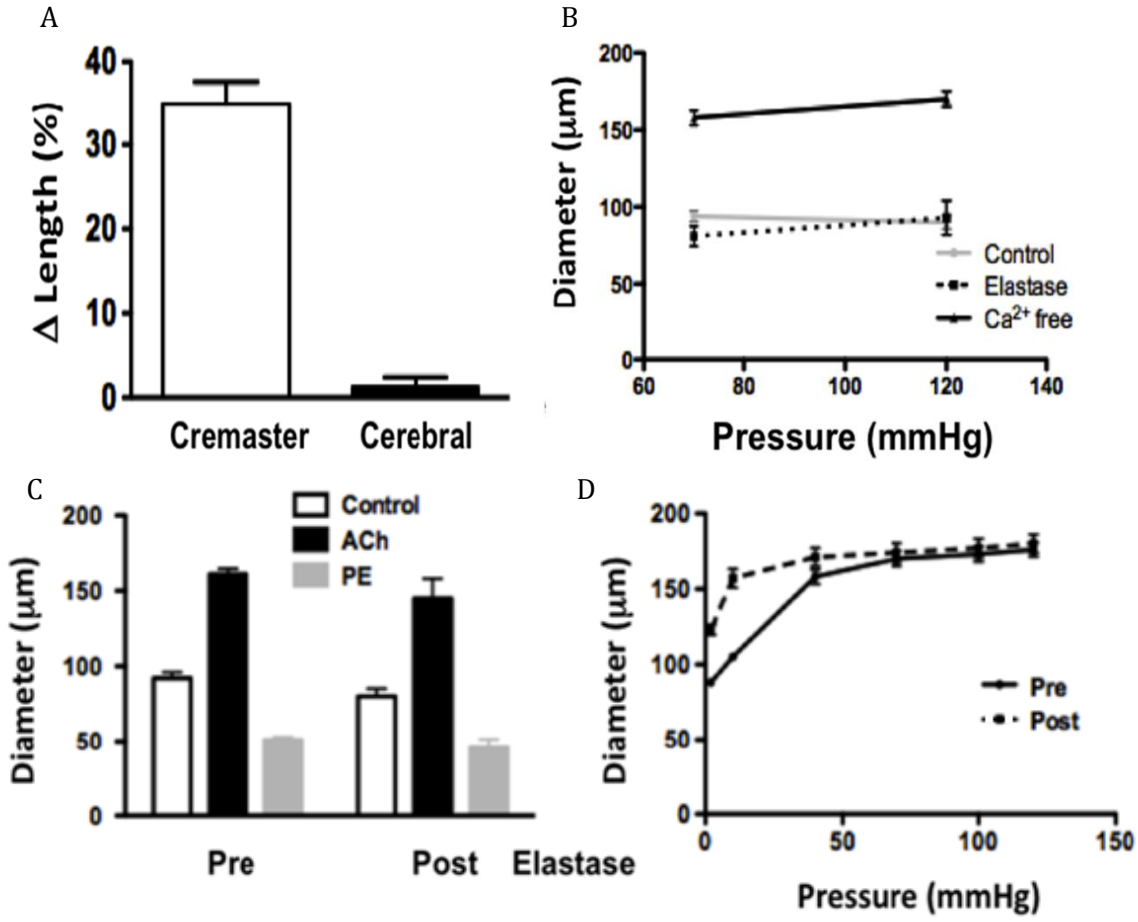

Figure 1.16: Effects of elastase treatments on arteriole properties. A) Changes in length between cremaster and cerebral, B) Pressure step in cremaster arterioles under passive, myogenically active, and elastase treated conditions, C) Responsiveness to vasoactive agents was not affected, D) Leftward shift in pressure-diameter relationship at low pressures.

Source: (Clifford et al., Unpublished data)

1.A Confocal Microscopy

With little known of the structure and orientation of elastin in the arteriolar wall, confocal microscopy offered the best possibility to understand the structural properties of elastin. The capabilities of confocal microscopy will be discussed briefly. The concept

of confocal microscopy is usually credited to Melvin Minsky, a postdoctoral student at Harvard, in the mid 1950s (Minksy, 1988). In trying to develop a protocol to image the neural networks of brain tissue, he attempted to develop an approach for imaging unstained sections. However, due to the lack of intense light sources and computing power to handle the large amounts of data, his ideas went largely unnoticed. The next step in developing the confocal system came from David Egger and Mojmir Petran in the form of multiple light sources and a spinning (Nipkow) disc in the late 1960s. The first images of recognizable corneal endothelial cells were produced by Davidovits and Egger (1973). After Minsky's patent ended in the late 1970s, the first practical confocal system was designed by a Dutch physicist, Fred Brakenhoff (1979). Advances in laser and computing algorithms and data storage power led to this latest development. Further advances in these fields led to the current state of confocal imaging where the microscope, lasers, and software are completely integrated.

The modern state of confocal imaging follows Minsky's principles with a point by point imaging model of the specimen. The laser's excitation light and out of focus emitted light are excluded from recording because of beam splitting mirrors and a pinhole in front of the light detector. Moving the light across the specimen avoided exposing the specimen to constant light (Webb, 1996).

1.A.1 General Principles of Confocal Microscopy

The main advantages of image enhancement through confocal microscopy are the low areas of excitation light projected on the specimen and the exclusion of out of focus

signals. As the schematic of confocal microscopy in Figure 1.17 shows, the excitation light is emitted by a laser and passes through the first pinhole aperture situated in a conjugate plane (confocal). The laser is reflected by a dichromatic mirror which directs the light to the objective. The objective focuses the light to the desired focal plane in the specimen (Webb, 1996). Fluorescent light is emitted from the specimen, which is directed by the dichromatic mirror to the photomultiplier tube (PMT). However a second or exit pinhole aperture is positioned in front of the PMT which focuses the light as a confocal point. The pinhole aperture in front of the PMT eliminates emitted light from the specimen that is above or below the focal plane, termed "out of focus" emission. The ability to eliminate out of focus light makes the imaging result much sharper and more defined than possible with widefield microscopy. Refocusing the objective shifts the focal plane, from which emitted light will then be detected. The adaptation of confocal microscopy to enable automated collection in different depths (z steps) of the focal plane led to the development of 3D confocal imaging (Paddock, 2000). The images collected are stored digitally and can be analyzed using numerous software programs.

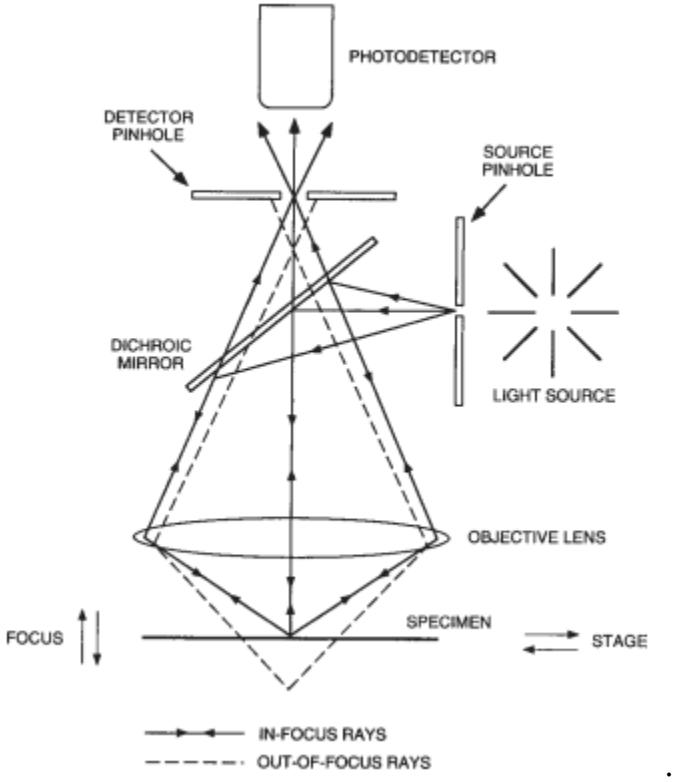

Figure 1.17: Following light detection of a fluorescent specimen in a confocal system.

Source: (Paddock, 2000)

1.A.2 Limitations of Confocal Microscopy

While the confocal system offers a number of advantages over more traditional microscopy methods, there are limitations to the design. Depending on the wavelength of the excitation light and the numerical aperture (NA) of the objective, the image produced is surrounded by diffracted light that appears as dark rings called "airy discs" (van den Berg et al., 2005). Therefore the optimal region of resolution is limited. The high intensity nature of the laser can be harmful to live specimens. This is less of a concern during imaging of fixed specimens. Also this high intensity light can cause a loss of fluorescence in stained specimens, which is the most consistent problem with

fluorescence microscopy. The constant excitation of the fluorescent molecules can either oxidize the fluorophore or leave electrons of the fluorophore in a triplet state that can ultimately lead to a nonfluorescent molecule through a process called photobleaching (Pawley, 1995). Photobleaching can be avoided by limiting exposure of the specimen to the light or through use of "laser dyes," which are highly resistance to photobleaching and often reversible from this state (Seward and Bagshaw, 2009).

1.A.3 Fluorescence Staining

Fluorescent imaging in cells and blood vessels began with specimens that were capable of primary fluorescence or autofluorescence. These specimens contained intrinsic properties that would emit light with a longer wavelength than the light used to excite the specimen. However, not all biological specimens have autofluorescent properties, such as bacteria (Lakowicz, 2006). The technique of secondary fluorescence was developed in the 1930s by an Austrian chemist, Max Haitinger. *In-vivo* and *in-vitro* fluorescent staining has largely increased the understanding of cellular structure and function and blood vessel structure. New developments in fluorescent labels and sensors and computer software for image acquisition and analysis continually improve the imaging capabilities. Fluorescent markers, also called fluorochromes or fluorophores, are available for a large variety of living or fixed biological structures including cell nuclei and proteins. Fluorescent markers are also used for measurement of chemical signals in vascular cells (Helmchen, 2011). Fluorochromes absorb the excitation light and emit a light with a longer wavelength. The separation of the excitation and emission spectra is

vital to fluorescent imaging (Harlow and Lane, 1999). The absorption and emission profile of a commonly used fluorochrome, Alexa 633 Hydrazide, is shown in Figure 1.18.

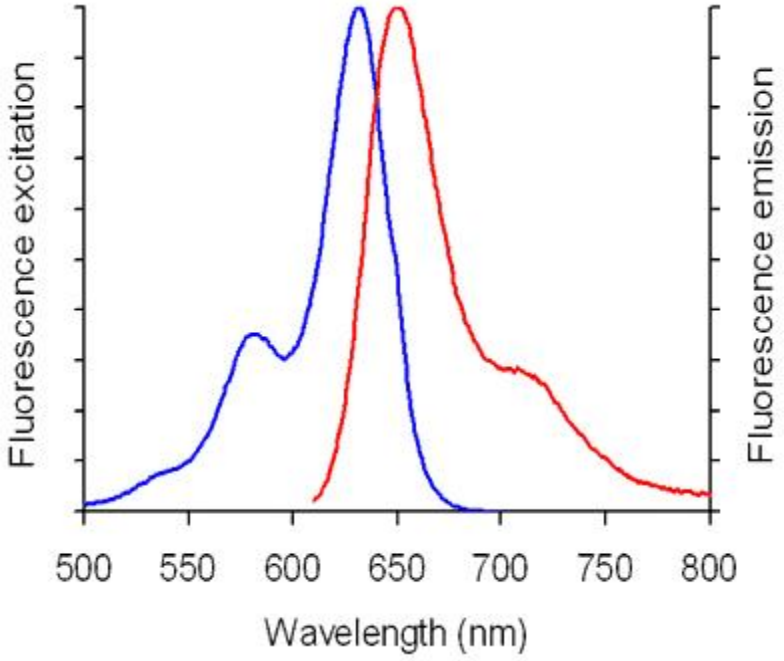

Figure 1.18: Excitation and emission spectra of Alexa 633. Excitation spectrum (blue), Emission spectrum (red).

Source: Molecular Probes specification sheet of Alexa 633 Hydrazide.

Specific staining of biological structures is often performed with the use of fluorescent antibody staining, through immunofluorescence. This process involves isolating specific antibodies from living animals that produce antibodies as part of their immune system. A primary antibody is designed to target a specific protein or structure. A fluorochrome is attached to the secondary antibody which binds with its conjugate antigen. Once this connection is made the fluorochrome can then be excited and the resulting fluorescence captured for image reconstruction. An example of such staining was performed by Iwasaki (2011) when studying the development of collagen type III in

the rat fetal tongue at different stages of embryonic development (Figure 1.19). Antigen-antibody binding is entirely dependent on noncovalent bonds and requires numerous bonds for stability. This binding is highly specific and therefore provides a sound basis for fluorescent markers. The two most common types of antibodies are monoclonal and polyclonal. Monoclonal antibodies are more specific for the target protein and provide low amounts of background fluorescence; however this high specificity often leads to lower signal strength. In contrast, polyclonal antibodies provide stronger signals but are also deemed less specific because the primary antibody recognizes and attaches to numerous sites on the target protein (Harlow and Lane, 1999). When an antibody attached to numerous sites, the likelihood that one of these sites occurs on a separate protein increases. These and other specific fluorescent stains have been extremely important in furthering the understanding of vascular development.

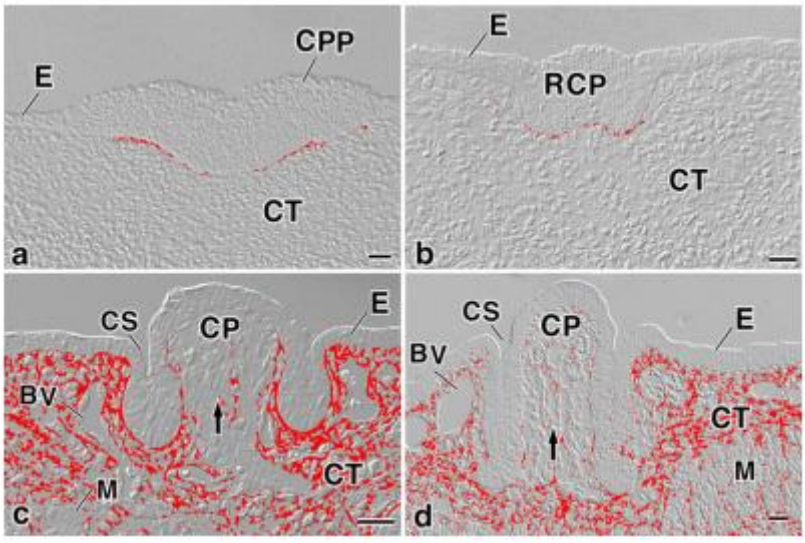

Figure 1.19: Immunofluorescence imaging of collagen type III in the tongue at different stages of embryonic development starting at embryonic day 13 (A) and progressing 2 days between image samples.

Source: (Iwasaki et al., 2011)

CHAPTER 2

HYPOTHESIS AND AIMS

The extracellular matrix (ECM) protein composition and organization are known to determine the mechanical properties of the arteriolar wall, particularly vascular stiffness and elasticity. These ECM proteins, including collagen, elastin, and glycoproteins, provide the vessel with mechanical support and physiological strength. A number of these proteins are also seen throughout multiple layers of the vascular wall, specifically elastin, collagen, and laminin. Support of the vascular wall comes in the form of longitudinal fibers in the adventitia, shorter, more branched fibers in the external elastic lamina, and a non-fibrillar sheet like structure in the internal elastic lamina.

These structural support ECM proteins have proven to be diverse as some have been shown to impact vascular function. For example, adventitial fibronectin is involved in sensing and relaying mechanical forces through the vessel wall in a process known as mechanotransduction. The signals span the membrane of smooth muscle cells (SMC) through proteins named integrins and ultimately result in vasoconstriction or dilation. These forces can also cause vasodilation through other ECM proteins, such as collagen, vitronectin, laminin, and fibronectin, which elicit SMC inhibitory responses from the endothelial cells. The SMCs in small arteries and arterioles possess the capability to autoregulate diameter in response changes in intraluminal pressure. This is a dominant property of small arteries and arterioles. Through mechanotransduction, fibronectin, collagen, laminin, and vitronectin are known to influence the myogenic response.

Elastin is an ECM protein that is known to provide the vessels with their elasticity in response to changes in length. This protein is a highly hydrophobic and cross-linked structure that is long lived and important to vascular viability. Elastic fibers are most commonly found in tissues that undergo repetitive lengthening like that of skeletal muscle and intestine (Butterfield and Herzog, 2005). This protein is known to be located in the adventitia, the nearby external elastic lamina, and the internal elastic lamina between the endothelial cells and vascular SMCs. Despite the importance of elastin, there exists little knowledge as to the 3D arrangement within the arteriolar wall. Further, how the vascular SMCs directly interact with this protein is uncertain. In preliminary studies, elastase treatment digested elastin fibers of arterioles from skeletal muscle resulting in the vessels showing significant lengthening. This lengthening was irreversible upon washout. Subsequent imaging showed a breakdown of longitudinal fibers exhibited in the adventitia of control vessels. This led to the ***hypothesis*** that adventitial elastin fibers are responsible for bearing longitudinal stress in blood vessels that would be exposed to longitudinal stretch. In order to test this hypothesis, the proposed studies ***aimed*** to:

- Determine staining patterns of 3 Alexa Hydrazides, nonspecific ECM dyes, with distinct emission spectra so as to determine the optimum dye for consistent elastin detection by fluorescence.
- Image the 3D structural properties of elastin in vessels from rat tissue known to be of different mechanical environments, specifically cremaster, cerebral, and the mesentery.
- Extend the imaging protocol to a pathological state of aging and see if any ECM or elastin variations exist.
- Begin to develop methods of quantification suited to describing characteristics of the arteriolar wall structure observed through the imaging approaches.

CHAPTER 3

MATERIALS AND METHODS

3.1 Isolated Vessel

For the majority of experiments described, male Sprague-Dawley rats weighing between 150-280 gms were used. A smaller group (n=5) of male Fischer 344 rats (333-465 gms) were also used. Prior to use, rats were housed in a temperature, humidity, and light controlled animal facility of the Dalton Cardiovascular Research Center with free access to standard rat chow and drinking water. All protocols were approved by the animal care and use committee of the University of Missouri, Columbia.

Rats were weighed on a balance and anesthetized with sodium pentobarbital (Nembutal, 100mg/kg), given by peritoneal injection using a sterile syringe and a 27 gauge needle. Rats were maintained in a warm environment until a surgical level of anesthesia was maintained. Appropriate levels of anesthesia were assessed by lack of response to foot/tail pinching and corneal reflexes. The cremaster muscle was surgically removed as described by Meininger *et al* (1987). Briefly, the hair was removed from the scrotum of the rat by shaving with an electric razor. The cremaster muscle was then removed when the testis was exposed by making an incision at the bottom of the scrotum. Connective tissue was removed from the testis and the cremaster muscle was identified. Arterioles were identified so as tissue removal could be done in the area with the lowest density of blood vessels. The cremaster muscle was slowly detached from the testis taking special care not to stretch the muscle and damage the tissue. During tissue

removal, the cremaster was periodically rinsed with cold saline (0.9%) solution. Once the tissue was removed, it was placed in a test tube containing refrigerated (-2°C) physiological salt solution (PSS), consisting of (in mM) 145 NaCl, 4.7 KCl, 2 $CaCl_2$, 1.0 $MgSO_4$, 1.2 NaH_2PO_4, 4.0 glucose, and 2.0 pyruvate.

The arterioles used in the current project were primarily isolated from rat cremaster, skeletal muscle tissue. Cremaster muscle tissue was used because isolation of the arterioles from the thin tissue is considerably easier than other skeletal muscle beds since the cremasteric arterioles are clearly visible when the tissue is transilluminated. First order arterioles (1A) are the largest of the arterioles and the main blood supply for the tissue. As branches form off the 1A, they become second order arterioles. This is shown in Figure 3.1. This branching and naming system continues until the terminal arterioles, from where the blood enters the capillaries.

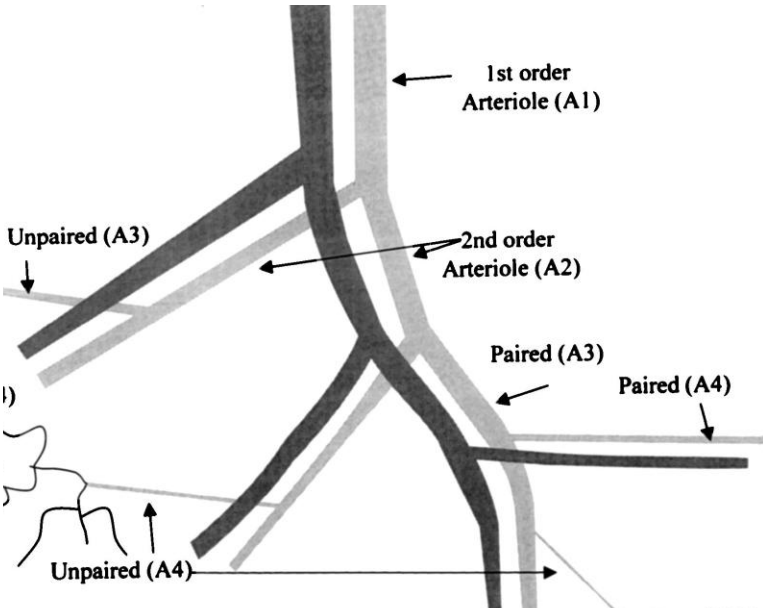

Figure 20: Example of cremaster tissue. Arterioles are the light colored blood vessels and are paired with the darker venules.

Source: (Hammer et al., 2001)

For microdissection of 1A segments, the muscle was spread out on a layer of silastic elastomer and pinned so the 1A (feed arteriole, as described in Chapter 1) was clearly visualized through a stereomicroscope (Olympus SZX12, Melville, NY). This dissection was completed in a vessel dissection chamber in the presence of vessel dissection buffer, which contained (in mM) 3.0 MOPS, 145 NaCl, 5.0 KCl, 2.5 $CaCl_2$, 1.0 $MgSO_4$, 1.0 NaH_2PO_4, 0.02 EDTA, 2.0 pyruvate, 5.0 glucose, and 1% albumin (endotoxin and fatty acid free) (Hill et al., 2000). The dissection chamber was maintained at a temperature of -5°C. Using ultra fine spring scissors and sharp forceps, segments in length of approximately 1-2 mm with no side branches were chosen for use in the studies (Meininger et al., 1991). These passive lengths were measured during previous elastase experiments (Clifford et al., 2009). Typical examples are shown in Figure 3.2. These segments were cleaned of surrounding tissue and isolated.

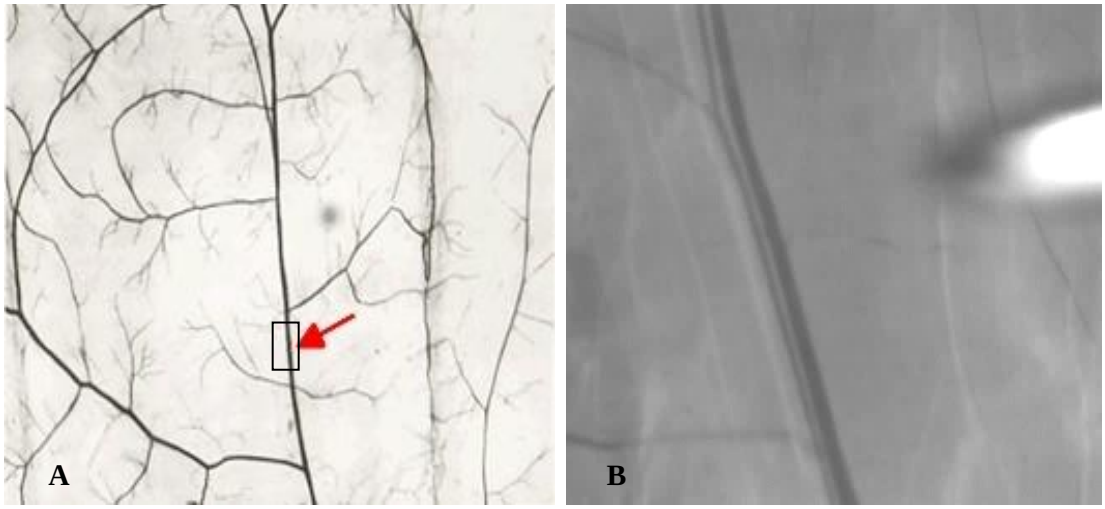

Figure 21: Pinned out segment of cremaster muscle (A) with enlarged image of suitable segment for isolation (B).

Mesenteric tissue was isolated after the cremaster muscle tissue was excised. Again, special care was used not to damage the tissue, which was also rinsed with cold

saline solution. Once removed the mesentery was placed in a separate test tube containing PSS. Microdissection of mesenteric third order arteries was performed under the same conditions as the cremaster arteriole isolation. These arteries were separated from connective tissue and prepared for cannulation (Sun et al., 1992).

Finally, a craniotomy was performed and the brain was removed from the rat. The brain was also placed in a test tube containing PSS. Small cerebral arteries were isolated in the presence of the same dissection buffer and the same conditions as cremasteric and mesenteric vessels. Branches of the posterior cerebral artery were isolated and prepared for cannulation (McCarron and Halpern, 1990).

3.2.1 Isolated Vessel Cannulation

The isolated segments were transferred to a chamber (model LS-CH-1-SH, Living Systems, St. Albans, VT) (Figure 3.3) filled with Krebs-bicarbonate buffer solution containing (in mM) 111 NaCl, 25.7 $NaHCO_3$, 4.9 KCl, 2.5 $CaCl_2$, 1.2 $MgSO_4$, 1.2 KH_2PO_4, 11.5 glucose, and 10 HEPES for cannulation (Hill et al., 2003). This buffer was titrated to 7.40 pH before use. Glass pipettes (tip diameter approximately 80 µm) were mounted in pipette holders of the cannulation chamber and attached by polyethylene tubing. The opposite end of the tubing was connected to a three way stopcock to allow for connection to a pressure reservoir. The tubing was filled with Krebs buffer containing 1% albumin. Careful observation was employed to avoid any air bubbles in the tubing and pipettes since an air bubble passing through the vessel would severely damage the endothelial layer. Each side of the isolated segments was then cannulated

onto the glass pipettes and secured with nylon mono-filament sutures (11-0, Alcon, Ft. Worth, TX) (Figure 3.4). Once the first end was secured, the vessel was gently flushed with the Krebs buffer containing 1% albumin.

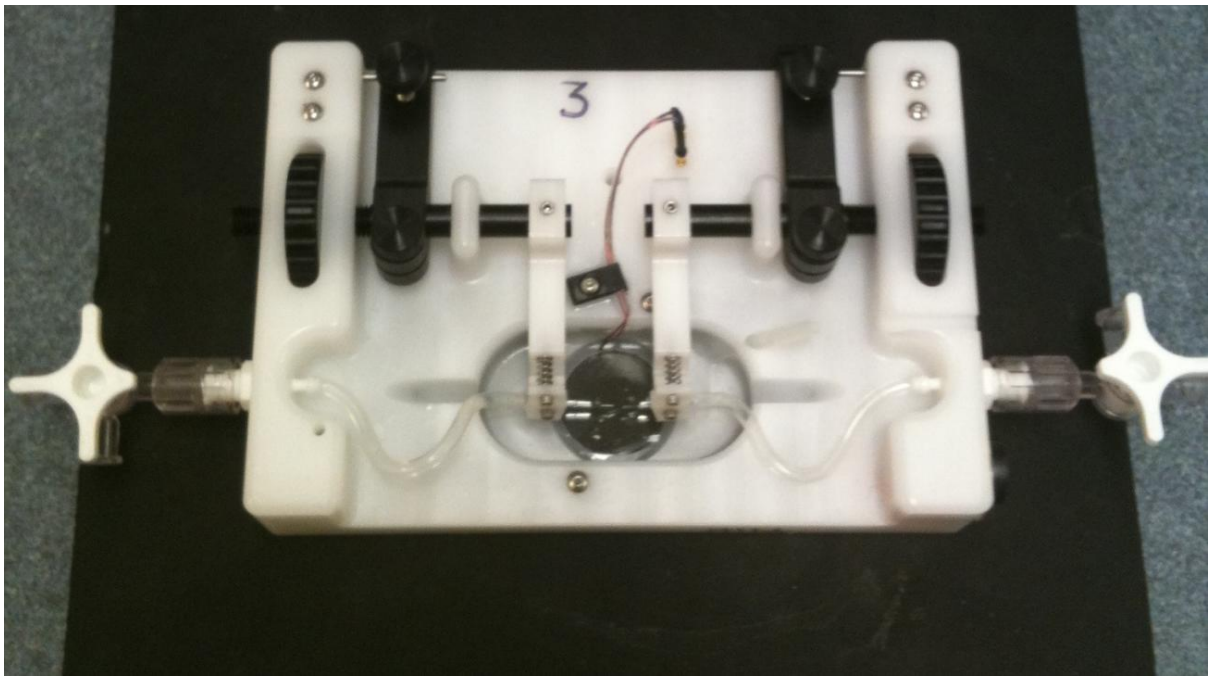

Figure 22: Chamber used for cannulation of freshly isolated arterioles. Glass pipettes were carefully leveled slightly above the glass coverslip.

Figure 23: Isolated vessel with each side cannulated and secured on glass pipettes.

3.2.2 Manufacture of Glass Pipettes

Six inch borosilicate glass capillaries (Harvard Apparatus, GC12OT-15, with an internal and external diameter of 0.94 mm and 1.2 mm, respectively) were pulled to a fine tip using a Sachs-Flaming Micropipette puller (Model # PC-84) (Figure 3.5). The program used to pull the pipettes for cannulation was looped 17 times, with each cycle providing heat, pull, and subsequent cooling.

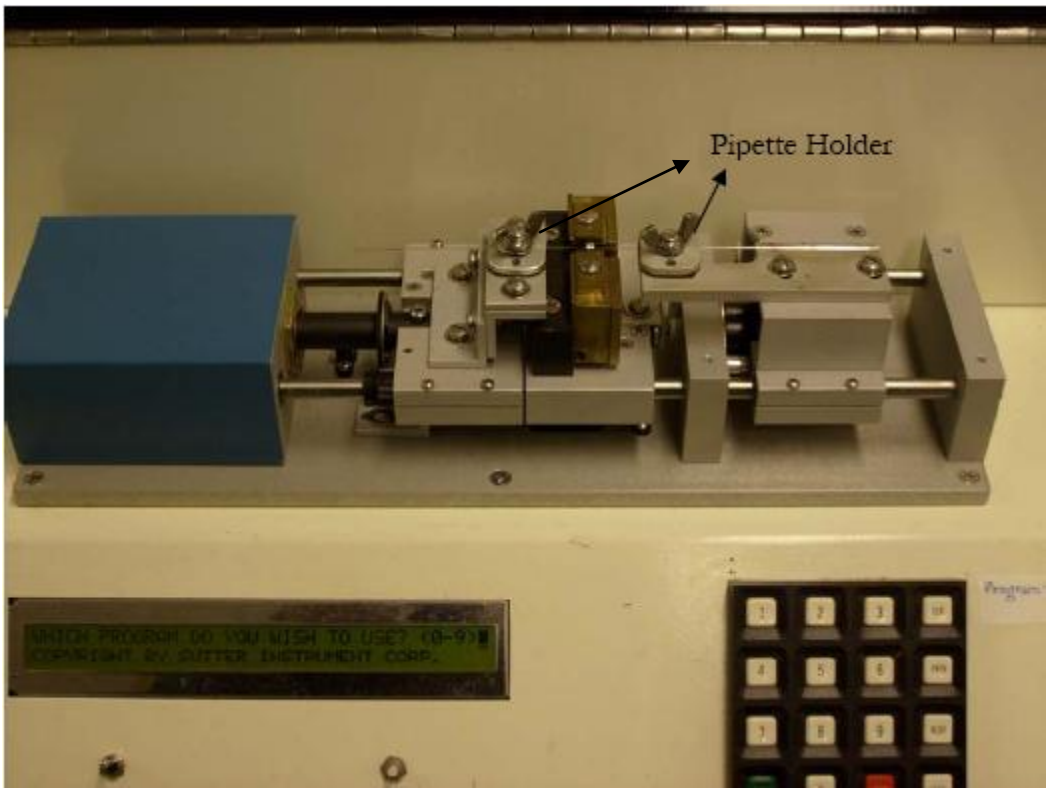

Figure 24: Sachs-Flaming Micropipette puller used to heat, pull, and cool pipettes for cannulation.

The pipette was placed in the chuck of a microforge (Stoetling Inc.) (Figure 3.6). The pipette was then heated to form a hook, to which a light weight was added. When heat was further added, the weight assisted in drawing out the tip of the pipette to the appropriate diameter until the weight broke off the hook of the pipette. The broken end was fire polished so as to not damage the vessel during cannulation.

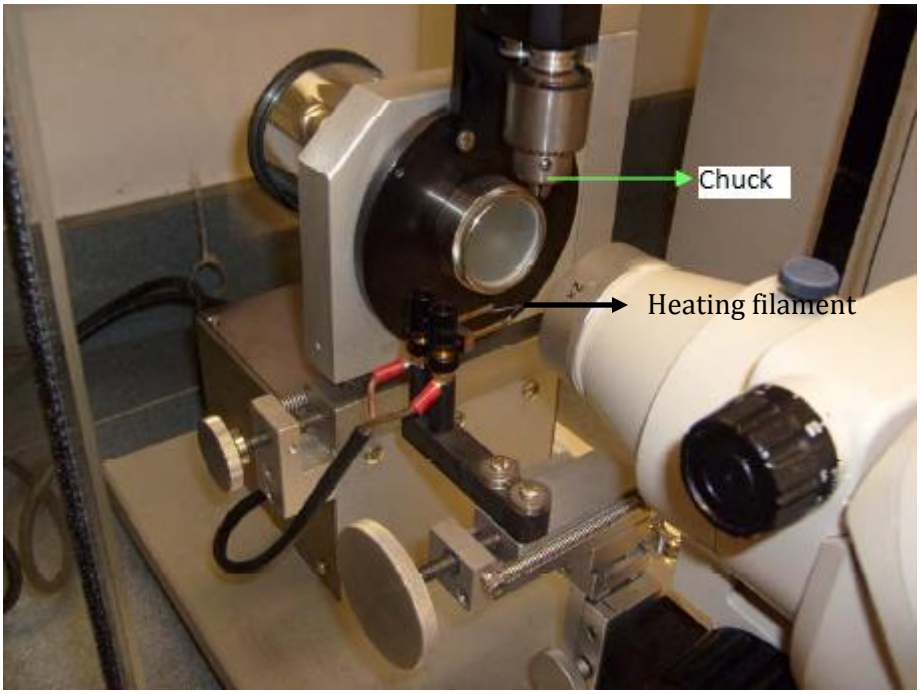

Figure 25: Stoelting microforge used for manipulating the tip of the micropipette. The chuck holds the micropipette and heating filament is used for fire polishing the tip.

3.3 Measurement of Internal Diameter and Development of Myogenic Tone

Once cannulated, the vessel chamber was transferred to an inverted microscope (model IX71, Olympus) coupled to a video camera (model TMC-7DSP, Pulnix, Glostrup, Denmark), electronic video caliper (Texas A&M, College Station, TX), and a data acquisition system (Powerlab, AD Instruments, Colorado Springs, CO), which allowed for continuous measurement of internal diameter. One side of isolated vessel was connected to a pressure reservoir, whose height could be adjusted to provide a hydrostatic pressure between 10 and 120 mmHg. The pressure reservoir was calibrated by measurement of height (in cm) with water. This configuration allowed for studies of the vessel under pressure but in the absence of flow. The pressure provided by the fluid

column was continuously monitored and recorded using a pressure transducer in parallel with output to the vessel. The vessel was checked for leaks at 40, 70, 100, and 120 mmHg and the vessel was stretched to eliminate any bowing of the vessel at each pressure (Hill et al., 2000). If a leak was observed, the chamber was removed and the branch would either be tied off with another suture or the segment of the vessel containing the leak would be tied to the glass pipette beyond the leak. After the vessel was rechecked for leaks, the bath was continuously superfused (approximately 2-4 ml/min) with Krebs buffer by use of a peristaltic pump (model Sci-Q 400, Watson Marlow, Wilmington, MA). For cremaster arterioles, intraluminal pressure was set to 70 mmHg and temperature in the bath was maintained at 34°C using an internal thermistor temperature sensor, which was connected to an external temperature controller (Hill et al., 1990). A suction tube was attached at the top of the bath to prevent overflow, which completed the superfusion circuit. Once the conditions were established, myogenic tone would generally spontaneously develop over the next 30-60 minutes. Any vessels not holding pressure or not gaining tone were discarded from experimentation.

All vessels exhibited myogenic tone, as demonstrated by a constriction of the arteriolar segment by 30-50% of the passive diameter and a constriction in response to a pressure step from 50-100 mmHg. Measurement of the internal diameter was monitored via electronic video calipers as described above. The calipers provided a set of lines on the video monitor for recording the internal diameter. The Powerlab Analog-Digital converter continuously sent measurements of diameter from the calipers and pressure from the pressure transducer to software, CHART 6.1, on the according computer. These values were recorded and saved for later analysis. Establishment of myogenic tone

confirmed that the dissection and cannulation techniques were performed without damaging the vessel or the SMCs. Imaging experiments would only use vessels fixed under passive conditions, however dissection and cannulation procedures had to be established that produced arterioles of physiological relevance.

3.4 3D Confocal Imaging Protocol and Vessel Reconstruction

In order to further understand the distribution/arrangement of elastin within the ECM of the arteriolar wall, 3D confocal microscopy was employed. All imaging presented below was performed on passive, fixed arterioles. Staining of ECM, cell nuclei, and specific proteins was needed before imaging. The pressurized (70 mmHg) arterioles were fixed (4% paraformaldyhe) for 20 minutes. Three separate Alexa Hydrazide dyes were tested for staining of the ECM: Alexa 350 Hydrazide (50 μM, Ex 350/Em 450 nm), Alexa 488 Hydrazide (10 μM, Ex 488/Em 550 nm), and Alexa 633 Hydrazide (0.2 μM, Ex 633/Em 700 nm). Alexa dyes were diluted in Krebs buffer. Each Alexa dye loading required 30 minutes incubation time. Two cell nuclei stains were used: 4'6-diamino-2-Phenylindol (DAPI, 500 ng/ml, Ex 350/Em 400-450nm), and Yo-Pro-1 iodide (1 μL/ml, Ex 491/Em 515 nm). Cell nuclei stains were diluted in Krebs buffer as well. Incubation time for each cell nuclei stain was 20 minutes. All Alexa and cell nuclei dyes were loaded at room temperature while maintained at 70 mmHg. Anti-elastin antibodies were required for imaging of specific elastin staining (1° antibody dilution- 1 mg/ml, 1:100; 2° antibody dilution- 2 mg/ml, 1:200 Ex 491/Em 515). Elastin primary and appropriate secondary antibodies were diluted in Krebs buffer containing 1%

albumin as a blocking agent for prevention of nonspecific labeling. The primary antibody required overnight abluminal loading (12-14 hours) at 4°C, while the secondary antibody was abluminally loaded, under 70 mmHg intraluminal pressure, the day of experimentation for 60 minutes at room temperature. An elastin antibody imaging experiment was performed in the absence of the primary and minimal, nonspecific staining was observed (Figure 5.17D.)

3D confocal microscopy was utilized in order to visualize the ECM of the arteriolar wall in conjunction with cellular location and elastin proteins. This imaging was performed using a Leica TCS-SP5 microscope with a Leica water immersion 63x objective lens (NA=1.2). Data acquisition was collected using Leica LAS AF software. Collection rate was 400 Hz. Image dimensions were 246 µm x 246 µm. Resolution was set at 8 bits. The z dimension step size was 0.3 µm for all z-stacks. A line average of 3 was used to reduce low frequency noise. All acquisitions represent 8-bit TIFF grey scale images.

Alexa 350 was excited by 700 nm light from a multiphoton laser and blue emission was collected from 400-450 nm with a gain of approximately 925. Alexa 488 was excited by an argon laser set to 488 nm while green emission was collected from 500-550 nm with an average gain of 748. Alexa 633 was excited at 633 nm from a HeNe 633 laser. Red emission was collected from 650-750 nm and used an average gain of 645. Laser powers were measured for quantum efficiency analysis using a photodiode power sensor (model S130A, ThorLabs, Newton, NJ).

Post image acquisition analysis and 3D reconstruction was performed using Image J (NIH, Bethesda, MD). Data were recorded as individual channels of dye

fluorescence in the form of image stacks. A composite stack containing all appropriate channels was created. Data quantification was performed using Imaris 7.2.3 (Bitplane, Switzerland). The ECM and EEL proteins were isolated from the IEL using a region of interest the size 123 µm x 123 µm. This region of interest included the entirety of the ECM and EEL down to the final slice before any fluorescence by the IEL. The z depth for the ECM and EEL varied between experiments due to the diameter of the vessel being examined. Measurements of length of fiber between branch points, fiber diameter, fiber straightness (a measure of linearity of each fiber), and number of branch points were calculated in the Imaris software. IEL measurements were also calculated using a consistent region of interest, 62 µm x 123 µm. The z depth of the IEL varied slightly between vessels but was in the range of 0.3-4µm. This ensured that the region studied was flat and curvature of the vessel would not impact measurements. The number and size of the fenestra were measured from the Imaris software as a collection of the individual areas showing no fluorescence.

3.5 Chemicals and Reagents

All Alexa Hydrazides, Yo-Pro-1 Iodide, and DAPI were obtained from Molecular Probes. Anti-elastin primary antibody was obtained from Chemicon International (Millipore, Billerica, MA), while the secondary elastin antibody was obtained from Molecular Probes (InVitrogen, Carlsbad, CA).

3.6 Statistical Analysis

Results are expressed as means ±S.E.M. and n denotes the number of animals used for each experiment. Differences in vessel properties such as diameter, fiber straightness, number of fiber branches, and IEL characteristics from different tissue environments were tested with a one-way analysis of variance (ANOVA). An ANOVA test was chosen because there were comparisons between multiple groups. A Bonferroni post-hoc test was used to compare individual values within groups. Specific two means comparisons were analyzed with Student's *t* test. A value of $P<0.05$ was considered significant.

CHAPTER 4

VESSEL RESPONSIVENESS

Although the isolated arterioles used for imaging were studied in the passive state, a reproducible dissection and cannulation protocol was first confirmed before any imaging studies were undertaken. This approach was taken to assure consistency of technique and used myogenic tone and agonist responsiveness as indicators of viable preparations. Thus, the dissection and cannulation techniques were considered successful if vessel gained myogenic tone as described above with a requirement for development of vessel constriction of 30-50% and completion of a successful myogenic constriction in response to a pressure step from 50 mmHg to 100 mmHg, as demonstrated in Figure 4.1 (n=5). Each step was held for a duration of 5 minutes. Acetylcholine (ACh) and phenylephrine (PE) dose response experiments (Figure 4.2) were performed following a successful constriction response to the pressure step. The vessel bath was given a thorough wash and pressure was held at 70 mmHg. PE and ACh doses were 1 nM, 3 nM, 10 nM, 30 nM, 100 nM, 300 nM, 1 µM, 3 µM, and 10 µM. Internal diameter was measured for 3 minutes at each concentration. Successful concentration-dependent responses for both drugs were considered to start with a passive period with little change in diameter, followed quickly by a significant change in diameter, and finally approaching a plateau as the vessel had reached the maximum steady state response. Once these characteristics were reproducible on a daily basis, the dissection and cannulation techniques were accepted as providing a preparation that was both viable and in a physiological state suitable for subsequent imaging studies.

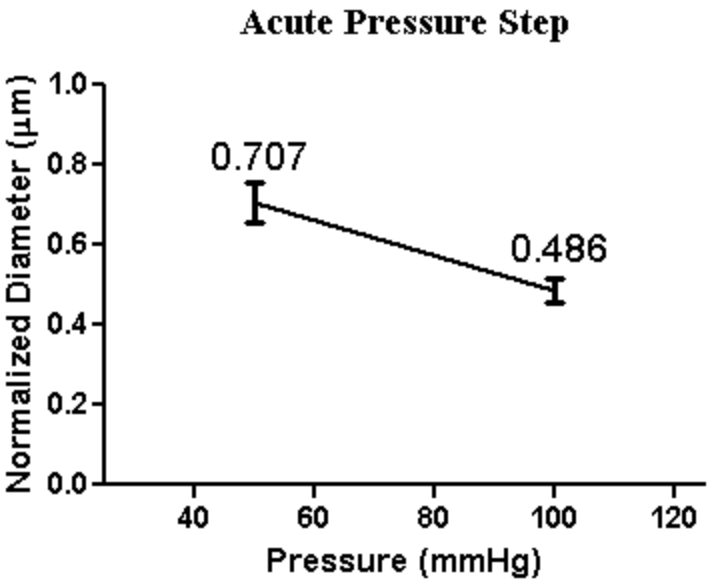

Figure 26: Group data showing the response to an acute pressure step from 50-100 mmHg. Diameters are normalized to passive diameter at 70 mmHg. Data are shown as mean ±S.E.M, n=5.

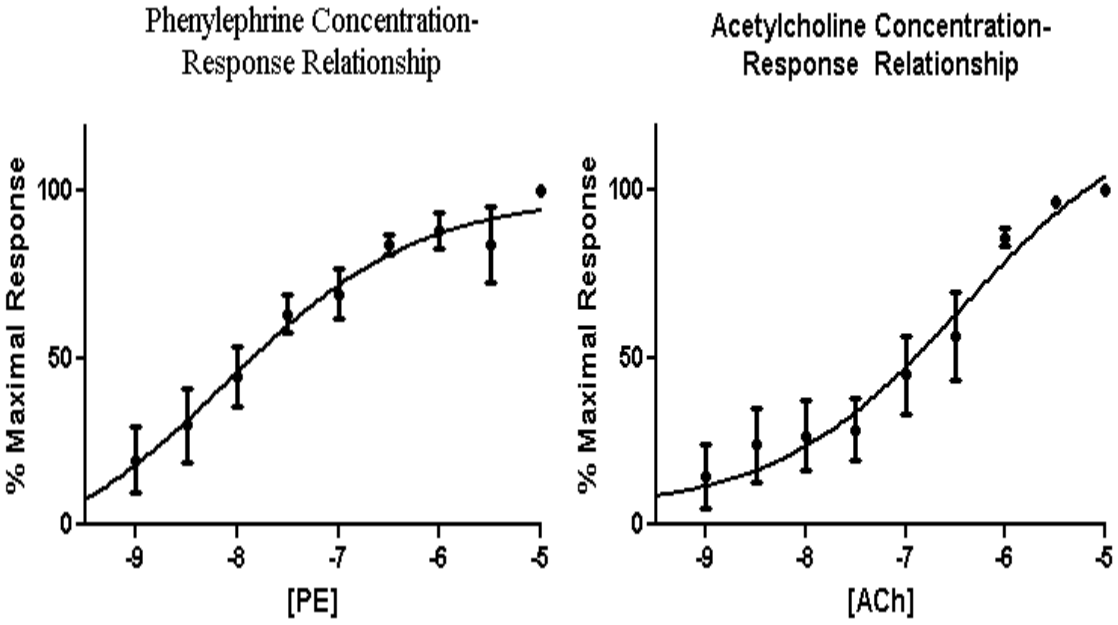

Figure 27: Phenylephrine and acetylcholine concentration response curve. Concentrations range from 1 nM to 10 µM. Data are shown as mean ±S.E.M, n=5.

CHAPTER 5

RESULTS

5.1 Staining Characteristics of Available Alexa Hydrazides

With a number of Alexa dyes being available, initial studies centered on identifying a suitable candidate for imaging the ECM distribution of isolated arterioles. Three Alexa Hydrazides, with distinct excitation (Figure 5.1) and emission (Figure 5.2) spectra were selected. The staining patterns of each were compared, as well as any possible impact the dyes would have on the stain distribution when loaded together. The three individual Alexa dyes were tested on sets of arterioles taken from the same rats (n=3), while the images containing all three Alexa dyes were collected on arterioles from different rats (n=4).

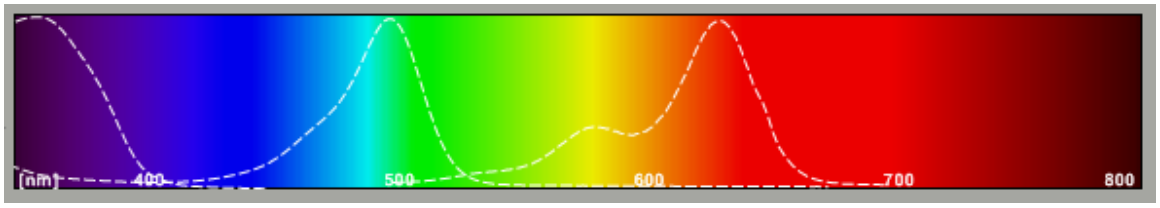

Figure 28: Excitation spectra of the three Alexa dyes.

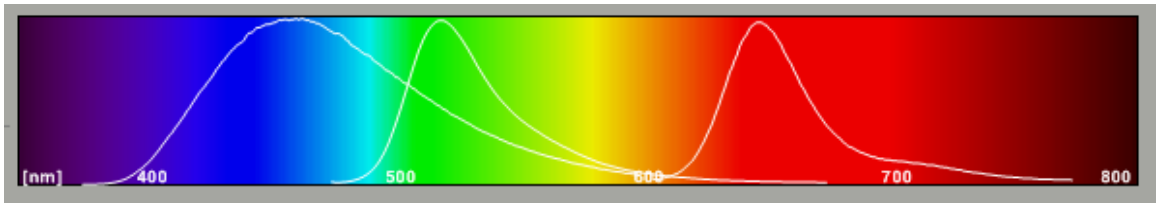

Figure 29: Emission spectra of the three Alexa dyes. The fluorescence of each dye is given: Alexa 350 (blue), Alexa 488 (green), and Alexa 633 (red).

Source: Figures 5.1 and 5.2 were taken from the computer that image acquisition was performed on.

Normalized quantum efficiencies, which is the amount of fluorescence divided by the energy input, are included in Table 5.1. Intensities from individual experiments with Alexa dyes were averaged over the entire collection stack. The laser power, as measured by the photodiode sensor, and average gain of the three Alexa dyes used for the entire collection stack was calculated. The fluorescence divided by the laser power and gain produced quantum yield. The dye with the largest quantum yield, Alexa 633, was normalized to 1.0. All quantum yields for the remaining two dyes were compared to this value of 1.0. The dye with the highest quantum efficiency is least likely to be affected by photobleaching. The size of the entire collection stack and depths of ECM, EEL, and IEL for each Alexa dye are also detailed in Table 5.1.

Table 5.1: Quantum yield of the Alexa dyes and properties of image stacks collected from rat cremasteric 1A.

	Alexa 350 (n=3)	**Alexa 488** (n=3)	**Alexa 633** (n=3)	**All Alexas** (n=4)
Normalized Quantum Efficiency	**0.1964**	**0.2975**	**1.0**	**-**
Entire Stack Size (µm)- (Fig 30)	**43.3**	**47.7**	**52**	**85.6**
ECM Stack Depth (µm)- (Fig 31)	**7**	**8.6**	**9**	**9**
EEL Stack Depth (µm)- (Fig 32)	**2.6**	**3.3**	**4**	**3**
IEL Stack Depth (µm)- (Fig 33)	**7**	**4.3**	**5.3**	**7.6**

All dyes appeared to stain the ECM, EEL, and IEL as shown below. Figure 5.3 is a composite image over the entire data range of A) Alexa 350, B) Alexa 488, C) Alexa 633, and D) the three Alexa dyes combined. Collection started outside the adventitial layer and ended midway through the lumen. When all Alexa dyes were loaded together

in the same arteriole, significant of colocalization was seen throughout the vessel. Detailed image collection parameters are provided in the Methods and Materials. Briefly, all images were collected as 246x246 μm^2 areas by a 63x water immersion objective.

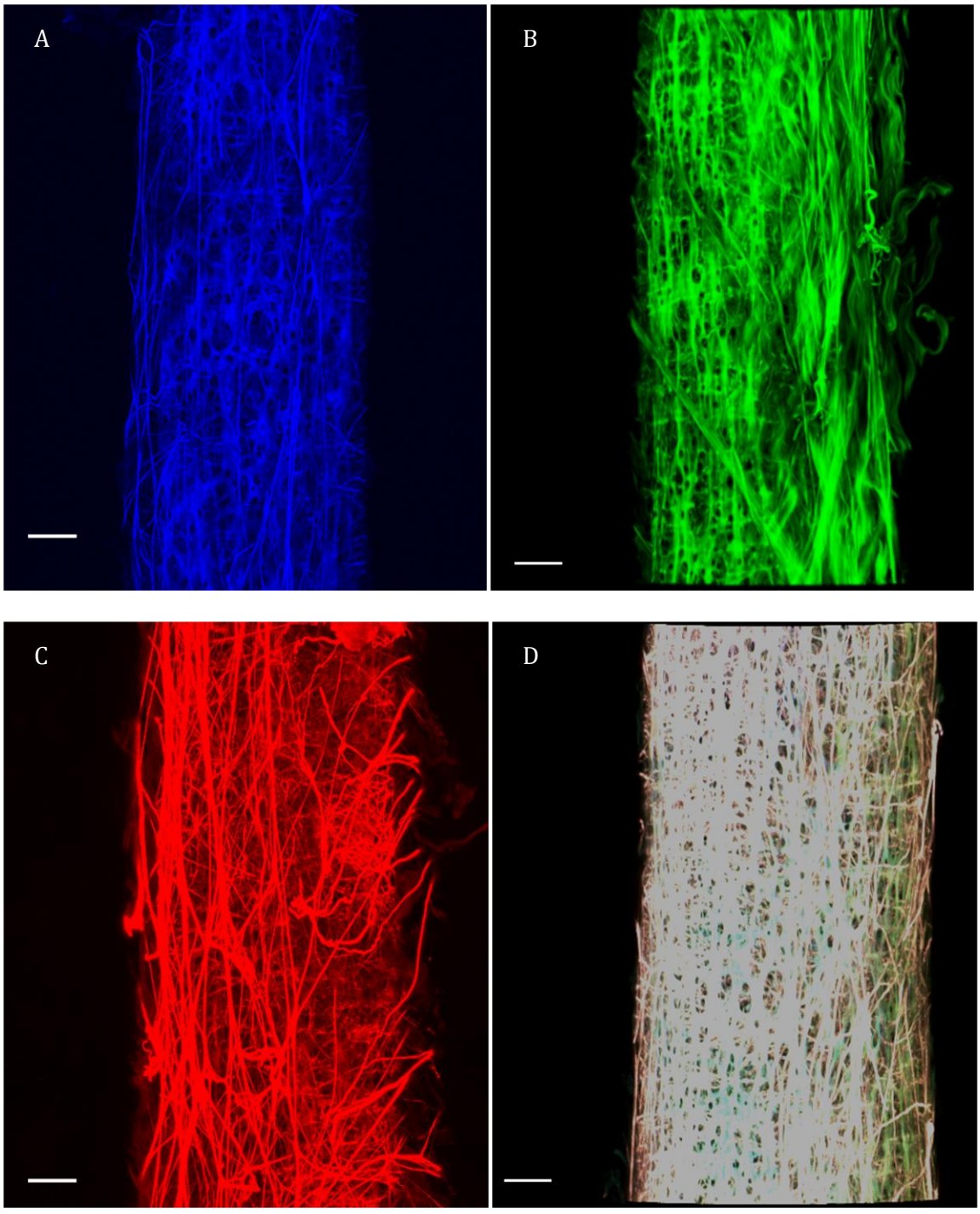

Figure 30: Alexa dye staining in cannulated cremaster 1A vessel segments. A) Alexa 350 (blue), B) Alexa 488 (green), C) Alexa 633 (red) D) All Alexa dyes. Scale bar= 25 µm.

Staining of the ECM proteins was the primary objective for testing the Alexa dyes. When imaged in cremasteric 1A, each dye showed staining of the ECM. Located particularly in the adventitia, the ECM is the most distal section from the lumen. This Alexa staining of ECM fibers is highlighted in Figure 5.4. Each image was optically sectioned from the first appearance of ECM fluorescence until the first image showing EEL. Alexa 350 (Figure 5.4A) and 633 (Figure 5.4C) both showed fluorescence of individual fibers varying in length from as little as 20 µm to longitudinal fibers that spanned the entire length of image collection (246 µm). The longitudinal fibers were oriented in the direction of blood flow. Alexa 488 (Figure 5.4B) stained fewer individual fibers, but bundles of fluorescence were observed that appeared to be weaved through one another and oriented in the direction of blood flow as well. Considerable colocalization was detected in the arteriole treated with all Alexa dyes together (Figure 5.4D). As shown, each Alexa dye provided staining consistent with where ECM proteins are believed to be located.

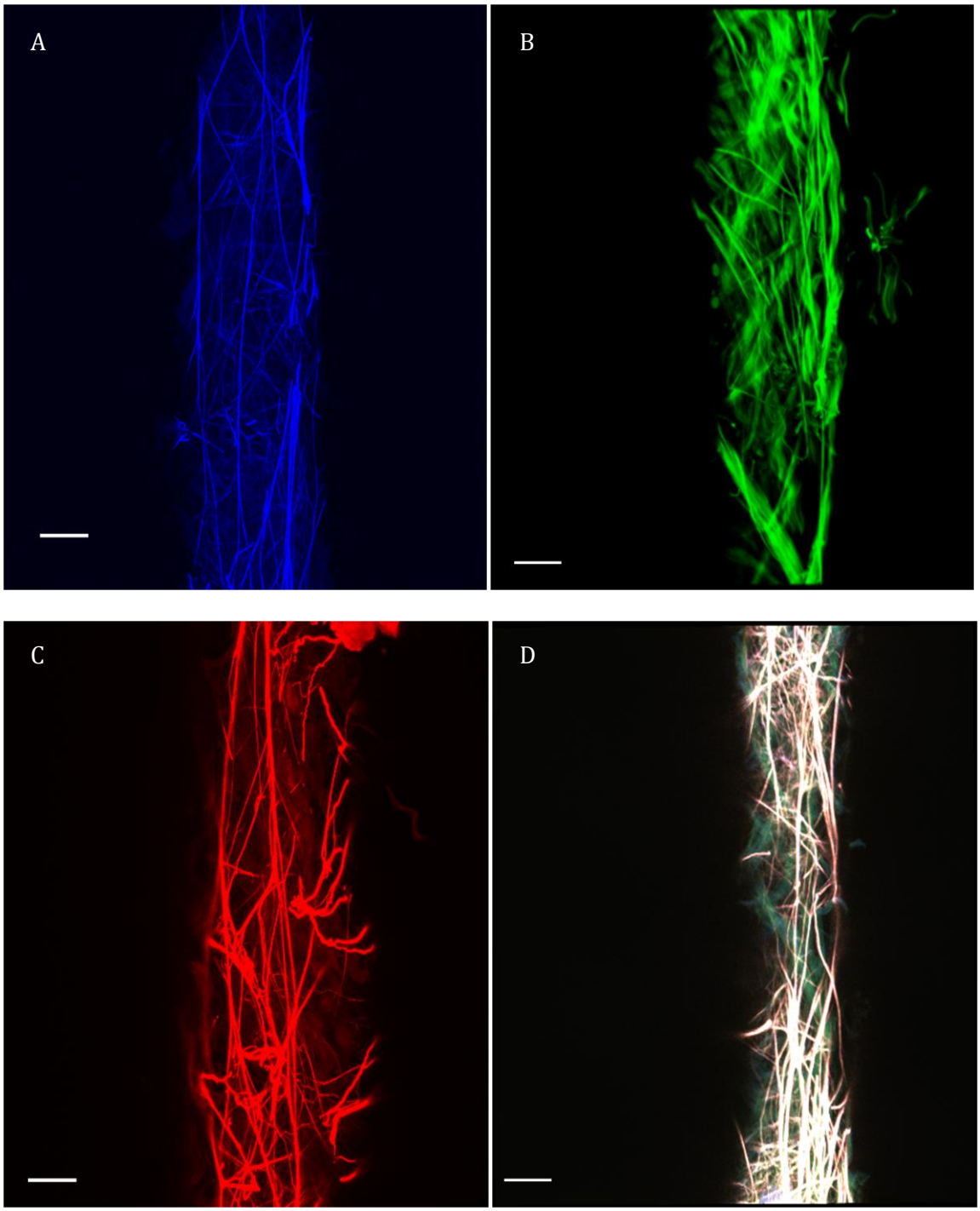

Figure 31: Alexa dye staining of the ECM from cremaster 1A. A) Alexa 350 B) Alexa 488 C) Alexa 633 D) Simultaneous loading of all three Alexas. Scale bar= 25 µm.

The EEL layer separating the ECM from the SMCs is also believed to be composed of proteins found in the ECM. This was confirmed by Alexa staining (Figure 5.5). Each Alexa dye stained fibers in the EEL. Staining with Alexa 350 (Figure 5.5A) did not show as many fibers as part of the EEL, when compared to the other Alexa dyes. Alexa 488 (Figure 5.5B) showed staining of short fibers as well as bundles of fibers, on the right side, that were seen as part of the ECM. With uneven amounts of ECM fibers on both sides of the EEL it appeared easy to mistake the precise position of the vessel lumen. Therefore a yellow box has been used to highlight the center of the vessel. Alexa 633 showed a vast array of fibers (Figure 5.5C), which were mostly shorter than fibers in the ECM (Figure 5.4C). Again, colocalization between the three dyes were seen when all dyes were loaded together (Figure 5.5D).

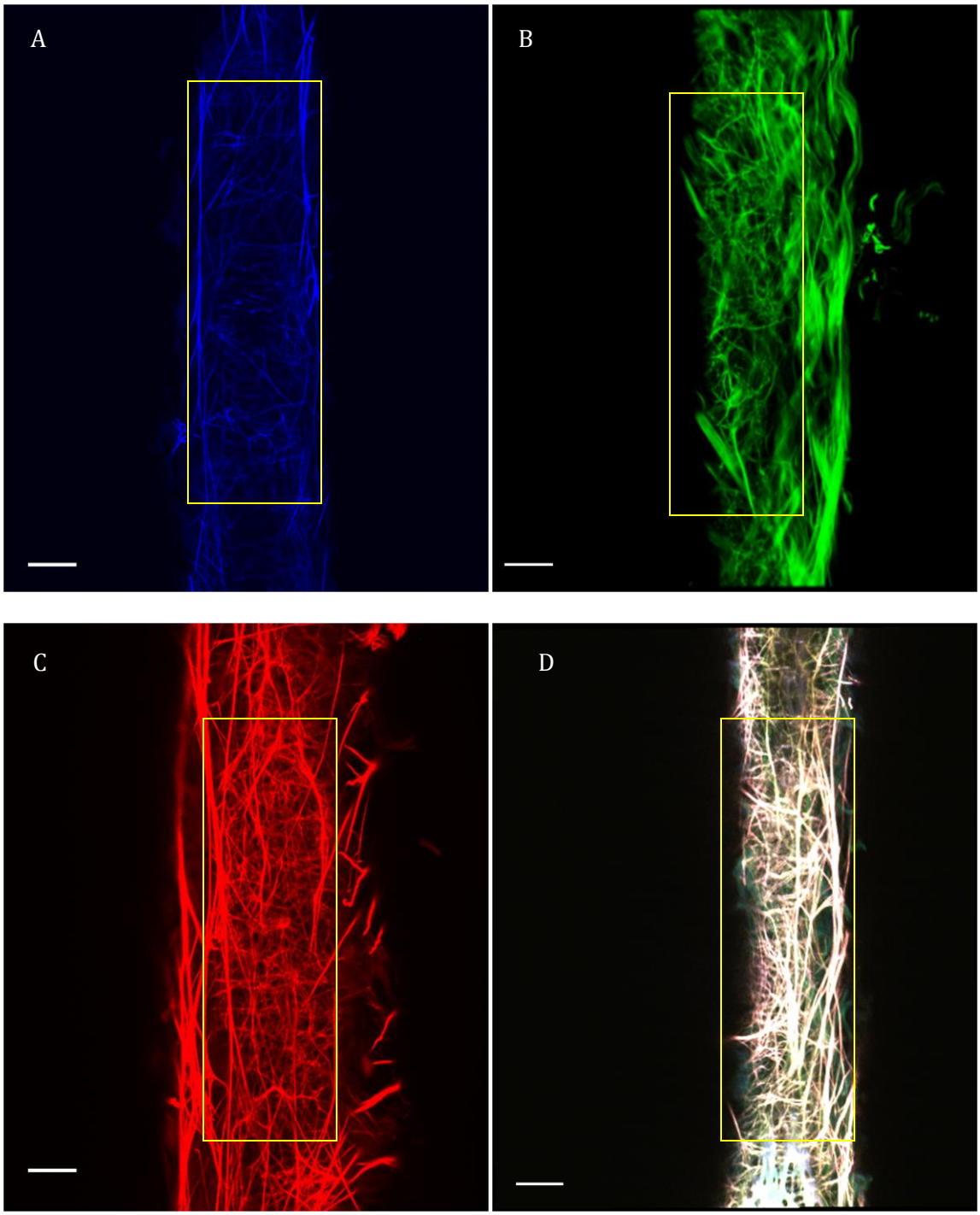

Figure 32: Alexa dye staining of the EEL from cremaster 1A. A) Alexa 350, B) Alexa 488, C) Alexa 633, D) Simultaneous loading of all three Alexas. The yellow box highlights the center of the vessel. Scale bar= 25 µm.

The IEL as a layer was also stained with each Alexa dye (Figure 5.6). The IEL separates the endothelial cells from the SMCs. The size of fenestra varies throughout this layer. There was little apparent variation in the staining patterns between the three Alexa dyes. Fluorescence was observed throughout the IEL, except in the areas of the fenestrae.

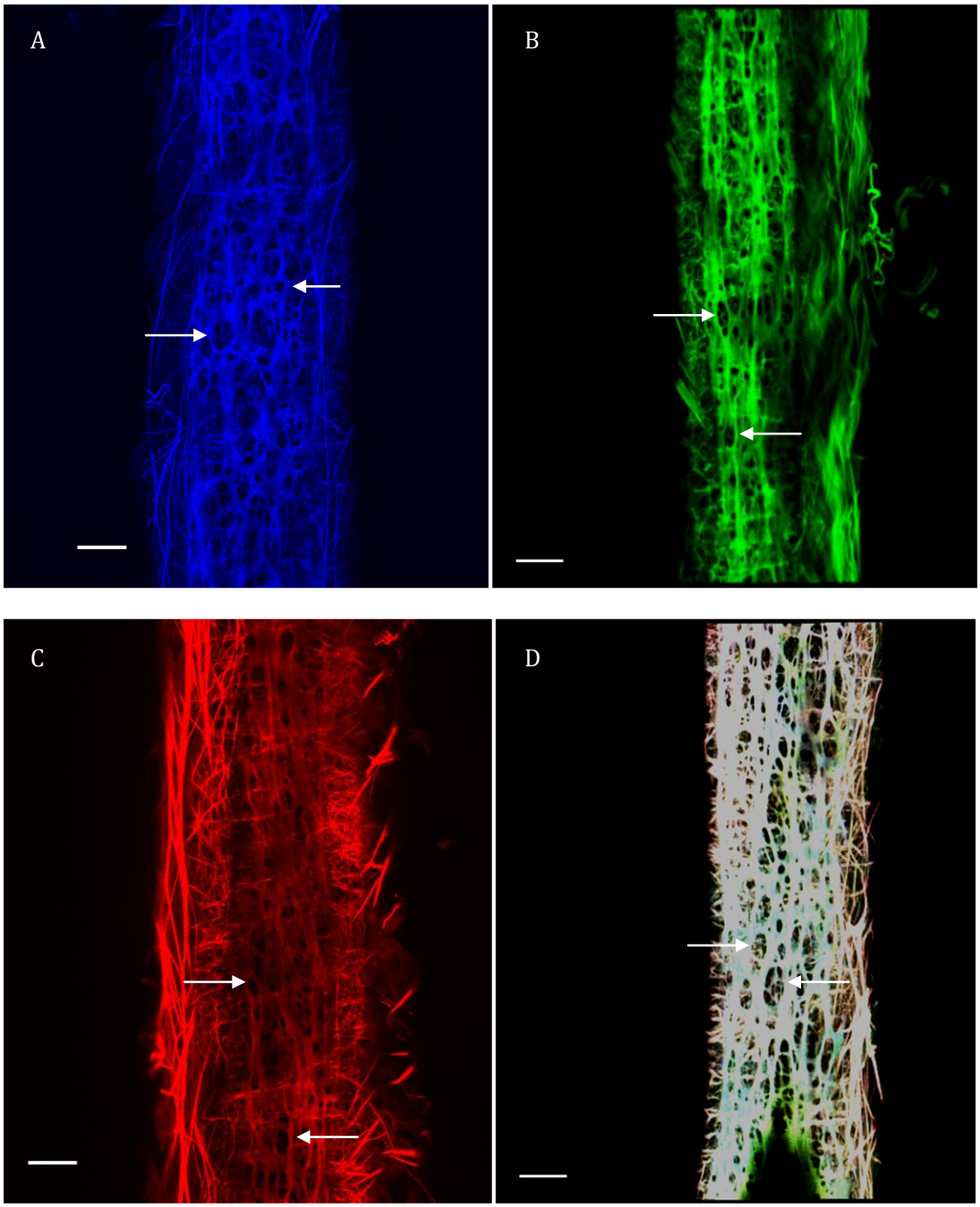

Figure 33: Alexa dye staining of the IEL from cremaster 1A. A) Alexa 350 B) Alexa 488 C) Alexa 633 D) Simultaneous loading of all three Alexas. Arrows indicate fenestrae in IEL. Scale bar= 25 µm.

5.2 Fluorescence Imaging of the Vessel Wall Using Cremaster Muscle, Cerebral, and Mesenteric Vasculatures

Once Alexa 633 Hydrazide was selected as the most efficient dye for imaging ECM content, 3D confocal imaging of arterioles and small arteries from cremaster, cerebral, and mesentery was performed. Since elastin is an important factor in the context of vessel stretch, elastin content in arteries from these tissue beds were imaged because of their differences in mechanical environment. Vessels from each tissue bed were stained and imaged with Alexa 633 Hydrazide and the nuclear stain Yo-Pro Iodide (Figures 5.7, 5.10, and 5.12). All vessel images are oriented vertically, in the same direction as blood flow. A summary of the fiber length, diameter, straightness, and branch points as well as fenestra area and density is provided in Table 5.2. Cremasteric 1A were initially imaged (Video 5.1). Figure 5.7A is a composite of all images collected as viewed from the lumen. Significant staining was recorded from long, thick fibers in the ECM that were oriented in the direction of blood flow, but there were also shorter fibers running obliquely around the arteriole (Figure 5.7B). Fluorescence in the IEL shows the sheet like fenestrated structure (Figure 5.7C). The EEL and IEL make up a double elastic wall in the arteriole (Figure 5.7D). Measurements of the length taken from all fibers outside the IEL showed that the greatest number of fibers were of distance less than 1 μm between branch points (Figure 5.8). The number of fibers distributed between 1-2 μm was also significantly higher than the remaining fibers. A distribution of the area of the fenestra in the cremaster arteriole (Figure 5.9) was constructed. Fenestra areas in the cremaster ranged from less than 1 μm^2 to as large as 260 μm^2. As calculated through an automated detection software, the only distribution with a statistically significant

difference from the one that followed was the total number of fenestra between 10-20 μm^2.

Cremaster- Alexa 633 and Yo-Pro.mpg

Video 5.1: Image stack of cremaster arteriole stained with Alexa 633 (elastin, red) and Yo-Pro (cell nuclei, green).

Table 5.2: Fiber and fenestra characteristics from rat cremaster, cerebral, and mesentery.. * $p<0.05$ when compared to mesenteric artery. Adventitial fibers were absent in the cerebral arteries. Differences in fiber diameter, straightness, length between branch points, and number of branch points were calculated by student t test. Fenestra area and density were calculated by ANOVA.

	Cremaster	**Cerebral**	**Mesentery**
Fiber Diameter (μm)	**1.07*±0.08**	**-**	**0.87±0.04**
Fiber Straightness	**0.94±0.004**	**-**	**0.95±0.01**
Length Between Branch Points (μm)	**2.03±0.25**	**-**	**1.60±0.32**
Number of Branch Points	**1454*±500**	**-**	**10003±5877**
Fenestra Area (μm^2)	**40.63±5.71**	**31.22±4.81**	**21.29±2.55**
Fenestra Density (number/ 123*62 μm^2)	**43.8±3.57**	**30.80±7.51**	**37.4±7.39**

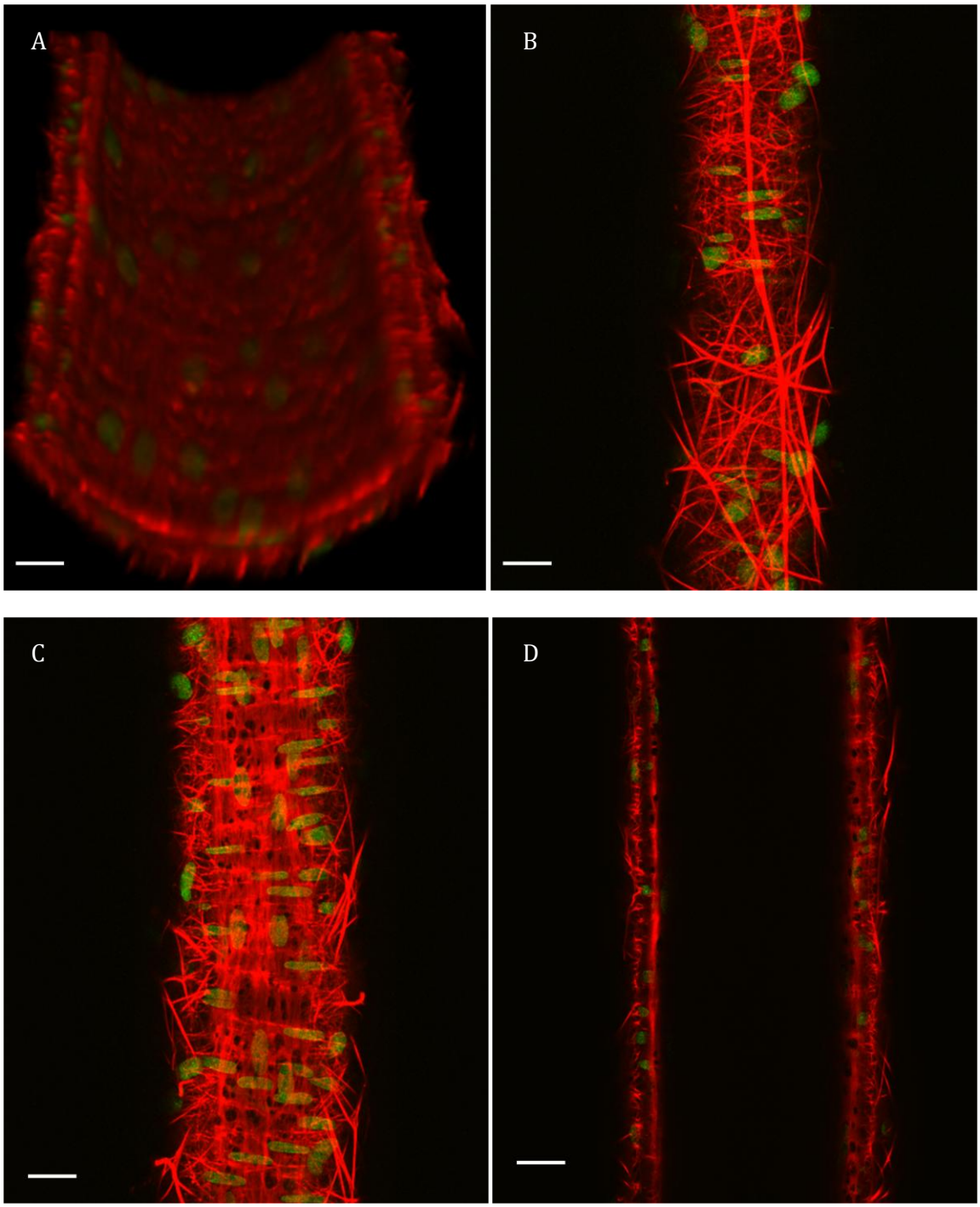

Figure 34: Cremaster 1A stained with Alexa 633 Hydrazide (red) and Yo-Pro Iodide (green). A) Whole vessel view from lumen, B) ECM, C) IEL, D) Double elastic wall. Scale bar= 25 µm.

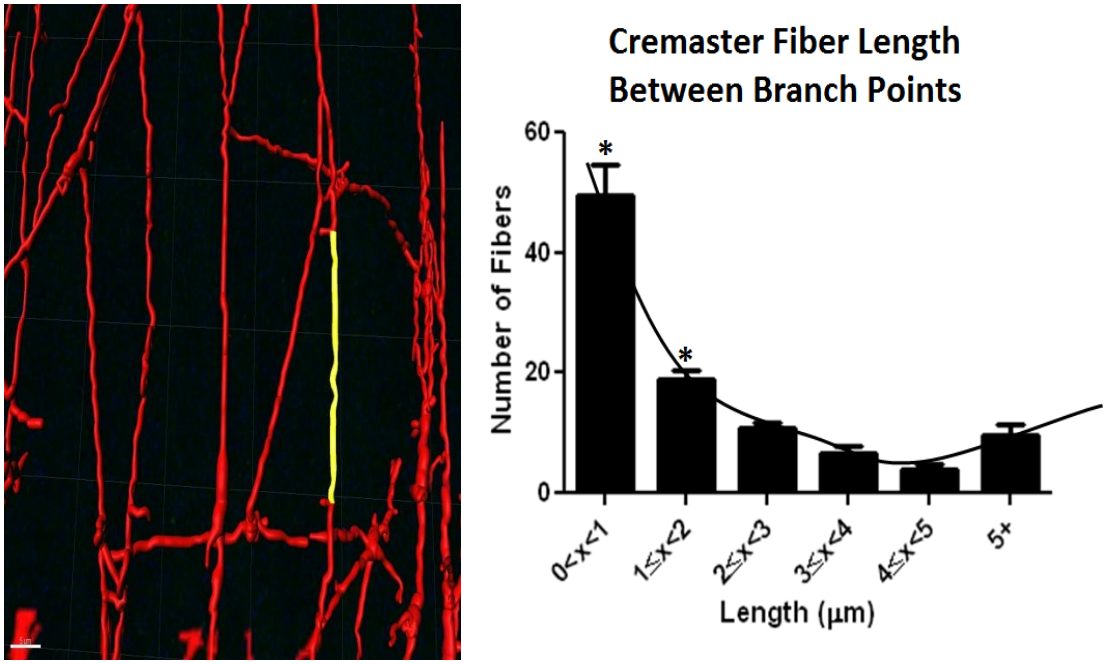

Figure 35: Left panel: Example of length measurement between branch points. Scale bar= 5 µm. Right panel: Cremaster distribution (+SEM) of fiber length between branch points (n=15). Results are normalized to total number of fibers collected from each image. * $p<0.05$ when compared to the remaining length distributions. Differences were calculated by one way ANOVA.

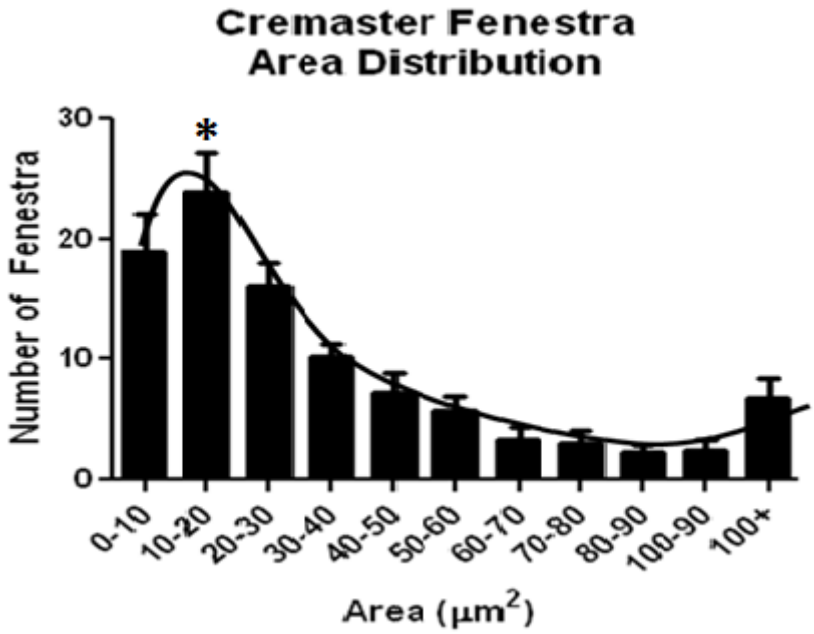

Figure 36: Distribution (+SEM) of the individual fenestra areas in the cremasteric arteriole. Results are normalized as averages of percentages of total number of fenestra calculated from individual experiments. * $p<0.05$ when compared to the following length distribution. Differences were calculated by one way ANOVA.

Small cerebral arteries were similarly stained with Alexa 633 Hydrazide and Yo-Pro Iodide (Video 5.2). A composite image as viewed from the lumen is provided in Figure 5.10A. There was a complete lack of fluorescence in the ECM area of the cerebral artery (Figure 5.10B). IEL staining, however, was similar to that of the cremasteric 1A. Fluorescence staining within the IEL was continuous throughout except for the areas within the fenestrae (Figure 5.10C). Cerebral fenestrae ranged from 2-119 μm^2 in area. As shown in Figure 5.11, the fenestra areas were varied and none of the distributions were significantly different from the ones that immediately followed. The cerebral artery exhibited a single elastic layer wall (Figure 5.10D) as compared to the double elastic wall of cremaster and mesenteric vessels (Figures 5.7D and 5.12D respectively).

Cerebral- Alexa 633 and Yo-Pro.mpg

Video 5.2: Cerebral small artery stained with Alexa 633 (elastin, red) and Yo-Pro (cell nuclei, green).

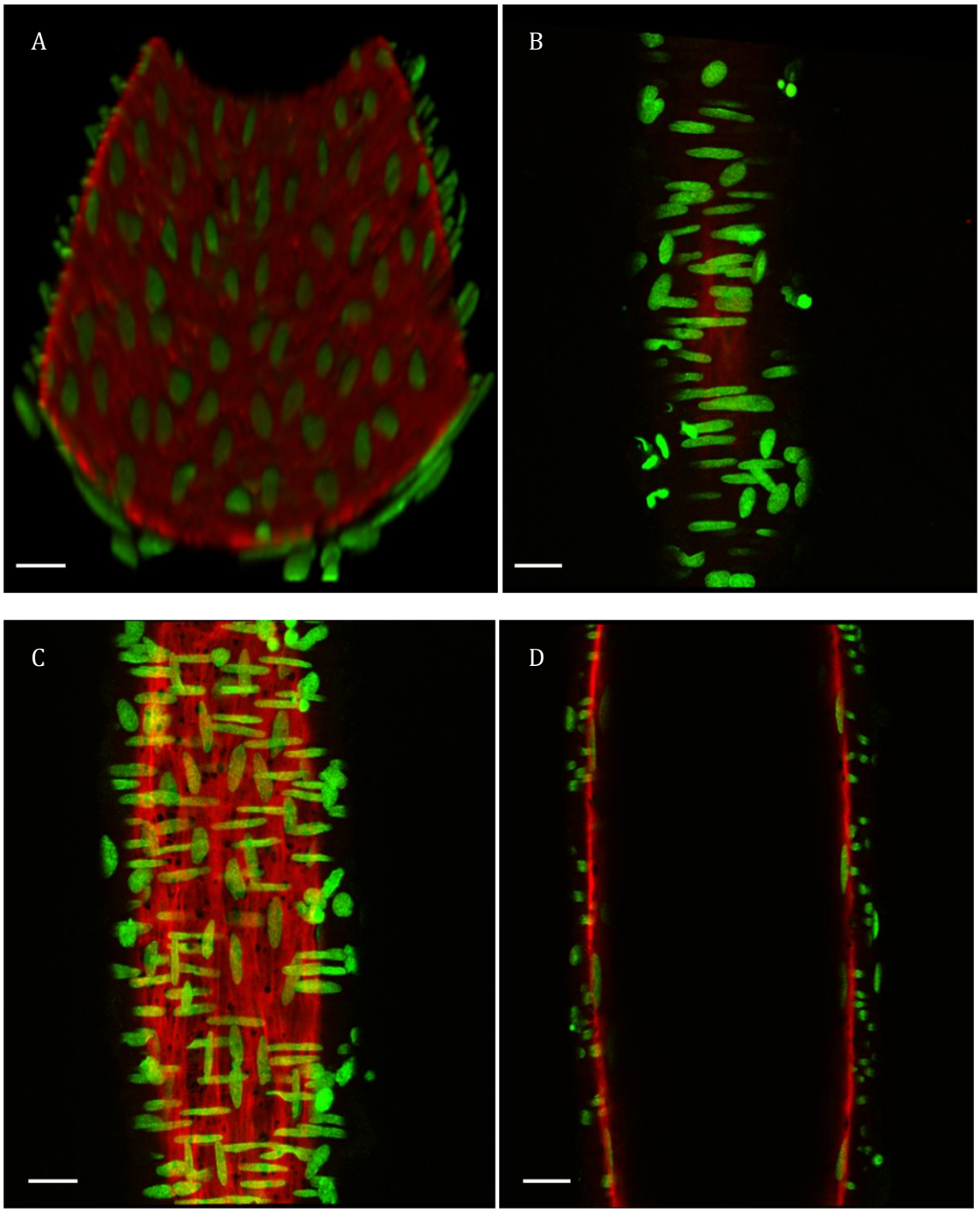

Figure 37: Cerebral small artery stained with Alexa 633 Hydrazide (red) and Yo-Pro Iodide (green). A) Whole vessel view from lumen, B) ECM section, C) IEL, D) Single elastic wall. Scale bar= 25 µm.

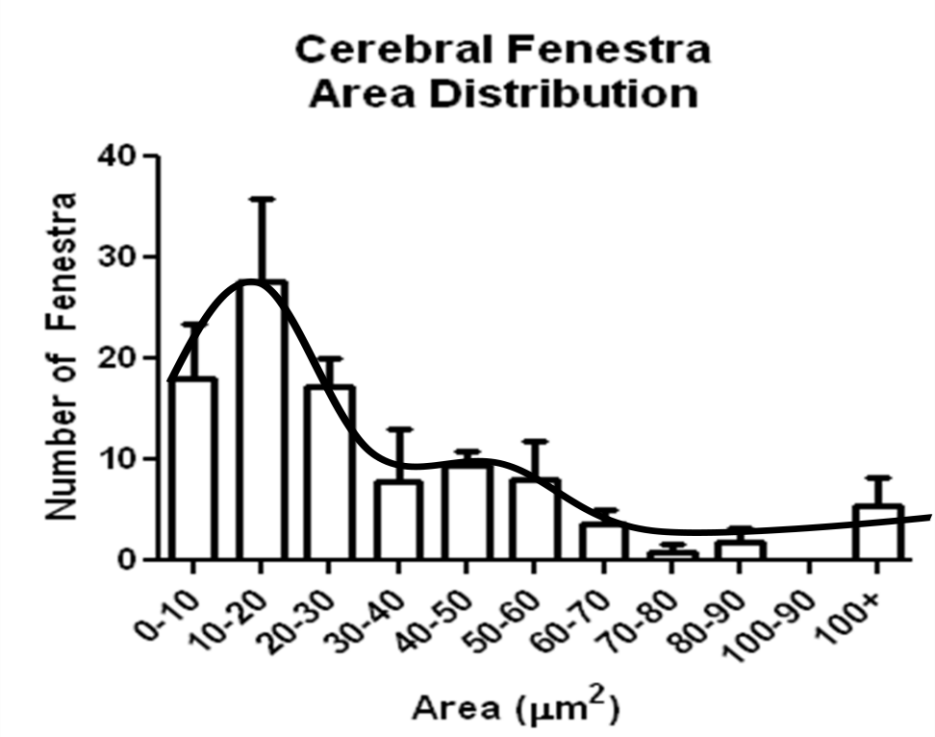

Figure 38: Distribution (+SEM) of individual cerebral artery fenestra areas. Results are normalized as averages of overall number of fenestra from individual experiments.

Small mesenteric third order arteries were imaged as examples of a third vascular bed (Video 5.3). A composite view from the lumen is provided in Figure 5.12A. The ECM of the mesenteric artery exhibited longitudinal fibers and a large amount of short, branched fibers (Figure 5.12B). Similar to that of the cremaster, the greatest number of ECM fibers was less than 1 μm between branch points (Figure 5.13). The fenestrated IEL was again similar to that of the other vessel types (Figure 5.12C). The fenestrae of the IEL ranged from 3-108 μm^2 in area. Over half of the fenestra areas in the mesentery were less than 20 μm^2 (Figure 5.14) as compared to the cremaster and cerebral distributions. An inner and outer elastic layer, similar to the cremaster 1A, was recorded in the mesenteric artery (Figure 5.12D).

Mesentery- Alexa 633 and Yo-Pro.mpg

Video 5.3: Mesenteric third order artery stained with Alexa 633 (elastin, red) and Yo-Pro (cell nuclei, green).

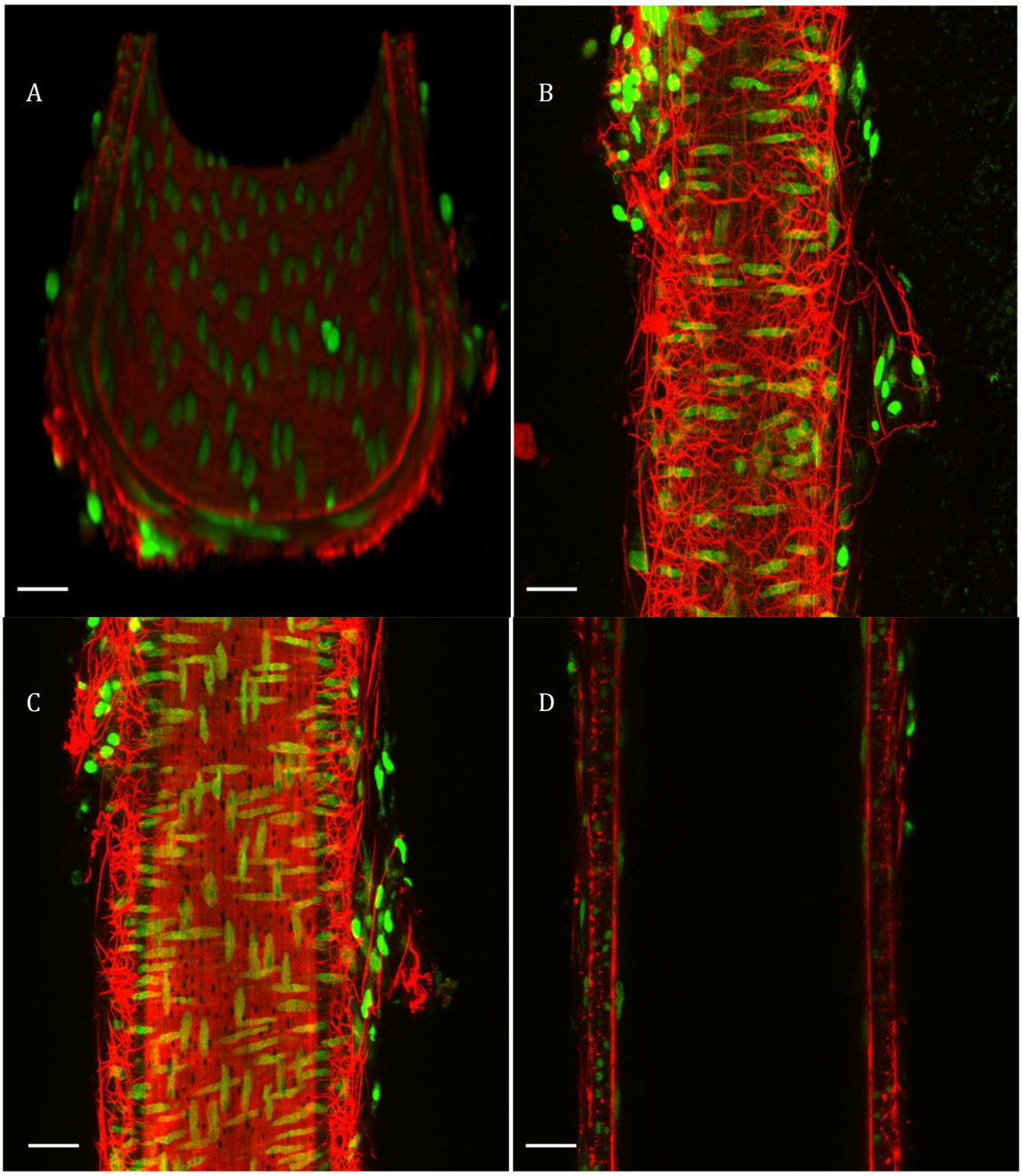

Figure 39: Mesenteric small artery stained with Alexa 633 Hydrazide (red) and Yo-Pro Iodide (green). A) Whole vessel view from lumen, B) ECM, C) IEL, D) Double elastic wall. Scale bar= 25 µm.

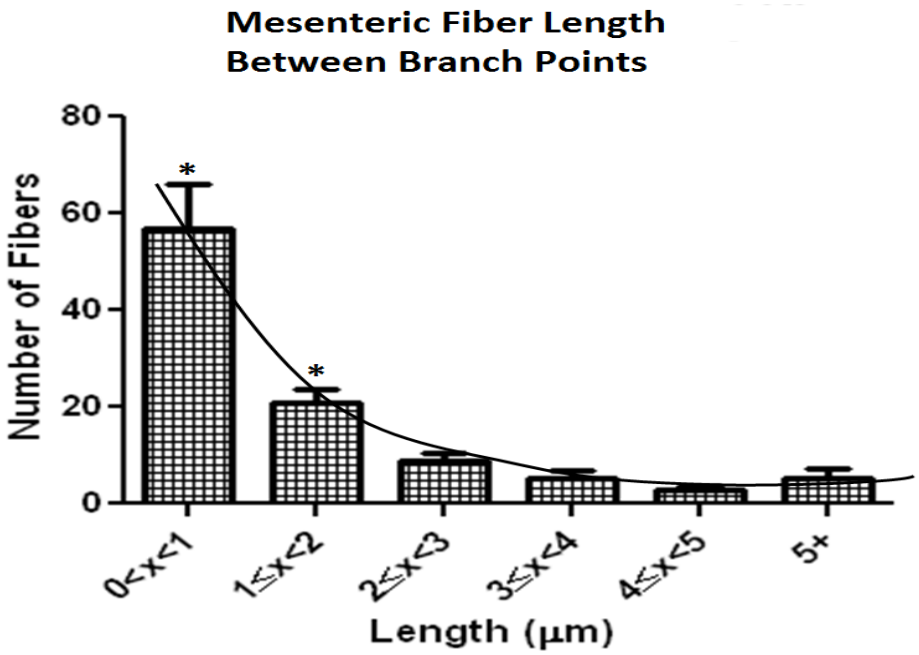

Figure 40: Mesenteric distribution (+SEM) of fiber length between branch points (n=5). Results are normalized to total number of fibers collected from each image. * $p<0.05$ when compared to the remaining length distributions. Differences were calculated by one way ANOVA.

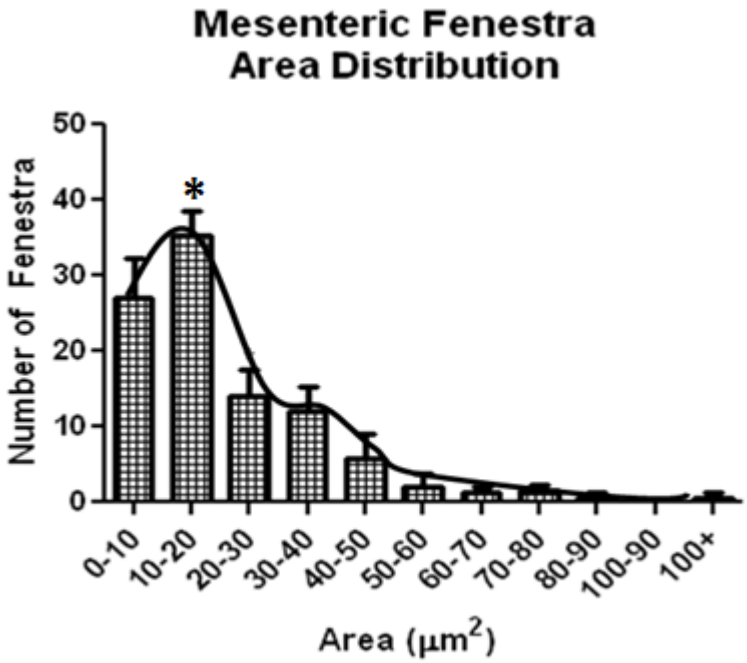

Figure 41: Distribution (+SEM) of individual mesenteric artery fenestrae areas. Results are normalized as averages of total number of fenestrae from individual experiments. * $p<0.05$ when compared to the following length distribution. Differences were calculated by one way ANOVA.

When the fiber length data between the cremaster and mesentery were compared, no significant differences were observed (Figure 5.15). The average of all fiber diameters in the cremaster was significantly higher than that of the mesenteric but the average of all fiber lengths was not significantly different (Table 5.2). All fibers from cremaster and mesentery were nearly linear as shown by the value of fiber straightness. This value was given on a scale of 0-1 in the linearity of the fibers. The number of branch points in the mesenteric ECM was significantly higher than that of the cremasteric arteriole (Table 5.2). The only difference in all measurements taken from fenestrae area was between the distributions of the mesentery and cremaster between 10-20 μm^2 (Figure 5.16). The density of fenestra studied was similar between all groups as well (Table 5.2). Overall, the fenestra area and density saw no differences between vessel types.

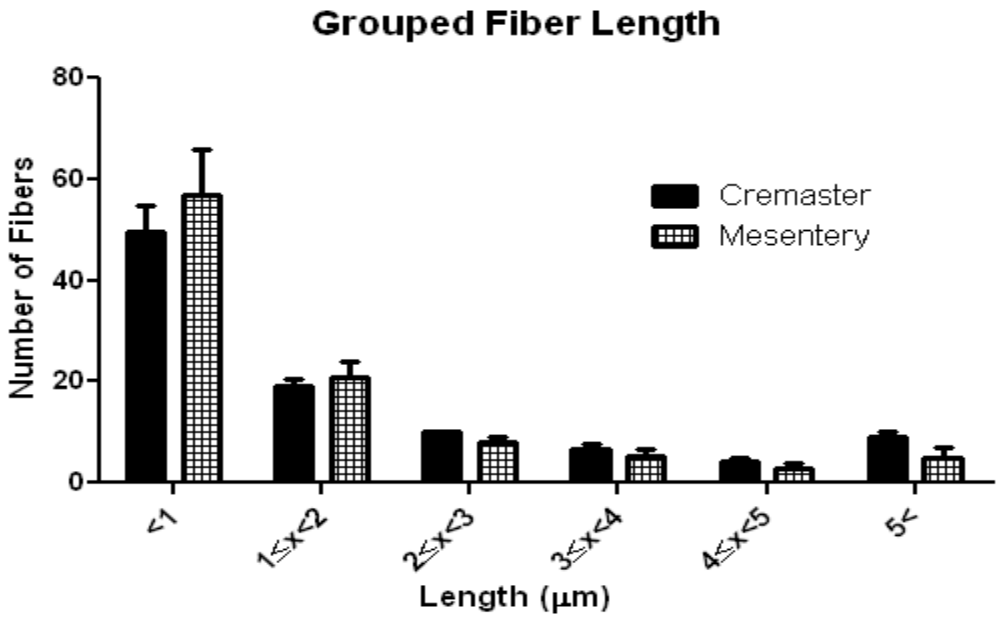

Figure 42: Group data (+SEM) from cremaster and mesentery length of fiber between branch points.

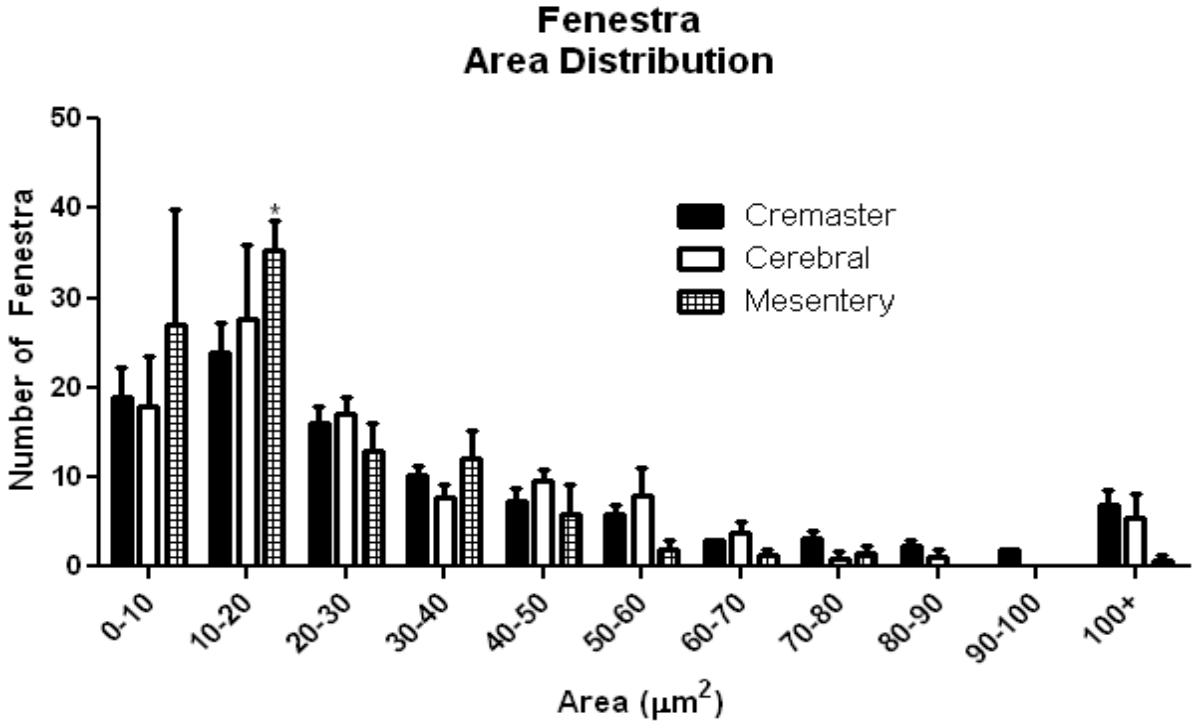

Figure 43: Group data (+SEM) from cremaster, cerebral, and mesentery of fenestrae areas. * $p<0.05$ when compared to cremaster distribution. Differences were calculated from two way ANOVA.

5.3 Localization of Vessel Wall Elastin by Immunohistochemistry: Comparison with Alexa Hydrazide Staining

In order to further understand what the Alexa 633 Hydrazide was staining, we performed elastin antibody staining on cremaster arterioles. These vessels were loaded with Alexa 633 and a primary and secondary elastin antibody (described in Methods). The Alexa 633 Hydrazide and 2° elastin antibody (Ex 491/ Em 515) had separate emission spectra and were therefore collected by different photomultiplier tubes (Figures 5.17A and 5.17B). The fibers that were stained with the Alexa 633 also showed double immunofluorescence staining with the elastin antibody when the images were overlaid (Figure 5.17C). Since the staining patterns matched, we concluded that the fibers being

stained by Alexa 633 were those of adventitial elastin. As a control experiment, no fluorescence of fibers was observed when the primary elastin antibody was omitted (Figure 5.17D).

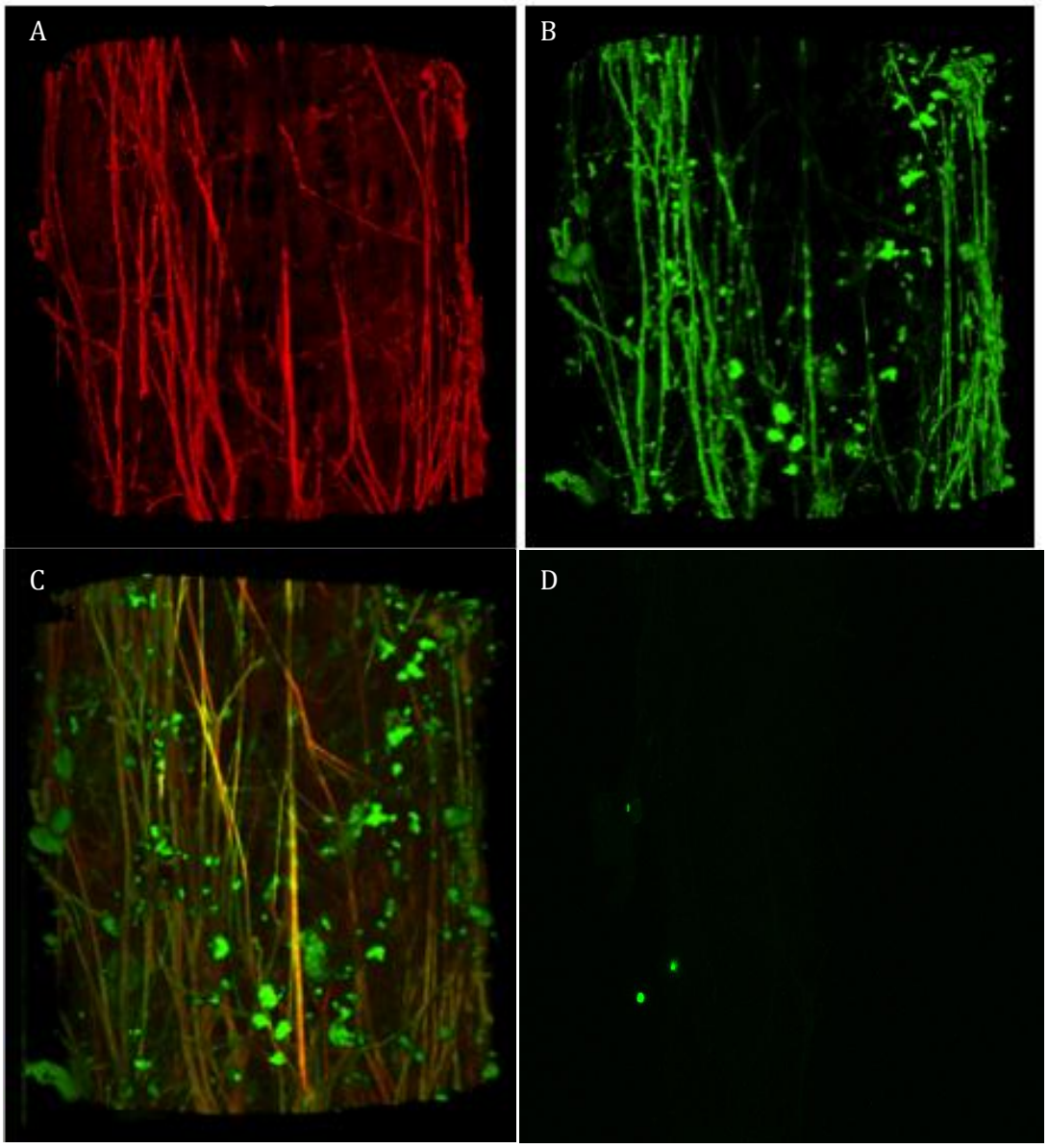

Figure 44: Elastin antibody staining in cremaster arteriole. A) Alexa 633 Hydrazide fluorescence, B) 2° Elastin antibody fluorescence, C) Merged image of panels A and B, D) Control image loaded with 2° antibody only.

5.4 Pathological Aging Model

After developing a successful image technique for blood vessel staining, the same method was extended to record the differences in a pathological aging model of rat. 3D confocal microscopy was performed in Fischer 344 male rats (n=5, 2= 9 month, 3= 24 month) weighing between 333-465 g. Mesenteric arteries were stained with Alexa 633 Hydrazide (Figure 5.18). The same quantifications were performed on these vessels. The IEL of the 9 month rat had an average of 25 fenestrae per quantification area, 62 x 123 μm^2 with an average fenestra area of 112 μm^2. The mesenteric from the 24 month rat exhibited 55 holes with an average area of 95.6 μm^2. This preliminary study did show a noticeable rearrangement of the IEL, however a large standard error led to neither value being significantly different.

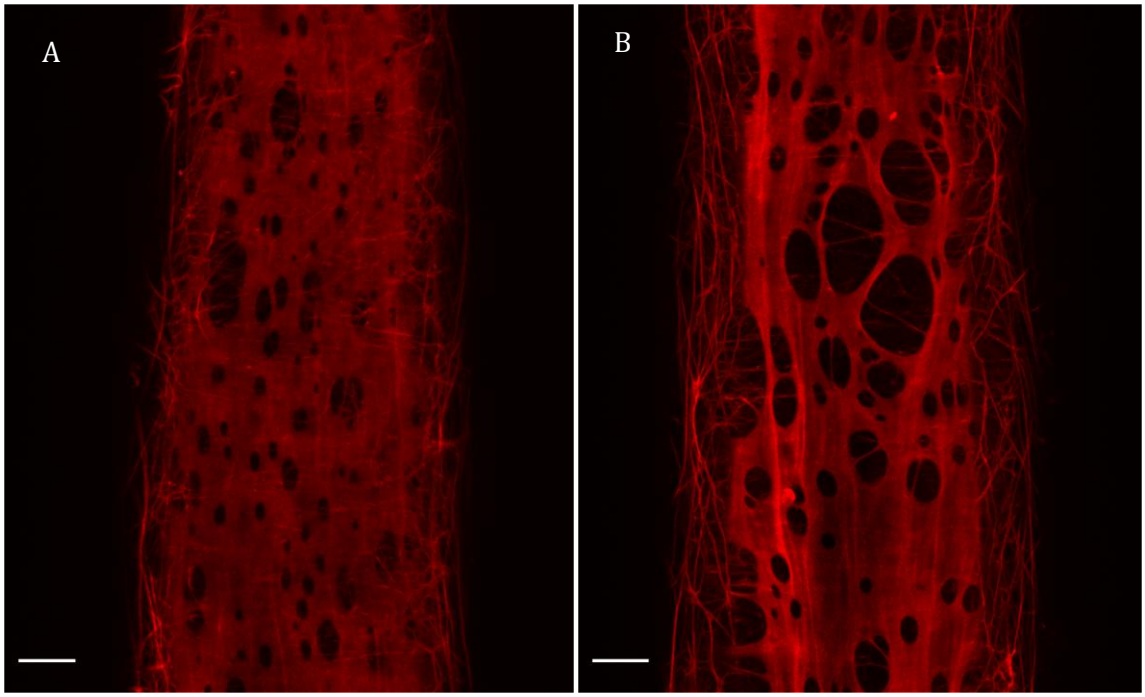

Figure 45: Alexa 633 Hydrazide staining in the mesentery of A) 9 and B) 24 month Fischer 344 rat. Scale bar =25 µm

CHAPTER 6
DISCUSSION

Elastin structure plays an important role in forming the vessels mechanical environment despite composing a relatively small amount of the overall protein content in the arteriolar wall (Kelleher et al., 2004). The focus of this study was to provide an understanding of the structural composition/arrangement of adventitial elastin fibers in the resistance arteries. This was accomplished using fluorescent stains, 3D confocal microscopy, and image analysis. Our results show considerable elastin staining in the extracellular matrix (ECM), external and internal elastic lamina (EEL and IEL, respectively) of the cremasteric arteriole wall. These imaging results raise the question as to whether the observed complex elastin network impacts both mechanical properties of the vessel as well as cellular function.

Individual Alexa Dyes

As the focus of this study was adventitial elastin, finding the most efficient dye for ECM staining of the cremaster arteriole was the first concern. ECM, EEL, and IEL content was fluoresced using three different, supposedly nonspecific ECM dyes, Alexa Hydrazides: 350, 488, and 633. Alexa 350 required the most energy input to obtain fluorescence. This increased laser power required for this dye would commonly interfere with other loaded dyes in the specimen. The binding pattern of Alexa 488 was greatest of the dyes. Alexa 488 marked the longitudinal fibers stained by Alexa 350 and 633 as well as thick, wavy bands or strips of fibers located in the ECM. These bands were always the

most distal structure from the lumen. Indeed, even the single, longitudinal fibers that were located in the adventitia were closer to the lumen. These thick bands were detected in the same location as those seen during fluorescent imaging studies from cremaster arterioles stained with a Type 1 collagen antibody (data not shown). This is in agreement with Arkill (2010), who used second harmonic generation in lymphatic vessels to image specifically for collagen. Thick, interwoven bands of collagen in the adventitia were observed that closely resembled those imaged with Alexa 488. Our results indicated that Alexa 633 was the most consistent dye between studies, requiring relatively low laser power, and showing the most extensive individual fiber staining. The ECM and EEL fibers stained by Alexa 633 were also stained with a selective elastin antibody suggesting that Alexa 633 staining shows specificity for elastin (Figure 5.17). Interestingly the elastin antibody did not stain the IEL. This may be attributable to three possible factors. One, although elastin is the main component of the IEL (Briones et al., 2003), there are numerous other proteins, such as fibrillin and others yet to be identified, composing the structure. Two, the conformational changes between elastin and these other components to form the elastic layer may block the binding sites used by the elastin antibody. Further, as antibody staining was applied from the adventitial surface, penetration to the IEL may be physically limited. The variability in staining between each Alexa Hydrazide could be a result of the biochemical properties of each. Without access to this information, it would be difficult to determine what the cause of this variation could be attributed to. Since these dyes are typically used for staining in cells, information on their staining patterns of ECM proteins is not widely known. Overall, these staining experiments showed that the longitudinal fibers of the ECM and shorter branched fibers

of the EEL are indeed elastin fibers and that the Alexa 633 Hydrazide provided the best choice for staining adventitial elastin.

Elastin Content in the Vascular Wall

Our results revealed elastin content in three separate sections throughout the vascular wall, each exhibiting a specialized arrangement. Elastic fibers in the adventitia were recorded as longitudinal fibers oriented parallel to blood flow. Little branching was seen in these fibers. These fibers are more common in vessels that undergo repetitive lengthening movements, such as skeletal muscle and the mesentery (Zou and Zhang, 2009). In the interstitium between the adventitial and medial layers were elastic fibers composing the EEL. These relatively short fibers branched often and formed a mesh encompassing the vascular wall. Therefore, the EEL elastin content appears to have the responsibility of not only protecting the vascular smooth muscle cells (SMC) from the extracellular environment, but also constraining the cells circumferentially around the lumen. This proposed function of EEL elastin is in agreement with a study by Clark and Glagov (1985) through scanning electron microscopy. Elastin fibers in the rabbit aorta were observed in between vascular SMCs in the medial layer (Clark and Glagov, 1985). The final location that elastin content was observed in our studies was in the IEL. This non-fibrillar, fenestrated sheet-like structure has been the focus of much current research. Primarily, the IEL serves as a scaffold for vessel growth on which vascular cells can assemble as well as a barrier between vascular SMCs and endothelial cells (McGrath et al., 2005). As more is known about the IEL, it appears to represent a primary component of vessel architecture and has the ability to influence vessel mechanics through remodeling.

The primary objective of this study was to classify differences in the composition of adventitial elastin from various tissues of stretch. Therefore cremasteric arterioles, small cerebral arteries, and third order mesenteric arteries were chosen as candidates to image elastin content and arrangement. During muscle recruitment of the cremaster muscle, the tissue retracts and relaxes. Therefore the arterioles in this muscle would undergo repetitive lengthening and relaxation cycles. The cremaster and mesenteric arterioles exhibited longitudinal elastic fibers in the adventitia, presumably to assist with these lengthening and relaxations. In contrast to this, the cerebral blood vessels are protected by the skull, with little movement in the tissue and are not subjected to these same stresses. No longitudinal elastic fibers were recorded in the adventitia of cerebral vessels. The EEL also showed an expansive array of fibers that completely encompassed the medial layer of cremasteric and mesenteric vascular walls. These fibers were shorter and much more branched than those fibers in the adventitia. Cerebral arteries however showed no sign of EEL elastin content. In agreement with our findings, Yamazoe (1990) found elastin content to be limited to the IEL in cerebral vessels. All vessel types imaged showed significant IEL elastin content.

There were no significant differences in the distributions of lengths of fibers between cremaster and mesenteric vessels. Both cremasteric and mesenteric vessels had significantly more fibers distributed less than 1 μm between branch points than any other length (Figure 5.15). While it is to be expected that a given vessel would have more short fibers than long fibers, the results may have been influenced by the composition of the EEL, which was shown to be composed of shorter fibers constraining the vascular SMCs. This could not be avoided during analysis due to the proximity of the two layers.

However the variations in fiber length may be due to the type of support they offer. The long fibers may be primarily responsible for bringing the vessel back to a resting state after longitudinal stretch thus relying on the elastic fibers rather than any energy input for vessel recoil. The shorter ECM and EEL fibers could have the primary role of protecting vascular stability during low levels of pressure increase (Intengan et al., 1999). The observation of irreversible lengthening caused by elastase and the variations in adventitial fiber staining in cremaster and mesentery vessels compared to cerebral vessels strongly supports the hypothesis that adventitial elastin is responsible for constraining the vessels depending on the mechanical environment.

While the variations in the ECM and EEL appeared marked between tissue beds, variation in the IEL was not as apparent under the conditions employed in this study. All imaged vessels contained the same basic structure of the IEL, a sheet-like structure wrapping around the lumen exhibiting a significant number of holes (fenestrae). The distributions in fenestra area of the IEL showed very little difference between vessel types (Figure 5.16). The largest number of holes in all vessel types was between 0-10 μm^2 in area. The mesenteric arteries were the only group to have more than 50% of all fenestrae fall below 20 μm^2 in area. It is conceivable that the size of the fenestra relates to physiological function such providing a pathway for myoendothelial gap junctions between SMCs and endothelial cells (Garland et al., 2010). Endothelium-derived hyperpolarizing factor (EDHF) and nitric oxide are generated in the vascular endothelium. These signal a current activation that ultimately causes hyperpolarization in SMCs and thus vasodilation. It is believed that this hyperpolarizing current travels through myoendothelial gap junctions to the SMCs (Garland et al., 2010; Jackson, 2011).

With an elastic layer separating the two, there would need to be channels through which the current could travel. However, classification of the fenestrae is beyond the scope of this study.

Elastin Remodeling

Vascular remodeling of elastin content throughout the vessel wall has been shown in both healthy physiological and pathological states. As flow was gradually increased in normal, adult rabbit carotid arteries, the lumen diameter increased as well as IEL fenestra size (Wong and Langille, 1996). Further, vascular remodeling of the IEL due to prolonged exposure to increased intraluminal pressure in carotid arteries from healthy animals was shown to be more significant than acute exposure to increased pressure (Masuda et al., 1999). Examination of the IEL in resistance vessels under hypertension has also shown that although IEL thickness and fenestra density do not change, fenestra area decreases significantly (Briones et al., 2003; Yao et al., 2009). Both IEL thickness and fenestra area variations could be attributed to changes in the mechanical environment and cellular function.

Decreases in IEL thickness and fenestra area are often associated with elastin reorganization and elastin degradation. Elastin reorganization would appear to be more plausible in hypertensive rats since elastin content resulted in no change (Gonzalez et al., 2005). Expression of elastin seen in the present study was observed to be structured in a number of different ways throughout the vascular wall (ECM, EEL, and IEL). These structures were not always the same between vessel types, which suggests that the conformational changes of elastin are common in different mechanical environments (Clifford et al., Unpublished data). These changes in elastin arrangement could be

regulated through production and organization of a family of glycoproteins named emilin. Emilin has displayed connections from the elastic fiber base structure, microfibrils, and vascular SMCs (Bressan et al., 1993; Doliana et al., 1999; Mongiat et al., 2000). The connections to microfibrils can influence tropoelastin binding to the microfibrils, thus allowing or disallowing overall production of elastin. The connections between elastic fibers and cell surfaces, however, do not appear to be characterized as well. These connections could be the signaling mechanism for elastin remodeling throughout the vascular wall.

Decreased elastin content has been associated with decreased distensibility and impaired cellular function. This is commonly seen in age related vascular remodeling. As part of this vascular remodeling is an increased stiffness of the vessels. This stiffness can be influenced by increases in the collagen to elastin ratio. This ratio could be affected through degradation of elastin through increased elastase activity or protein glycation as described above (Konova et al., 2004). Elastin degradation through elastase caused significant vessel lengthening and shifts in the passive pressure-diameter relationship, but no noticeable effect on vascular reactivity to vascular agents was observed under the conditions of the study (Clifford et al., Unpublished data). The vessel lengthening and shifts in pressure-diameter relationship could be associated with degradation of adventitial and internal elastin. Further confirmation of aging stiffness due to elastin degradation was provided by Hodis and Zamir (Hodis and Zamir, 2009). They provided a fractional derivative model in which elastin fatigue occurred throughout the life cycle and the load bearing function of elastin was taken over by collagen. This would result in increased stiffness and decreased distensibility.

As a preliminary study into the effects of aging, the imaging protocol was extended to the Fischer 344 rat, the preferred rat model to mimic aging (Cizza et al., 1995; Goel et al., 2010). Cremaster arterioles and mesenteric arteries were isolated from nine and twenty four month rats. The vessels were subjected to the same imaging technique as cremaster, cerebral, and mesenteric vessels from Sprague Dawley rats. Successful results were able to be collected from each vessel. As our results show, the structure of the IEL from a mesenteric artery was noticeably different between the young and old. This change in structure could be attributable to elastin degradation. In small mesenteric arteries, Briones *et al.* (2003) showed that elastase treatments caused fragmenting of the IEL and decreased distensibility at low pressures, though no measurement was taken on vessel length. This is in agreement with elastin degradation resulting in increased vessel stiffness of aging individuals. Extensive data quantification was not performed on these results because the number of samples was too small. Fenestra area and density measurements were recorded but the data varied between groups and produced a large standard error. With a low number of trials, no significant difference existed between ages. Further studies using the imaging protocol given could provide significant results.

Another theory on the decreased distensibility of arteries stems from elastin reorganization in the IEL. Changes in the organization of the IEL of small and large arteries have been recorded while elastin content was unchanged (Boumaza et al., 2001; Briones et al., 2003). Decreases of fenestra area in mesenteric arteries were also observed in spontaneously hypertensive rats (Gonzalez et al., 2005). These changes in fenestra area could have a twofold effect on distensibility. First the smaller fenestrae

together with the thickened wall seen in hypertension would increase stiffness. Second the deceased area of fenestrae would decrease the amount of area that blood and endothelium derived factors could travel through to reach the SMCs. Few studies on IEL changes in arterioles and perhaps none on EEL or adventitial elastin have been performed due in part to the relatively low amounts of elastin in these vessels. Additional studies could be performed to narrow the focus of IEL remodeling.

The lack of significant differences in characteristics between vessel types may be attributed to the process used for data quantification. Using the automated detection software in Imaris, the number of fiber branch points and IEL fenestrae were determined. It was noted that bends in elastin fibers would often be interpreted/counted as branch points, which would lead to the overall computed length between branch points being lower than the actual length. In addition, dark areas, or shadows, in the IEL would often be counted as fenestra. Dark areas around IEL fenestrae would also increase the apparent size of individual fenestra. While the automated detection did not produce accurate results of quantified data, these measurements, if done correctly, would offer an excellent classification for vessel types.

Summary

The current nomenclature for structure of the vascular wall recognizes three distinct layers: intima, media, and adventitia based on cellular location. As more research is presented and 3D structure of the vascular wall becomes better understood, the nomenclature begins to fall short. For example, adventitial proteins such as elastin and collagen are located throughout the vascular wall. In the present study, we show that

elastin is also located in between each layer. More and more research shows that IEL structure, composition, and remodeling can have significant impacts on vascular function. Collagen, located in the basement membrane, has not been a focus of this study but it also forms a significant layer in the vascular wall. Updated nomenclature or further classification of the vascular wall to include five or six layers could further a general understanding of vascular structure.

In summary, the adventitial elastin content and arrangement has been proven to vary greatly between tissue environments. Cremaster and mesenteric vessels exhibited extensive adventitial elastin content as well as an external elastic layer believed to be responsible for protecting the vascular SMCs and keeping them in place, while cerebral vessels showed none of these features. Cerebral vessels do contain adventitial proteins; however none of the Alexa dyes or antibodies used in this study ever showed staining in the adventitia of cerebral arteries. The differences in mechanical environment of these tissue beds have been thoroughly discussed. The purpose of these adventitial fibers is believed to be responsible keeping the vessels constrained on the axis of blood flow and therefore be able to lengthen when required. This function is necessary cremasteric and mesenteric arteries that would be expected to experience longitudinal strain. To the best of our knowledge, our approach for fluorescent staining of elastin in arterioles is novel and could provide a valuable tool for future investigations of the vascular wall. Importantly, this provided a 3D basis for understanding elastin structure in small arteries and arterioles. All vessel types exhibited an IEL between the SMCs and endothelial cells. Sizes of fenestra area and density were not significantly different between the vessels studied from each tissue bed. The imaging protocol for staining these small arteries and

arterioles clearly shows these differences in elastin structure. Understanding of the 3D structure of elastin in healthy arteries will further advance the research into pathological states associated with elastin changes.

CHAPTER 7

CONCLUSIONS

A detailed imaging protocol has been developed for staining elastin content and arrangement in the arteriolar wall. Fluorescent staining with Alexa 633 Hydrazide visualized elastin in the ECM, EEL, and IEL. The approach can be complemented with other fluorochromes, including that of the stains similarly loaded into the same vessel, such as nuclear dyes and antibodies to specific proteins. The staining was applied across vascular beds including those of cremaster muscle, cerebral circulation, and mesentery, as well as the same tissues in a rat model of aging.

Several Alexa Hydrazides with separate emission spectra have been shown to stain elastin and in some cases other ECM components in these vessels. The variations between dyes have been recorded and characterized. Loading different Alexa stains into the same vessel allows for imaging before and after experimentation while knowing what differences are to be expected in dye staining patterns. This also allows for development of customizable experiments. If the emission of one Alexa will influence the emission of a different fluorochrome, two separate ECM stains are available.

Alexa 633 specifically targeted elastin, which showed differing arrangements of elastin throughout the vascular wall. In cremaster arterioles, elastin was observed as longitudinal elastin fibers in the ECM, a shorter, mesh of fibers in the EEL, and the fenestrated sheet of the IEL. Similar arrangements of elastin were observed in mesenteric arteries. Elastase treatment cleaved ECM and EEL elastin fibers in the cremasteric

arteriole and the result was an irreversible lengthening. Through the described 3D confocal imaging technique, we concluded that elastase primarily digested the longitudinal fibers which confirmed our hypothesis that elastin constrains these vessels in a longitudinal direction. This permanent state of constraint would allow for vessels to lengthen when required with no damage to the vascular wall. However, elastin fluorescence was only generated in the IEL of cerebral arteries. One reason for the heterogeneity of elastin structure between vessel types could be due to the differences in the mechanical environments. The cerebral arteries may not require as much elastin if the mechanical environment of the brain is relatively stable. The IEL could adequately provide the stability needed for these vessels.

Changes in elastin arrangement have been recorded in physiological and pathological states, which indicate that elastin contributes a necessary mechanical property on the vascular wall. Brief increases in intraluminal pressure have resulted in a rearrangement of the IEL. Prolonged exposure to increased intraluminal pressure has also been shown to result in remodeling of the IEL. When elastin is degraded through enzymatic activity or fatigue, the stress bearing function relies entirely on collagen which culminates in stiffer blood vessels.

CHAPTER 8

FUTURE DIRECTIONS

Although elastin structure has been shown to be important to vascular mechanical properties, the arrangements of other ECM proteins are almost certainly vital to vascular function. Collagen has been shown to provide strength to the arterial wall (Barnes and Farndale, 1999). Fibronectin has been shown to have connections to vascular SMCs and endothelial cells and influence cellular activity (Sun et al., 2008). Further probing into the structure and arrangement of these proteins as well as other ECM proteins such as vitronectin and laminin, will also significantly advance understanding of vascular mechanics.

The heterogeneity of the elastin between vessel types has been shown here but the exact causes of these differences are unknown. One candidate is the mechanical environment in which these vessels exist. However, this is certainly not the only possible cause. Further understanding of the biomechanical properties of blood vessels with and without elastin could narrow the number of possible causes. Since cremasteric arterioles treated with elastase are still capable of myogenic activity, it can be concluded that elastin primarily influences tension on the vessel wall. The fenestrae in the IEL could certainly impact vascular responses to stimuli from the blood stream or endothelial cells. What effects various tensions and fenestra areas have on the vascular wall is still unknown.

Mechanotransduction through ECM-SMC and ECM-endothelial cell integrin connection has been studied (Martinez-Lemus et al., 2005). Most current research into mechanotransduction focuses on fibronectin, but a protein like elastin that is closely connected with vessel length would almost certainly have an impact on mechanosensing. One possible integrin connection, $\alpha_v\beta_3$, between elastin and vascular cells has been implicated during elastin synthesis. However, there are other possible integrin connections during mechanosensing. High resolution imaging through the technique provided here could highlight possible connections between the ECM and vascular wall. Short fibers in the EEL could connect the ECM to the IEL and thus transmit forces between the two structures.

Imaging elastin defects in the ECM composition in diabetic and other pathological states will need to be performed. Individuals suffering from diabetes mellitus have been shown to have increased vascular stiffness (Soldatos et al., 2011; Thelwall et al., 2011). This cause of the increased stiffness in these blood vessels is the basis for much current debate on the subject. This imaging technique for small arteries and arterioles could lead to answers that would change the focus of this controversy.

REFERENCES

Ahmed, A., C. M. Waters, C. W. Leffler and J. H. Jaggar (2004). "Ionic mechanisms mediating the myogenic response in newborn porcine cerebral arteries." Am J Physiol Heart Circ Physiol **287**(5): H2061-2069.

Alenghat, F. J. and D. E. Ingber (2002). "Mechanotransduction: All Signals Point to Cytoskeleton, Matrix, and Integrins." Sci STKE **PE6**.

Arkill, K. P., J. Moger and C. P. Winlove (2010). "The structure and mechanical properties of collecting lymphatic vessels: an investigation using multimodal nonlinear microscopy." J Anat **216**(5): 547-555.

Badylak, S. F., D. O. Freytes and T. W. Gilbert (2009). "Extracellular matrix as a biological scaffold material: Structure and function." Acta Biomater **5**(1): 1-13.

Bakker, E. N., A. Pistea and E. VanBavel (2008). "Transglutaminases in vascular biology: relevance for vascular remodeling and atherosclerosis." Journal of Vascular Research **45**(4): 271-278.

Barnes, M. J. and R. W. Farndale (1999). "Collagens and atherosclerosis." Exp Gerontol **34**(4): 513-525.

Baumbach, G. L. and D. D. Heistad (1989). "Remodeling of cerebral arterioles in chronic hypertension." Hypertension **13**(6 Pt 2): 968-972.

Bax, D. V., U. R. Rodgers, M. M. Bilek and A. S. Weiss (2009). "Cell adhesion to tropoelastin is mediated via the C-terminal GRKRK motif and integrin alphaVbeta3." J Biol Chem **284**(42): 28616-28623.

Bayliss, W. M. (1902). "On the local reactions of the arterial wall to changes of internal pressure." J Physiol **28**(3): 220-231.

Bellingham, C. M., K. A. Woodhouse, P. Robson, S. J. Rothstein and F. W. Keeley (2001). "Self-aggregation characteristics of recombinantly expressed human elastin polypeptides." Biochim Biophys Acta **1550**(1): 6-19.

Berne, R. M. (2004). Physiology. St. Louis, Mosby**:** 368-379.

Bohlen, H. G., R. W. Gore and P. M. Hutchins (1977). "Comparison of microvascular pressures in normal and spontaneously hypertensive rats." Microvasc Res **13**(1): 125-130.

Borisov, A. B., S. K. Huang and B. M. Carlson (2000). "Remodeling of the vascular bed and progressive loss of capillaries in denervated skeletal muscle." Anat Rec **258**(3): 292-304.

Boumaza, S., S. M. Arribas, M. Osborne-Pellegrin, J. C. McGrath, S. Laurent, P. Lacolley and P. Challande (2001). "Fenestrations of the carotid internal elastic lamina and structural adaptation in stroke-prone spontaneously hypertensive rats." Hypertension **37**(4): 1101-1107.

Brakenhoff, G. J., P. Blom and P. Barends (1979). "Confocal scanning light microscopy with high aperture immersion lenses." Journal of Microscopy **117**(2): 219-232.

Bressan, G. M., D. Daga-Gordini, A. Colombatti, I. Castellani, V. Marigo and D. Volpin (1993). "Emilin, a component of elastic fibers preferentially located at the elastin-microfibrils interface." J Cell Biol **121**(1): 201-212.

Briones, A. M., J. M. Gonzalez, B. Somoza, J. Giraldo, C. J. Daly, E. Vila, M. C. Gonzalez, J. C. McGrath and S. M. Arribas (2003). "Role of elastin in spontaneously hypertensive rat small mesenteric artery remodelling." J Physiol **552**(Pt 1): 185-195.

Burton, A. C. (1954). "Relation of structure to function of the tissues of the wall of blood vessels." Physiol Rev **34**(4): 619-642.

Butterfield, T. A. and W. Herzog (2005). "Quantification of muscle fiber strain during in vivo repetitive stretch-shortening cycles." J Appl Physiol **99**(2): 593-602.

Chilian, W. M., L. Kuo, D. V. DeFily, C. J. Jones and M. J. Davis (1993). "Endothelial regulation of coronary microvascular tone under physiological and pathophysiological conditions." Eur Heart J **14 Suppl I**: 55-59.

Christensen, K. L. and M. J. Mulvany (2001). "Vasodilatation, not hypotension, improves resistance vessel design during treatment of essential hypertension: a literature survey." J Hypertens **19**(6): 1001-1006.

Cizza, G., P. W. Gold and G. P. Chrousos (1995). "Aging is associated in the 344/N Fischer rat with decreased stress responsivity of central and peripheral catecholaminergic systems and impairment of the hypothalamic-pituitary-adrenal axis." Ann N Y Acad Sci **771**: 491-511.

Clark, J. M. and S. Glagov (1985). "Transmural organization of the arterial media. The lamellar unit revisited." Arteriosclerosis **5**(1): 19-34.

Clifford, P. S., S. R. Ella, A. J. Stupica, Z. Nourian, L. A. Martinez-Lemus, K. A. Dora, Y. Yang, M. J. Davis, U. Pohl, G. A. Meininger and M. A. Hill (Unpublished data). "Spatial distribution and mechanical functino of elastin in resistance arteries- a role in bearing longitudinal stress." Arterioscler Thromb Vasc Biol(Submitted Manuscript).

Clifford, P. S., S. R. Ella, Y. Yang, M. J. Davis, G. A. Meininger and M. A. Hill (2009). "Differential effects of collagenase and elastase on arteriolar vasomotor responses." The FASEB Journal **23**(1_MeetingAbstracts): 951.955.

Coats, P. (2003). "Myogenic, mechanical and structural characteristics of resistance arterioles from healthy and ischaemic subjects." Clin Sci (Lond) **105**(6): 683-689.

Davidovits, P. and M. D. Egger (1973). "Photomicrography of corneal endothelial cells in vivo." Nature **244**(5415): 366-367.

Davis, M. J., J. A. Donovitz and J. D. Hood (1992). "Stretch-activated single-channel and whole cell currents in vascular smooth muscle cells." Am J Physiol **262**(4 Pt 1): C1083-1088.

Davis, M. J., P. N. Ferrer and R. W. Gore (1986). "Vascular anatomy and hydrostatic pressure profile in the hamster cheek pouch." Am J Physiol Heart Circ Physiol **250**(2): H291-H303.

Davis, M. J. and M. A. Hill (1999). "Signaling Mechanisms Underlying the Vascular Myogenic Response." Physiological Reviews **79**(2): 387-423.

Deng, L. Y. and E. L. Schiffrin (1992). "Effects of endothelin on resistance arteries of DOCA-salt hypertensive rats." Am J Physiol **262**(6 Pt 2): H1782-1787.

Dodds, S. R., N. K. Bourne and A. D. Chant (1996). "Effect of flow on the resistance of modelled femoral artery stenoses." Br J Surg **83**(7): 957-961.

Doliana, R., M. Mongiat, F. Bucciotti, E. Giacomello, R. Deutzmann, D. Volpin, G. M. Bressan and A. Colombatti (1999). "EMILIN, a component of the elastic fiber and a new member of the C1q/tumor necrosis factor superfamily of proteins." J Biol Chem **274**(24): 16773-16781.

Faury, G. (2001). "Function-structure relationship of elastic arteries in evolution: from microfibrils to elastin and elastic fibres." Pathol Biol (Paris) **49**(4): 310-325.

Fedosov, D. A., B. Caswell and G. E. Karniadakis (2010). "A multiscale red blood cell model with accurate mechanics, rheology, and dynamics." Biophys J **98**(10): 2215-2225.

Folkow, B. (1949). "Intravascular pressure as a factor regulating the tone of the small vessels." Acta Physiol Scand **17**(4): 289-310.

Fomovsky, G. M., S. Thomopoulos and J. W. Holmes (2010). "Contribution of extracellular matrix to the mechanical properties of the heart." J Mol Cell Cardiol **48**(3): 490-496.

Fung, Y. C. (1993). Biomechanics: Mechanical Properties of Living Tissues, Springer- Verlag.

Garland, C. J., C. R. Hiley and K. A. Dora (2010). "EDHF: spreading the influence of the endothelium." Br J Pharmacol.

Gelman, S. (2008). "Venous function and central venous pressure: a physiologic story." Anesthesiology **108**(4): 735-748.

Goel, A., B. Su, S. Flavahan, C. J. Lowenstein, D. E. Berkowitz and N. A. Flavahan (2010). "Increased endothelial exocytosis and generation of endothelin-1 contributes to constriction of aged arteries." Circ Res **107**(2): 242-251.

Gonzalez, J. M., A. M. Briones, B. Starcher, M. V. Conde, B. Somoza, C. Daly, E. Vila, I. McGrath, M. C. Gonzalez and S. M. Arribas (2005). "Influence of elastin on rat small artery mechanical properties." Exp Physiol **90**(4): 463-468.

Greenlee, T. K., Jr., R. Ross and J. L. Hartman (1966). "The fine structure of elastic fibers." J Cell Biol **30**(1): 59-71.

Hammer, L. W., A. L. Ligon and R. L. Hester (2001). "Differential Inhibition of Functional Dilation of Small Arterioles by Indomethacin and Glibenclamide." Hypertension **37**(2): 599-603.

Harlow, E. and D. Lane (1999). Using antibodies : a laboratory manual. Cold Spring Harbor, N.Y., Cold Spring Harbor Laboratory Press.

Helmchen, F. (2011). "Calibration of fluorescent calcium indicators." Cold Spring Harb Protoc **2011**(8).

Hill, M. A., S. J. Potocnik, L. A. Martinez-Lemus and G. A. Meininger (2003). "Delayed arteriolar relaxation after prolonged agonist exposure: functional remodeling involving tyrosine phosphorylation." Am J Physiol Heart Circ Physiol **285**(2): H849-856.

Hill, M. A., B. E. Simpson and G. A. Meininger (1990). "Altered cremaster muscle hemodynamics due to disruption of the deferential feed vessels." Microvasc Res **39**(3): 349-363.

Hill, M. A., H. Zou, M. J. Davis, S. J. Potocnik and S. Price (2000). "Transient increases in diameter and [Ca(2+)](i) are not obligatory for myogenic constriction." Am J Physiol Heart Circ Physiol **278**(2): H345-352.

Hodis, S. and M. Zamir (2009). "Mechanical events within the arterial wall: The dynamic context for elastin fatigue." J Biomech **42**(8): 1010-1016.

Huang, H., R. D. Kamm and R. T. Lee (2004). "Cell mechanics and mechanotransduction: pathways, probes, and physiology." Am J Physiol Cell Physiol **287**(1): C1-C11.

Intengan, H. D., L. Y. Deng, J. S. Li and E. L. Schiffrin (1999). "Mechanics and composition of human subcutaneous resistance arteries in essential hypertension." Hypertension **33**(1 Pt 2): 569-574.

Intengan, H. D. and E. L. Schiffrin (2000). "Structure and mechanical properties of resistance arteries in hypertension: role of adhesion molecules and extracellular matrix determinants." Hypertension **36**(3): 312-318.

Iwasaki, S. I., H. Yoshizawa and H. Aoyagi (2011). "Localization of type III collagen in the lingual mucosa of rats during the morphogenesis of circumvallate papillae." Odontology.

Jackson, W. F. (2000). "Ion channels and vascular tone." Hypertension **35**(1 Pt 2): 173-178.

Jackson, W. F. (2011). "Quick change artist: endothelium-derived relaxing factor in resistance arteries." Hypertension **57**(4): 686-688.

Johnson, P. (1981). Myogenic Response Handbook of Physiology. The Cardiovascular System. Vascular Smooth Muscle. MD, Bethesda**:** 409-442.

Kagan, H. M. and W. Li (2003). "Lysyl oxidase: properties, specificity, and biological roles inside and outside of the cell." J Cell Biochem **88**(4): 660-672.

Keeley, F. W., C. M. Bellingham and K. A. Woodhouse (2002). "Elastin as a self-organizing biomaterial: use of recombinantly expressed human elastin polypeptides as a model for investigations of structure and self-assembly of elastin." Philos Trans R Soc Lond B Biol Sci **357**(1418): 185-189.

Kelleher, C. M., S. E. McLean and R. P. Mecham (2004). "Vascular extracellular matrix and aortic development." Curr Top Dev Biol **62**: 153-188.

Kielty, C. M., M. J. Sherratt and C. A. Shuttleworth (2002). "Elastic fibres." J Cell Sci **115**(Pt 14): 2817-2828.

Konova, E., S. Baydanoff, M. Atanasova and A. Velkova (2004). "Age-related changes in the glycation of human aortic elastin." Exp Gerontol **39**(2): 249-254.

Kuo, L., M. J. Davis and W. M. Chilian (1990). "Endothelium-dependent, flow-induced dilation of isolated coronary arterioles." Am J Physiol **259**(4 Pt 2): H1063-1070.

Lakowicz, J. R. (2006). Principles of Fluorescence Spectroscopy. New York, Springer Science+Business Media.

Martinez-Lemus, L. A., Z. Sun, A. Trache, J. P. Trzciakowski and G. A. Meininger (2005). "Integrins and regulation of the microcirculation: from arterioles to molecular studies using atomic force microscopy." Microcirculation **12**(1): 99-112.

Masuda, H., Y. J. Zhuang, T. M. Singh, K. Kawamura, M. Murakami, C. K. Zarins and S. Glagov (1999). "Adaptive remodeling of internal elastic lamina and endothelial lining during flow-induced arterial enlargement." Arterioscler Thromb Vasc Biol **19**(10): 2298-2307.

McCarron, J. G. and W. Halpern (1990). "Impaired potassium-induced dilation in hypertensive rat cerebral arteries does not reflect altered Na+,K(+)-ATPase dilation." Circ Res **67**(4): 1035-1039.

McGrath, J. C., C. Deighan, A. M. Briones, M. M. Shafaroudi, M. McBride, J. Adler, S. M. Arribas, E. Vila and C. J. Daly (2005). "New aspects of vascular remodelling: the involvement of all vascular cell types." Exp Physiol **90**(4): 469-475.

Mecham, R. P. (2008). "Methods in elastic tissue biology: elastin isolation and purification." Methods **45**(1): 32-41.

Meininger, G. A., C. A. Mack, K. L. Fehr and H. G. Bohlen (1987). "Myogenic vasoregulation overrides local metabolic control in resting rat skeletal muscle." Circ Res **60**(6): 861-870.

Meininger, G. A., D. C. Zawieja, J. C. Falcone, M. A. Hill and J. P. Davey (1991). "Calcium measurement in isolated arterioles during myogenic and agonist stimulation." Am J Physiol **261**(3 Pt 2): H950-959.

Minksy, M. (1988). "Memoir in inventing the confocal microscope." Scanning **10**: 128-138.

Mithieux, S. M. and A. S. Weiss (2005). "Elastin." Adv Protein Chem **70**: 437-461.

Mogford, J. E., G. E. Davis and G. A. Meininger (1997). "RGDN peptide interaction with endothelial alpha5beta1 integrin causes sustained endothelin-dependent vasoconstriction of rat skeletal muscle arterioles." J Clin Invest **100**(6): 1647-1653.

Mongiat, M., G. Mungiguerra, S. Bot, M. T. Mucignat, E. Giacomello, R. Doliana and A. Colombatti (2000). "Self-assembly and Supramolecular Organization of EMILIN." J Biol Chem **275**(33): 25471-25480.

Ng, W. and S. Ikeda (2011). "Standardized, defined serum-free culture of a human skin equivalent on fibroblast-populated collagen scaffold." Acta Derm Venereol **91**(4): 387-391.

Nozynski, J., M. Zakliczynski, D. Konecka-Mrowka, R. Przybylski, M. Zembala, T. Zielinska, A. Mrowka, D. Lange, E. Zembala-Nozynska, B. Nikiel and J. Mlynarczyk-Liszka (2011). "Advanced glycation end-products in myocardium-supported vessels: effects of heart failure and diabetes mellitus." J Heart Lung Transplant **30**(5): 558-564.

O'Rourke, M. F. (2007). "Arterial aging: pathophysiological principles." Vasc Med **12**(4): 329-341.

Paddock, S. W. (2000). "Principles and practices of laser scanning confocal microscopy." Mol Biotechnol **16**(2): 127-149.

Patel, D., R. Menon and L. J. Taite (2011). "Self-assembly of elastin-based peptides into the ECM: the importance of integrins and the elastin binding protein in elastic fiber assembly." Biomacromolecules **12**(2): 432-440.

Pawley, J. B., Ed. (1995). Handbook of Biological Confocal Microscopy. New York, Plenum Press.

Petersen, E., F. Wagberg and K. A. Angquist (2002). "Serum concentrations of elastin-derived peptides in patients with specific manifestations of atherosclerotic disease." Eur J Vasc Endovasc Surg **24**(5): 440-444.

Pickering, A. E., A. E. Simms and J. F. Paton (2008). "Dominant role of aortic baroreceptors in the cardiac baroreflex of the rat in situ." Auton Neurosci **142**(1-2): 32-39.

Purves, W. K., G. H. Orians and H. C. Heller (1995). Life, the science of biology. Sunderland, Mass. Salt Lake City, Utah, Sinauer Associates ; W.H. Freeman.

Segal, S. S., D. G. Welsh and D. T. Kurjiaka (1999). "Spread of vasodilatation and vasoconstriction along feed arteries and arterioles of hamster skeletal muscle." J Physiol **516 (Pt 1)**: 283-291.

Seward, H. E. and C. R. Bagshaw (2009). "The photochemistry of fluorescent proteins: implications for their biological applications." Chem Soc Rev **38**(10): 2842-2851.

Shepherd, A. P. and G. L. Riedel (1982). "Effect of pulsatile pressure and metabolic rate on intestinal autoregulation." Am J Physiol **242**(5): H769-775.

Shiraishi, T., S. Sakaki and Y. Uehara (1990). "Architecture of the medial smooth muscle of the arterial vessels in the normal human brain: a scanning electron-microscopic study." Scanning Microsc **4**(1): 191-199; discussion 199.

Shyy, J. Y. and S. Chien (2002). "Role of integrins in endothelial mechanosensing of shear stress." Circ Res **91**(9): 769-775.

Sims, F. H., X. Chen and J. B. Gavin (1993). "The importance of a substantial elastic lamina subjacent to the endothelium in limiting the progression of atherosclerotic changes." Histopathology **23**(4): 307-317.

Small, J. V. and M. Gimona (1998). "The cytoskeleton of the vertebrate smooth muscle cell." Acta Physiol Scand **164**(4): 341-348.

Soldatos, G., K. Jandeleit-Dahm, H. Thomson, M. Formosa, K. D'Orsa, A. C. Calkin, M. E. Cooper, A. A. Ahimastos and B. A. Kingwell (2011). "Large artery biomechanics and diastolic dysfunctionin patients with Type 2 diabetes." Diabet Med **28**(1): 54-60.

Sun, D., E. J. Messina, G. Kaley and A. Koller (1992). "Characteristics and origin of myogenic response in isolated mesenteric arterioles." Am J Physiol **263**(5 Pt 2): H1486-1491.

Sun, Z., L. A. Martinez-Lemus, M. A. Hill and G. A. Meininger (2008). "Extracellular matrix-specific focal adhesions in vascular smooth muscle produce mechanically active adhesion sites." Am J Physiol Cell Physiol **295**(1): C268-278.

Sylvester, F. A., J. C. Frisbee and J. H. Lombard (2000). "Longitudinal Differences in Vascular Control Mechanisms in Isolated Resistance Arteries of the Rat Cremaster Muscle." Microvasc Res **60**(2): 160-167.

Tamarina, N. A., W. D. McMillan, V. P. Shively and W. H. Pearce (1997). "Expression of matrix metalloproteinases and their inhibitors in aneurysms and normal aorta." Surgery **122**(2): 264-272.

Thelwall, P. E., R. Taylor and S. M. Marshall (2011). "Non-invasive investigation of kidney disease in type 1 diabetes by magnetic resonance imaging." Diabetologia.

Uchida, E. and D. F. Bohr (1969). "Myogenic tone in isolated perfused resistance vessels from rats." Am J Physiol **216**(6): 1343-1350.

Uitto, J., A. M. Christiano, V. M. Kahari, M. M. Bashir and J. Rosenbloom (1991). "Molecular biology and pathology of human elastin." Biochem Soc Trans **19**(4): 824-829.

Urban, Z. and C. D. Boyd (2000). "Elastic-fiber pathologies: primary defects in assembly-and secondary disorders in transport and delivery." Am J Hum Genet **67**(1): 4-7.

van den Akker, J., M. J. Schoorl, E. N. Bakker and E. Vanbavel (2010). "Small artery remodeling: current concepts and questions." J Vasc Res **47**(3): 183-202.

van den Berg, T. J., M. P. Hagenouw and J. E. Coppens (2005). "The ciliary corona: physical model and simulation of the fine needles radiating from point light sources." Invest Ophthalmol Vis Sci **46**(7): 2627-2632.

von Anrep, G. (1912). "On local vascular reactions and their interpretation." J Physiol **45**(5): 318-327.

Vuori, K. (1998). "Integrin signaling: tyrosine phosphorylation events in focal adhesions." J Membr Biol **165**(3): 191-199.

Wagenseil, J. E., C. H. Ciliberto, R. H. Knutsen, M. A. Levy, A. Kovacs and R. P. Mecham (2009). "Reduced vessel elasticity alters cardiovascular structure and function in newborn mice." Circ Res **104**(10): 1217-1224.

Wagenseil, J. E. and R. P. Mecham (2009). "Vascular extracellular matrix and arterial mechanics." Physiol Rev **89**(3): 957-989.

Wang, N., J. P. Butler and D. E. Ingber (1993). "Mechanotransduction across the cell surface and through the cytoskeleton." Science **260**(5111): 1124-1127.

Watanabe, M., T. Sawai, H. Nagura and K. Suyama (1996). "Age-related alteration of cross-linking amino acids of elastin in human aorta." Tohoku J Exp Med **180**(2): 115-130.

Webb, R. H. (1996). "Confocal optical microscopy." Rep Prog Phys **59**(3): 427-471.

Wong, L. C. and B. L. Langille (1996). "Developmental remodeling of the internal elastic lamina of rabbit arteries: effect of blood flow." Circ Res **78**(5): 799-805.

Wu, W. J. and A. S. Weiss (1999). "Deficient coacervation of two forms of human tropoelastin associated with supravalvular aortic stenosis." Eur J Biochem **266**(1): 308-314.

Wu, X., Y. Yang, P. Gui, Y. Sohma, G. A. Meininger, G. E. Davis, A. P. Braun and M. J. Davis (2008). "Potentiation of large conductance, Ca2+-activated K+ (BK) channels by alpha5beta1 integrin activation in arteriolar smooth muscle." J Physiol **586**(6): 1699-1713.

Yamazoe, N., N. Hashimoto, H. Kikuchi, Y. Kang, H. Nakatani and F. Hazama (1990). "Study of the elastic skeleton of intracranial arteries in animal and human vessels by scanning electron microscopy." Stroke **21**(5): 765-770.

Yao, Q., D. M. Hayman, Q. Dai, M. L. Lindsey and H. C. Han (2009). "Alterations of pulse pressure stimulate arterial wall matrix remodeling." J Biomech Eng **131**(10): 101011.

Zou, Y. and Y. Zhang (2009). "An experimental and theoretical study on the anisotropy of elastin network." Ann Biomed Eng **37**(8): 1572-1583.